ÓBUDAI EGYETEM
ÓBUDA UNIVERSITY

DOCTORAL (PhD) THESIS FOR HOME DEFENSE

István Gőzse

Applications of Hyperbolic Geometry in the Theory of Linear Time-Invariant Systems

Supervisor: Prof. Dr. habil. Róbert Szabolcsi DSc

DOCTORAL SCHOOL ON SAFETY AND SECURITY SCIENCES

Budapest, 2026-02-04

Contents

Chapter 1

Introduction

Geometry is one of the most important areas of matematics. Initially geometry was a natural consequence of our everyday life.

Our first geometrical records were created in ancient times. The process of abstraction began in Greece, where the basics of geometry were logically described. Concepts of line, point, distance, angle were lay down. One of the most important mathematician and philosopher of the time was Euclid who summarized the results in his famous book Elements that determined the geometrical way of thinking for millennia.

To solve engineering problems we most commonly use analysis, algebra and geometry. In order to make geometry an even more reliable engineering tool there is a need to correlate geometrical facts to useful algorithms. The vast majority of the engineering problems are handled by Euclidean geometry and only few works exploit the much richer content of geometry. Following this in this thesis aspect of hyperbolic geometry is examined in conjunction with engineering problems.

Although hyperbolic geometry is difficult to visualize it is more common than we would think. The truth according to Einstein's relativity theory is that the world we live in is a hyperbolic space.

1.1 Motivation and Background

Hyperbolic geometry view on dynamical systems can offer a unique insight and reveal connections between certain properties of linear systems. Investigation of this connection has led to the successful utilization of the hyperbolic approach on various engineering problems.

The most successful application area is the system identification, where various methodologies are developed in the literature.

The problem of Linear Time Invariant (LTI) system identification is discussed in [1] from a

hyperbolic geometric point of view. The identification method is based on a hyperbolic wavelet construction that parametrizes the location of poles by operations similar to the basic mother wavelet transformations that are translation and dilatation. Furthermore, a hyperbolic wavelet transformation is proposed on the conceptual base of the Blaschke function, operating as a translation operator.

Another identification method, based on the intersection of hyperbolic circles is proposed in [2]. The system is represented in Laguerre basis and the convergence of the Laguerre series expansion is connected to the hyperbolic radius of a hyperbolic circle.

The 2-dimensional Poincaré disc model is utilized in [3] in order to aid system identification of Linear Parameter Varying (LPV) systems. The work connects Kolmogorov n-width optimal orthogonal basis (see [4]) functions with objects in hyperbolic geometry.

The basis of the motivation is that hyperbolic geometry has been successfully utilized in system identification and analysis. Following this, the dissertation provides novel results on the basic underlying correspondence of hyperbolic geometry and system theory (Thesis1.) and a novel application of hyperbolic geometry on gridded parametric LTI interpolation(Thesis 2.) and identification of pole location of LTI systems(Thesis 3.). The next sections provide basic introduction for the hyperbolic geometry, parametric LTI interpolation, and system identification.

1.1.1 Hyperbolic geometry

The foundation of geometry is dated back to Thales (600 BC) with the formalised discussion while the axiomatic construction of geometry was started by Euclid around 300 BC. His axioms can be expressed as the following:

1. Any two points lie on a unique line.
2. Any straight line can be continued indefinitely in either direction.
3. A circle of any center and any radius can be drawn.
4. All right angles are equal.
5. The parallel postulate: If a straight line, crossing another two straight lines l, l' , makes angles α, β with l, l' on one side, and if $\alpha + \beta < \pi$ then l, l' meet on that same side. Equivalently for every line l, and a point P not on l, there is only one line through P which does not cross l.

The last axiom started a series of attempts to prove it using the other four postulates but the problem could not be solved until the first half of the 19th century, when independently from each other, Gauss (c. 1822), Bolyai (1829) and Lobachevsky (1826) were able to develop a

consistent geometry in which the parallel postulate is modified but the rest of Euclid's axioms are kept. Later this became known as non-Euclidean geometry. It is worth to mention that the modern treatment of Euclidean geometry is attributed to David Hilbert (1899).

One of the non-Euclidean geometries is hyperbolic geometry where the fifth postulate is substituted with the following: for every line h, and a point P not on h, there are infinitely many lines through P which do not cross h. It is obvious that such a geometry can not exist in Euclidean space, therefore, the models of hyperbolic geometry were constructed that follow the axioms of hyperbolic geometry and can be illustrated in Eucledean space. In this thesis the Poincaré disc model is used that is a model of a hyperbolic plane (see chapter 3).

1.1.2 Parametric LTI interpolation

Ordinary differential equations are one of the most powerful tools for modeling dynamical systems but accurate models usually contain large number of equations. The main purpose of these models is to study complex underlying physical phenomena. However, if they are used for simulation, control design or optimization using the available computational resources can be ineffective in terms of execution time and available memory. In order to overcome this problem methods of model order reduction (MOR) have been proposed. The reduced order model approximates the input-output behavior of the original large-scale system by a significantly lower order one. In addition, it is usual in engineering practice that the dynamics of the high-order system depends on a set of parameters. These parameters may influence the dynamics in many ways for example material properties, system geometry, system configuration. In this case, application of parametric model order reduction (pMOR) [5] is needed.

Generating and reducing a large-scale model can be a very costly procedure. For example a complex computer fluid dynamics (CFD) calculation can take days to evaluate at one certain parameter. Optimization of a mechanical structure that is modeled by finite element method (FEM) can require evaluation of a model at each step of the optimization even with several thousand states. Thus the main goal for pMOR is to obtain a reduced model for any parameter value without the need to repeat the modeling and reduction. It is crucial and it is in the main focus that the algorithm that solves the pMOR problem should have significantly less computational requirement than the evaluation of the original system.

In most of the cases, the parameter-dependent high-dimensional model is known at certain parameter values that is why the vast majority of the pMOR methods are interpolation-based methods. The standard work-flow of interpolation based methods is as follows: given a set of high-dimensional models at certain parameter values, each is reduced independently then the reduced model at different parameter values is calculated (interpolated) using the known reduced models ([6, 7]). Since the behavior of the complex system is unknown at the parameter value

of interest, apart from the initially known models, some additional a priori information needs to be incorporated into the interpolation algorithm in order to relate the interpolated models to the original behavior. For example if it is known that the original system is stable everywhere in the valid parameter domain then the interpolated system should be stable as well. Many stability preserving techniques were developed and applied on dissipative systems [8], Port-Hamiltonian systems [9], passive systems [10], and general class of linear time-invariant (LTI) systems [5,11]. Interpolation-based pMOR algorithms interpolate between LTI systems which are samples of a parametric LTI system so the term parametric LTI interpolation is used to denote the action required to accomplish an interpolation-based pMOR algorithm.

In this work a stability and minimal phase preserving interpolation method is proposed for parametric MIMO LTI systems with a scalar parameter.

1.1.3 Identification of LTI system

Determining pole locations is fundamental in many linear-system modeling tasks, and a variety of methods have been developed to address it. In particular, identifying spectral peaks in noisy measurements can be viewed as a pole-identification problem. Such situations arise frequently in the analysis of vibrating mechanical structures, rotating electrical machines, and industrial processes (e.g., in power-generation systems such as nuclear power plants).

For use of parametric methods in time domain one can cite variations of Prony–methods [12] and those assuming linear signal- and system-models, i.e. applying autoregressive (AR) or autoregressive moving-average (ARMA) model identifications and associated spectral analysis [13], as well as identification of matrix partial fraction models [14], and subspace approaches [15]. Disadvantage of these approaches is that associated to the parametrization problem, both the structure and the parameters have to be estimated, leading to, in many situations, unreliable results.

Another approach is the use of rational orthogonal bases [16] that needs a priori knowledge on the pole locations. Special attention is paid on the problems of pole selection and validation [17]. There exist methods to refine the pole locations starting from an approximate placement of poles [18].

This work proposes a new approach that is closely related to signal and system representations using discrete rational Laguerre–basis in $\mathrm{H}^2(\mathbb{D})$. ($\mathbb{D} := \{z \in \mathbb{C} : |z| < 1\}$) The poles of the system can be identified by applying Fourier transform on the Laguerre–coefficient that can be computed using frequency domain data.

1.2 Overview of the thesis

After the introduction, the literature related to the application of hyperbolic geometry in engineering is discussed in Chapter 2.

Chapter 3 presents mathematical preliminaries that are used in the upcoming material. The basic features of hyperbolic geometry is presented along with a discussion of H^2 Hardy space and discrete Laguerre transformation.

In Chapter 4 results are reported, connecting the H_∞ norm and the ν-gap metric with the hyperbolic distance; under specified assumptions, the equivalence of (i) the H_∞ norm of the difference of two first-order LTI systems, (ii) the ν-gap of these systems and (iii) the hyperbolic distance is also proved.

A new application of hyperbolic geometry is described in Chapter 5. A stability preserving interpolation method is proposed for parametric SISO LTI systems with a scalar parameter that also guarantees minimum phase property. The parametric SISO LTI system is sampled over a grid of parameter values and the interpolated system is calculated between these samples. The proposed method is based on the geometrical interpolation of the poles and the zeros. The poles and the zeros travel on a particular trajectory while the scalar parameter changes and the samples of these trajectories are known. As the real paths are unknown between samples, artificial trajectories are proposed which are hyperbolic lines. The method is extended for MIMO systems as well.

In Chapter 6 a new method of identification of the poles is proposed for discrete time linear system. The discrete rational transfer function is represented in a rational Laguerre basis. Laguerre coefficients are considered as a sum of oscillating signals that gives us the opportunity to estimate the places of poles of the system by the Fourier transform of the Laguerre–coefficients.

Finally, a conclusion is given in Chapter 7 and future research is stated.

Disclosure of AI assistance. In line with the Committee on Publication Ethics (COPE) recommendations regarding transparency, I hereby disclose the usage of artificial intelligence in the preparation of this manuscript. A large language model (ChatGPT 5.2) was used solely to improve English grammar, wording, and readability. All suggestions generated by the AI were carefully reviewed, verified, and edited by the author, who takes full responsibility for the final content of the manuscript.

Chapter 2

Literature review

In this section the application of hyperbolic geometry in engineering is reviewed. The general mathematical description has a vast literature (just to name some: [19] [20] [21]) and the discussion of it is beyond the scope of this thesis. The hyperbolic geometry is also used in physics for example in special relativity [22] but we focus on the applications relevant in engineering. In the last part of this chapter we focus on the summary of the literature of parametric interpolation of LTI systems. The application of hyperbolic geometry in parametric LTI interpolation is a new approach that is introduced in this thesis.

Material science

Certain crystal structures are linked with hyperbolic surfaces [23] [24].

Apart from the well known morphologies, such as lamellae, cylinders and spheres, other new microdomain morphologies have been described. Those new morphologies are important from both academic and industrial points of view as these belong to a new class of microdomain structures and their interfaces are hyperbolic surfaces. Novel morphologies can be predicted with mathematical modelling of microdomain interfaces with a variety of hyperbolic surfaces. The shape of the interface between two phases plays a key role in description of microdomain morphology. The base of the classification can be the local curvature of the interfaces with the given topological continuity.

Network science

A geometric framework for complex networks was developed (see [25] [26] [27]) to study the structure and function of complex networks. As it is described under some realistic assumptions, hyperbolic geometry naturally appears. The underlying geometric properties make some forms of analyses of complex networks less complicated.

Impedance matching

Problems such as finding a proper solution for transmission lines and matching circuits can be efficiently handled by Smith chart [28] [29]. The graph of the chart that is plotted on the complex plane can be used to depict multiple parameters such as impedances, admittances, scattering parameters, noise figure circles, constant gain contours and regions for unconditional stability, including mechanical vibrations analysis. The correspondence between hyperbolic geometry and Smith chart can be captured in the fact that Smith chart can aid performing Möbius transformation. More general aspect of the correspondance of hyperbolic geometry and impedance matching problem is discussed in [30] [31] [32].

Robust control

Certain kinds of robust control synthesis problems are considered in [33] [34] [35] from a complex function theoretic point of view. The usage of hyperbolic metric on the unit disk gives us the opportunity to simplify the robust stabilization problem into an easily solvable problem in hyperbolic geometry. More general can be built up on this approach to treat several different problems.

System identification

The most successful application area of hyperbolic geometry is system identification, where various methodologies are developed in the literature. In [36] [37] [38] the hyperbolic metric on Poincaré disk model is applied in LPV identification framework. A bases-selection algorithm is developed based on hyperbolic geometric results that can be used for selecting bases of orthogonal bases function based LPV model structure.

In the field of LTI identification and signals and systems theory principles of the hyperbolic geometry are extensively applied in [39] [18] [40] [41] [42] [43] [40] [44] [45] [1] [46] [2]. Hyperbolic metric and Laguerre representation of analytic functions can be outlined to give us the opportunity to derive the poles of the functions. Pole determination in such a way leads to the intersection of hyperbolic circles.

The presented work in section 4 is loosely connected to the work of [33] [34] [35], so the analysis of the correspondence of linear systems are further investigated. In section 5 a new way of application of the hyperbolic geometry in engineering is introduced on the field of parametric LTI interpolation. As it is discussed, the hyperbolic geometry is applied on the field of system identification and in section 6 a new identification method is presented that is connected to the usage of hyperbolic geometry.

Parametric LTI interpolation

Various pMOR techniques have been developed and applied to different classes of systems. Balanced truncation for parameter-dependent systems was explored in [47] that extends classical balanced truncation to parameter-dependent systems (including differential-algebraic equations) by computing reduced models on a set of parameter samples and constructing a single projection subspace valid for all parameters. This approach has a computationally expensive offline part and a much more efficient online part. Matrix interpolation techniques for local reduced order model (ROM) interpolation appeared in [8]. The study introduces a framework for parametric MOR via matrix interpolation. High-fidelity models are first reduced at various fixed parameter values, producing stable local ROMs. Then, the system matrices of these ROMs are interpolated across the parameter domain. This method ensures the interpolated ROM remains stable (using a matrix-measure criterion). Stability-preserving interpolation was comprehensively tackled in [5,11]. The papers propose an enhanced matrix-interpolation method that guarantees asymptotic stability of the parametric ROM. Here, each local ROM is post-processed via semidefinite programming to enforce strict dissipativity (passivity) so that it is stable. By interpolating these modified (dissipative) reduced models, the resulting parametric ROM remains stable for any intermediate parameter value. A data-driven Loewner framework for aeroelastic systems is introduced in [48]. The authors explore data-driven identification for parametric ROMs of aeroelastic systems. It uses a technique for modeling unsteady aerodynamic forces with parameter dependence. The approach employs the Loewner framework to fit parametric state-space models to frequency-domain data at multiple parameter settings, effectively interpolating transfer-function data into a reduced-order model. Optimization-based $\mathcal{H}_2 \otimes \mathcal{L}_2$ reduction was advanced in [49]. The paper has demonstrated that the $\mathcal{H}_2 \otimes \mathcal{L}_2$ reduction framework extends to parametric LTI systems: first-order optimality conditions for structured ROMs were derived, and a stability-preserving optimisation routine was devised that yields locally optimal, stable reduced models with markedly lower errors at modest computational cost. Port-Hamiltonian structure preservation for pMOR was addressed by [50]. The study contributes a method aimed at preserving the inherent structure (e.g., port-Hamiltonian) of the original system in the reduced models. The approach integrates structure-preserving constraints into the MOR process so that the parametric ROM inherits properties like stability and passivity from the full-order model. Passivity-preserving reduction across parameter ranges was discussed in [10]. The authors focuses on preserving physical system structure during parametric reduction. It introduces a pMOR technique that ensures the ROM remains passive (energy non-generating and stable) for all parameter values.

Chapter 3

Mathematical preliminaries

3.1 Hyperbolic geometry

In the followings a short summary is presented about the most important features of the hyperbolic geometry (for further information see [19, 20]). The basis of hyperbolic geometry is that

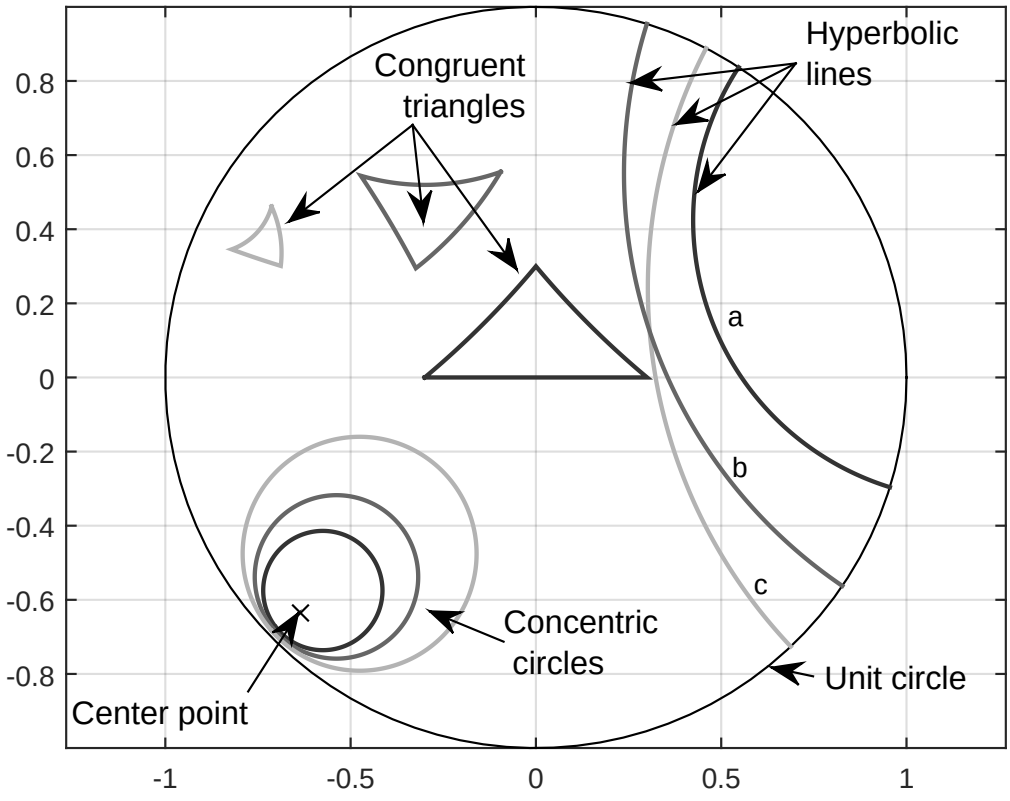

Figure 3.1: Basic geometric objects on Poincaré disk model of hyperbolic geometry

the Euclid's parallel postulate is substituted by the axiom stating that for every line h, and a point P not on h, there are infinitely many lines through P which does not cross h. There are many models with this property, in this paper the Poincaré disk model is applied which is also used in the control engineering for other purposes [3, 43].

Lines are represented by Euclidean circles that are orthogonal to the unit circle, while the hyperbolic line is the part of a circle which lies strictly inside the unit circle. In Fig. 3.1 line a is parallel to line b and line c and it is easy to see that infinite number of lines can be drawn that is parallel to line a and go through the intersection of lines b and c.

The Poincaré disk model is defined on the complex unit disk $\mathbb{D} := \{z \in \mathbb{C} : |z| < 1\}$ with the following distance metric:

$$d_h(\gamma_1, \gamma_2) = 2 \tanh^{-1} \frac{|\gamma_1 - \gamma_2|}{|1 - \gamma_2 \overline{\gamma}_1|}, \tag{3.1}$$

where $\gamma_1, \gamma_2 \in \mathbb{D}$ and $\overline{\gamma}$ is the complex conjugate of γ. It can be shown:

$$\lim_{|\gamma_1| \to 1} d_h(\gamma_1, \gamma_2) \to \infty, \tag{3.2}$$

i.e. the distance approaches infinity as one of the points approaches the unit circle. In other words: the complex unit disk $\mathbb{D}$ represents the infinite hyperbolic 2-dimensional space in this model.

Hyperbolic circles are the set of all points that are at a given hyperbolic distance from a given center point (see Fig. 3.1). In Poincaré disk model the hyperbolic circles can be represented by Euclidean circles meaning that there is an Euclidean circle for every hyperbolic circle so that each circle has the same set of points.

It is also important to note that one can define a so called pseudo-hyperbolic distance as:

$$d_{hp}(\gamma_1, \gamma_2) = \left| \frac{\gamma_1 - \gamma_2}{1 - \overline{\gamma}_1 \gamma_2} \right|. \tag{3.3}$$

The Poincaré disk model equipped with the pseudo-hyperbolic distance has the same geometric properties except that the pseudo-hyperbolic distance is not additive along geodesics (i.e., the hyperbolic lines).

Three important theorem is presented here that express the isometric transformations on the hyperbolic space (see [20]).

Theorem 3.1.1. *Any holomorphic homeomorphism $f : \mathbb{D} \to \mathbb{D}$ is an isometry of the hyperbolic metric.*

Theorem 3.1.2. *Any holomorphic homeomorphism f of $\mathbb{D}$ to itself is a Möbius transformation*

$$f(z) = \frac{az + b}{cz + d} \quad ad - bc \neq 0 \tag{3.4}$$

Theorem 3.1.3. *The general formula for all isometric transformation of the Poincaré disk model is:*

$$w = \frac{\alpha z + \beta}{\overline{\beta} z + \overline{\alpha}} \quad \alpha, \beta \in \mathbb{C},\ |\beta|^2 - |\alpha|^2 = 1. \tag{3.5}$$

3.2 H^2 Hardy space

Let $H^2(\mathbb{D})$ be the set of all functions that are analytic outside the unit circle plate $\mathbb{D}$ and have a finite norm with respect to the following norm definition [51].

Let $f \in H^2(\mathbb{D})$ and let $M_2(f, r)$ be the following function:

$$M_2(f, r) = \left\{ \frac{1}{2\pi} \int_{-\pi}^{\pi} \left| f\left(re^{\mathrm{i}\,\omega}\right) \right|^2 d\omega \right\}^{\frac{1}{2}}, \tag{3.6}$$

where r and ω are the magnitude and argument of the complex number with i being the imaginary unit. For any $f \in H^2(\mathbb{D})$ the 2-norm is defined as:

$$\|f\|_2 = \lim_{r \to 1} M_2(f, r). \tag{3.7}$$

The $L^2(\partial\,\mathbb{D})$ space is the space of functions g on the unit circle $\partial\,\mathbb{D}$ for which the following norm

$$\|g\| = \left\{ \frac{1}{2\pi} \int_{-\pi}^{\pi} \left| g\left(e^{\mathrm{i}\,\omega}\right) \right|^2 d\omega \right\}^{\frac{1}{2}}$$

is bounded.

In the followings useful theorems are summarized regarding $H^2(\mathbb{D})$ (see [51]).

- If $f \in H^2(\mathbb{D})$ then f has radial limits $f^*(e^{i\omega})$ at almost all points of $\partial\,\mathbb{D}$.
- $f^* \in L^2(\partial\,\mathbb{D})$.
- The mapping $f \to f^*$ is an isometry of $H^2(\mathbb{D})$ onto the subspace of $L^2(\partial\,\mathbb{D})$.
- Let $f, g \in H^2(\mathbb{D})$ and the inner product in $H^2(\mathbb{D})$ is defined by

$$\langle f, g \rangle = \frac{1}{2\pi} \int_{-\pi}^{\pi} f^*\left(e^{i\omega}\right) \overline{g^*\left(e^{i\omega}\right)} d\omega, \tag{3.8}$$

then the $H^2(\mathbb{D})$ space is a Hilbert space equipped with the above described inner product.

Every $F(z) \in H^2(\mathbb{D})$ under investigation is a strictly proper rational transfer function that do not have zeros on the unit circle. In this case the followings are true (see [16]):

- The radial limits $f^*(e^{i\omega})$ of $f \in H^2(\mathbb{D})$ are equal to $f(e^{i\omega})$.
- The inner product among these functions can be expressed as:

$$\langle f, g\rangle = \frac{1}{2\pi}\int_{-\pi}^{\pi} f\left(e^{i\omega}\right)\overline{g\left(e^{i\omega}\right)}d\omega \quad and$$
$$\langle f, g\rangle = \frac{1}{2\pi\,\mathrm{i}}\oint_{\mathbb{T}} f(z)\overline{g\left(\frac{1}{\bar{z}}\right)}\frac{dz}{z} \tag{3.9}$$

Note that the there is an orthogonal complement of H^2 in L^2 and it is denoted by $H^2_\perp$. In short $H^2_\perp$ is the set of all functions that is analytic inside the unit circle plate $\mathbb{D}$ and has a finite norm. From engineering point of view the H^2 space is more important since the convention is that a discrete stable LTI systems have their poles inside the unit circle.

3.3 The discrete Laguerre-system

The discrete Laguerre system based upon parameter b ($b \in \mathbb{D}$) is defined as:

$$\Phi_n(z) = \frac{\sqrt{1-|b|^2}}{1-\overline{b}\,z}\,B_b^n(z) \quad (n = 0, 1, 2\ldots), \tag{3.10}$$

where

$$B_b(z) = e^{\mathrm{i}\delta}\frac{z-b}{1-\overline{b}\,z}$$

is the Blaschke function with the arbitrary constant $\delta \in [0, 2\pi)$.

It is well known – see [52] – that the discrete Laguerre system forms an orthonormal basis in the Hardy space $\mathrm{H}^2(\mathbb{D})$. Any function $F \in \mathrm{H}^2(\mathbb{D})$ can be expressed by the representation:

$$F(z) = \sum_{n=0}^{\infty} l_n \Phi_n(z), \tag{3.11}$$

where the coefficients $\{l_n\}$ – the so-called Laguerre coefficients – can be computed by using the inner-product belonging to the space $\mathrm{H}^2(\mathbb{D})$ as:

$$l_n = \langle F, \Phi_n\rangle.$$

By substituting the expression of the Blaschke function in (3.10) by selecting 0 for the value of

the arbitrary parameter δ, the elements of the Laguerre system get the form

$$\Phi_n(z) = \sqrt{1-|b|^2}\,\frac{(z-b)^n}{(1-\overline{b}\,z)^{n+1}} \quad (n = 0, 1, 2\dots)$$

The representation of any function $F \in \mathrm{H}^2(\mathbb{D})$ can be expressed on the basis of an orthogonal projection upon the Laguerre system components, i.e. the representation coefficients can be expressed as:

$$\begin{aligned} l_n &= \left\langle F(z), \sqrt{1-|b|^2}\,\frac{(z-b)^n}{(1-\overline{b}\,z)^{n+1}} \right\rangle = \\ &= \frac{\sqrt{1-|b|^2}}{2\pi}\int_{-\pi}^{\pi} F(e^{\mathrm{i}t})\frac{(e^{-\mathrm{i}t}-\overline{b})^n}{(1-b\,e^{-\mathrm{i}t})^{n+1}}\,dt = \\ &= \frac{\sqrt{1-|b|^2}}{2\pi}\int_{-\pi}^{\pi} F(e^{\mathrm{i}t})\frac{(1-\overline{b}e^{\mathrm{i}t})^n}{(e^{\mathrm{i}t}-b)^{n+1}}e^{\mathrm{i}t}\,dt \end{aligned}$$

Rewriting this form into a complex contour integral upon the unit circle, i.e. by applying the substitution $z = e^{\mathrm{i}t}$ and considering $\mathbb{T} := \{z \in \mathbb{C} : |z| = 1\}$,

$$\begin{aligned} l_n &= \frac{\sqrt{1-|b|^2}}{2\pi\mathrm{i}}\oint_{\mathbb{T}} F(z)\frac{(1-\overline{b}z)^n}{(z-b)^{n+1}}\,dz = \\ &= \sqrt{1-|b|^2}\,\frac{1}{2\pi\mathrm{i}}\oint_{\mathbb{T}} F(z)(1-\overline{b}z)^n\frac{dz}{(z-b)^{n+1}}. \end{aligned} \tag{3.12}$$

According to Cauchy's integral formula the Laguerre coefficients can be expressed in the form

$$l_n = \frac{\sqrt{1-|b|^2}}{n!}\left[\frac{d^n(1-\overline{b}z)^n F(z)}{dz^n}\right]_{z=b} \tag{3.13}$$
$$(n = 0, 1, 2\dots)$$

Chapter 4

Investigation of the correspondence between hyperbolic geometry and LTI system analysis

4.1 Introduction

The connection between hyperbolic geometry and linear time invariant systems is not obvious, these two fields seem to be distinct from each other. As an introduction a simple example is presented.

Consider a nominal second order, strictly proper SISO discrete transfer function $H_N(z)$ with the complex eigenvalue pair $0.9e^{\pm i\frac{\pi}{8}}$ inside the unit disk. Take the perturbed systems $H_1(z)$ and $H_2(z)$ with the poles $0.99e^{\pm i\frac{\pi}{8}}$ and $0.81e^{\pm i\frac{\pi}{8}}$ respectively. Set the static gain of each system equal to 1 and compare their time-domain behaviors.The result is plotted in Fig. 4.1. In this example the euclidean distance between the corresponding poles of the nominal and $H_1(z)$, $H_2(z)$ equals, it is 0.09. Their time domain behavior greatly differ from each other so it is clear that the euclidean distance does not capture the dynamic behavior of these systems. The hyperbolic distance of the corresponding poles respect to $H_N(z)$ and $H_1(z)$ is 2.3489 and respect to $H_N(z)$ and $H_2(z)$ it is 0.6904. The hyperbolic distances between the poles suggest that the hyperbolic metric is more suitable for comparing dynamic behavior based only on pole locations.

The hyperbolic distance has another important feature that it is meaningless if one compares stable poles with unstable poles which is coherent with the expectations. This feature does not hold for Euclidean distance. On the other hand, measuring the hyperbolic distance between unstable poles is possible since one can transform them with the transformation $\hat{p} = 1/\overline{p}$ where $\hat{p}$ is the transformed pole and bar means complex conjugate.

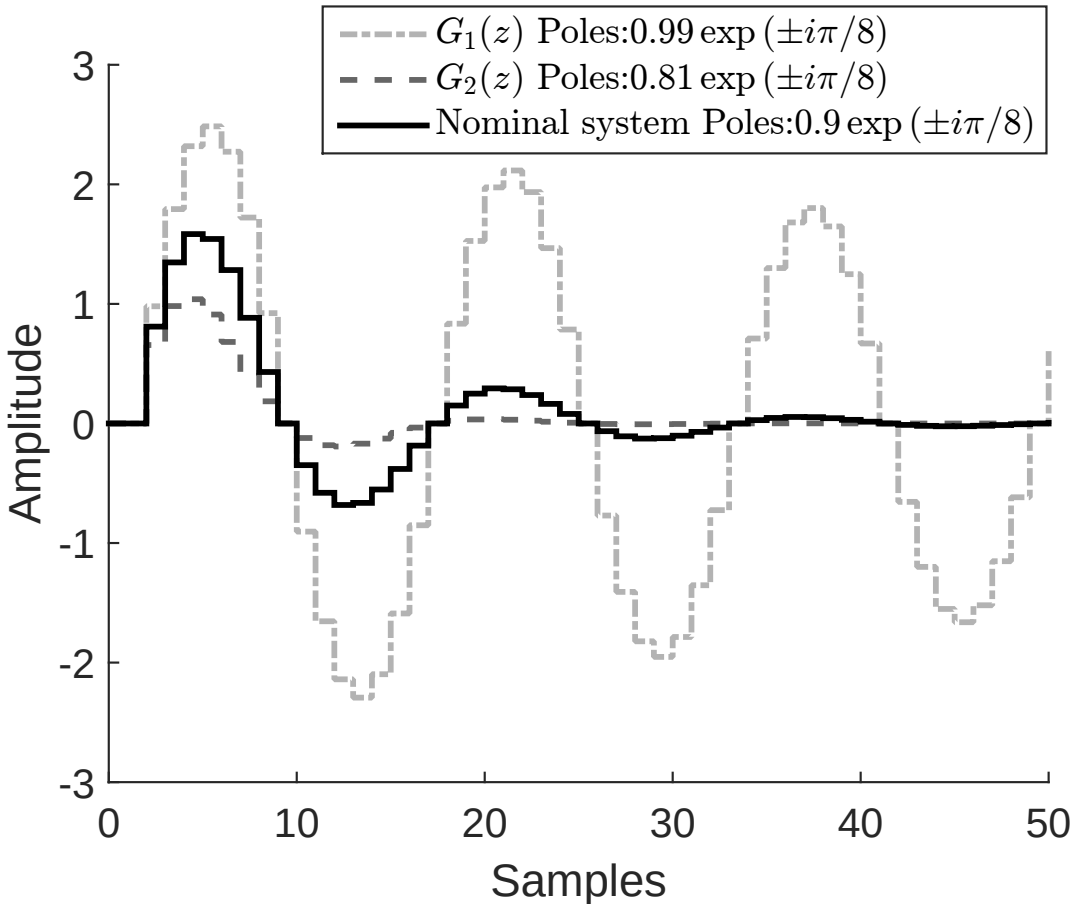

Figure 4.1: Impulse responses of $H_1(z)$, $H_2(z)$ and $H_N(z)$ systems

Special properties of Laguerre series expansion

The introductory example above motivates why a non-Euclidean geometry is natural when one compares discrete-time dynamics through pole locations within the unit disk the pseudo-hyperbolic (and hence hyperbolic) metric reflects stability-related distortions and provides a more meaningful notion of "closeness" than the Euclidean distance. In the sequel we make this connection more explicit from a representation point of view.

In particular, we consider the Laguerre series expansion, an orthonormal basis expansion on the Hardy space $H^2(\mathbb{D})$ that is widely used for approximating stable discrete-time LTI systems. The basis depends on a free parameter $b \in \mathbb{D}$ (the Laguerre parameter), and the practical performance of the expansion is governed by its rate of convergence. This section shows that for a first-order discrete LTI system the convergence factor is exactly the pseudo-hyperbolic distance between the Laguerre parameter and the corresponding pole. Similar derivations can be found in the literature: in [2] equivalence in the Hardy space $H^2_\perp$ is proven, while in [16] only real poles are considered. The present derivation is carried out in the H^2 Hardy space which is important from the engineering point of view. Furthermore, it is not limited to real poles.

4.1 Introduction

In the following the convergence factor is precisely defined for orthogonal series expansion of functions in H^2.

Convergence factor

The unit pulse response $g(t)$ of a stable casual LTI system can be expressed in an orthonormal series expansion as:

$$g(t) = \sum_{k=1}^{\infty} c_k f_k(t), \tag{4.1}$$

where $f_k(t)$ is the k-th element of an orthonormal basis and c_k is the k-th coefficient. In practical applications all the elements of the series expansion can not be used so $g(t)$ is approximated by the first n elements of the series expansion. Let $g(t;n)$ be the approximation of $g(t)$ of order n. The error of this approximation is

$$\epsilon_g(t;n) = g(t;n) - g(t). \tag{4.2}$$

The convergence factor describes the rate of convergence for the series expansion. Under exponential approximation error one can write,

$$\left\|\epsilon_g(t;n+k)\right\| \approx \rho^k \left\|\epsilon_g(t;n)\right\| \tag{4.3}$$

where ρ is the convergence factor ($0 \leq \rho < 1$).

Derivation of the convergence factor of the Laguerre series expansion

The Laguerre basis on $H^2(\mathbb{D})$ is defined by the following basis functions:

$$\Phi_n(z) = \frac{\sqrt{1-|b|^2}}{z-b}\left(\frac{1-\bar{b}z}{z-b}\right)^n \quad n = 0, 1, 2\ldots$$
$$b \in \mathbb{D};\ b \neq 0 \tag{4.4}$$

Let $F(z) \in H^2(\mathbb{D})$ be a strictly proper rational function that is analytic outside the unit circle and has no pole on the unit circle. Then compute the n-th Laguerre coefficient l_n of $F(z)$ as:

$$l_n = \langle \Phi_n(z), F(z) \rangle = \frac{1}{2\pi \mathrm{i}} \oint_{\mathbb{T}} \Phi_n(z) \overline{F\left(\frac{1}{\bar{z}}\right)} \frac{dz}{z} =$$
$$= \frac{\sqrt{1-|b|^2}}{2\pi \mathrm{i}} \oint_{|z-b|=\epsilon} \frac{(1-\bar{b}z)^n \overline{F\left(\frac{1}{\bar{z}}\right)} \frac{1}{z}}{(z-b)^{n+1}} dz +$$
$$+ \frac{1}{2\pi \mathrm{i}} \oint_{|z|=\epsilon} \frac{\frac{(1-\bar{b}z)^n}{(z-b)^{n+1}} \overline{F\left(\frac{1}{\bar{z}}\right)}}{z} dz \tag{4.5}$$

where $0 < \epsilon < |b|$.

Applying the Cauchy integral formulas to (4.5) the Laguerre coefficients are rewritten as:

$$l_n = \left[\frac{\sqrt{1-|b|^2}}{n!} \frac{d^n}{dz^n} \left(\frac{1}{z} (1-\bar{b}z)^n \overline{F\left(\frac{1}{\bar{z}}\right)} \right) \right]_{z=b} +$$
$$+ \left[\sqrt{1-|b|^2} \frac{(1-\bar{b}z)^n}{(z-b)^{n+1}} \overline{F\left(\frac{1}{\bar{z}}\right)} \right]_{z=0} \tag{4.6}$$

At this point we restrict ourselves for stable, first-order transfer functions, in the following form:

$$F(z) = \frac{A}{z-a} \tag{4.7}$$
$$\overline{F\left(\frac{1}{\bar{z}}\right)} = \frac{Az}{1-\bar{a}z} \tag{4.8}$$

where $a \in \mathbb{D}$. When substituting (4.7) and (4.8) into (4.6), the Laguerre coefficients for the given $F(z)$ are computed as follows:

$$l_n = \left[\frac{A\sqrt{1-|b|^2}}{n!} \frac{d^n}{dz^n} \left(\frac{(1-\bar{b}z)^n}{1-\bar{a}z} \right) \right]_{z=b} +$$
$$+ \left[\sqrt{1-|b|^2} \frac{(1-\bar{b}z)^n}{(z-b)^{n+1}} \frac{Az}{1-\bar{a}z} \right]_{z=0} \tag{4.9}$$

It is obvious that the second term of (4.9) is zero, therefore the Laguerre coefficients of (4.7)

are:

$$l_n = \left[\frac{A\sqrt{1-|b|^2}}{n!} \frac{d^n}{dz^n} \left(\frac{\left(1-\bar{b}z\right)^n}{1-\bar{a}z} \right) \right]_{z=b} . \tag{4.10}$$

In order to calculate l_n the n-th derivative of

$$\frac{\left(1-\bar{b}z\right)^n}{1-\bar{a}z} = \left(1-\bar{b}z\right)^n (1-\bar{a}z)^{-1} \tag{4.11}$$

has to be computed, for which the generalized Leibniz rule can be applied. Let u and v be two n-times differentiable functions, then:

$$(uv)^{(n)} = \sum_{k=0}^{n} \binom{n}{k} u^{(n-k)} v^{(k)} \tag{4.12}$$

Applying (4.12) for (4.11), we get:

$$\begin{aligned} u^{(n-k)} &= \left(\left(1-\bar{b}z\right)^n\right)^{(n-k)} = \\ &= (-1)^{n-k} (n-k)! \binom{n}{n-k} \left(1-\bar{b}z\right)^k \left(\bar{b}\right)^{n-k} \\ v^{(k)} &= \left((1-\bar{a}z)^{-1}\right)^{(k)} = k! (1-\bar{a}z)^{-1-k} (\overline{a})^k \end{aligned} \tag{4.13}$$

Notice that:

$$(n-k)! \binom{n}{n-k} = \frac{n!}{k!},$$

so equation (4.12) takes the following form:

$$\begin{aligned} &(uv)^{(n)} = \\ &\sum_{k=0}^{n} \binom{n}{k} (-1)^{n-k} \frac{n!}{k!} \left(1-\bar{b}z\right)^k \left(\bar{b}\right)^{n-k} k! (1-\bar{a}z)^{-1-k} (\overline{a})^k \end{aligned} \tag{4.14}$$

After some algebraic manipulation the binomial theorem can be applied to get:

$$(uv)^{(n)} = \frac{n!}{(1-\bar{a}z)^{n+1}} K(z) \tag{4.15}$$

where

$$K(z)=\sum_{k=0}^{n}\binom{n}{k}(-1)^{n-k}\left(\bar{b}\right)^{n-k}(1-\bar{a}z)^{n-k}\left(\overline{a}\right)^{k}\left(1-\bar{b}z\right)^{k}=$$
$$=\left(\bar{a}\left(1-\bar{b}z\right)-\bar{b}\left(1-\bar{a}z\right)\right)^{n}=\left(\bar{a}-\bar{b}\right)^{n}. \tag{4.16}$$

Therefore, we arrive to the following formula:

$$(uv)^{(n)}=\frac{n!\left(\bar{a}-\bar{b}\right)^{n}}{(1-\bar{a}z)^{n+1}} \tag{4.17}$$

Consequently, the Laguerre coefficients (4.10) are:

$$l_n=\left[\frac{A\sqrt{1-|b|^2}}{n!}\frac{n!\left(\bar{a}-\bar{b}\right)^{n}}{(1-\bar{a}z)^{n+1}}\right]_{z=b}=$$
$$=\frac{A\sqrt{1-|b|^2}}{1-\bar{a}b}\frac{\left(\bar{a}-\bar{b}\right)^{n}}{(1-\bar{a}b)^{n}}. \tag{4.18}$$

From (4.18) it is obvious that the convergence factor ρ of $F(z)$ is

$$\rho=\frac{\left|\bar{a}-\bar{b}\right|}{|1-\bar{a}b|}=\frac{|a-b|}{|1-\bar{a}b|} \tag{4.19}$$

which is equal to the pseudo-hyperbolic distance between a and b in (3.3). It is worth to mention that this result is true in more general cases. If $F(z)$ has a partial fractional representation and every pole is distinct and stable, the contribution of each partial fraction to the series expansion has the form of (4.18). For large n the convergence factor of $F(z)$ is obviously equal to the convergence factor of the term in partial fractional representation whose convergence factor is the largest.

4.2 Relation of ν-gap metric with hyperbolic geometry

In this section two preliminary results are presented on the correspondence of H_∞ norm and ν-gap metric with hyperbolic distance.

Theorem 4.2.1. *Let $P_1(s)$ and $P_2(s)$ be two first order continuous time LTI SISO systems and let $H_1(z)$ and $H_2(z)$ be the discrete zero-order hold equivalent of $P_1(s)$, $P_2(s)$. Then if the static gains are equal to* 1 *and the sampling time is approaching zero:*

4.2 Relation of ν-gap metric with hyperbolic geometry

- *the ν-gap metric of continuous systems and the pseudo-hyperbolic distance of the poles of the discrete systems are equivalent metrics*
- *the H_∞ norm of the difference of the continuous systems and the pseudo-hyperbolic distance of the poles of the discrete systems are equivalent*

Proof. Let the system be a first order LTI system in the form:

$$P(s) = \frac{A}{s+b}. \tag{4.20}$$

The normalized right graph symbol of $P(s)$ is

$$G_r = \begin{bmatrix} N(s) \\ D(s) \end{bmatrix} = \begin{bmatrix} \frac{-A}{s+\sqrt{A^2+b^2}} \\ \frac{-s-b}{s+\sqrt{A^2+b^2}} \end{bmatrix}. \tag{4.21}$$

In order to see that $N(s)$ and $D(s)$ in (4.21) are the co-prime factorization of (4.20) we write:

$$P(s) = ND^{-1} = \frac{-A}{s+\sqrt{A^2+b^2}} \frac{s+\sqrt{A^2+b^2}}{-s-b} = \frac{A}{s+b}, \tag{4.22}$$

Furthermore, to see that (4.21) is normalized it has to satisfy the following Bezout identity:

$$N^*N + D^*D = I \tag{4.23}$$

where $N(s)^* = N(-s)^T$ and $D(s)^* = D(-s)^T$. Substitute (4.21) in (4.23):

$$\begin{aligned} &\frac{-A}{-s+\sqrt{A^2+b^2}} \frac{-A}{s+\sqrt{A^2+b^2}} + \frac{s-b}{-s+\sqrt{A^2+b^2}} \frac{-s-b}{s+\sqrt{A^2+b^2}} = \\ &= \frac{A^2}{A^2+b^2-s^2} + \frac{b^2-s^2}{A^2+b^2-s^2} = \frac{A^2+b^2-s^2}{A^2+b^2-s^2} = 1 \end{aligned}$$

so one can conclude that (4.21) is the normalized right graph symbol of $P(s)$. The same argument can be applied to the left normalized graph symbol that is:

$$G_l = \begin{bmatrix} -D(s) & N(s) \end{bmatrix} = \begin{bmatrix} \frac{s+b}{s+\sqrt{A^2+b^2}} & \frac{-A}{s+\sqrt{A^2+b^2}} \end{bmatrix}. \tag{4.24}$$

Now we are at the position to compute the ν-gap between two stable systems $P_1(s)$ and $P_2(s)$,

by using the corresponding co-prime factorizations. The definition of ν-gap metric (see [53]) is

$$\delta_\nu(P_1, P_2) = \begin{cases} \|G_{l2}G_{r1}\|_\infty & \text{if } det(G_{r2}^* G_{r1})(j\omega) \neq 0 \\ & \forall \omega \in (-\infty, \infty) \\ & \text{and winding number of} \\ & det(G_{r2}^* G_{r1}) = 0 \\ 1 & \text{otherwise} \end{cases} \tag{4.25}$$

Now, substitute the first order dynamics of $P_1(s)$ and $P_2(s)$ into (4.25) using (4.21) and (4.24)

$$\delta_\nu(P_1, P_2) = \left\| \begin{bmatrix} \frac{s+b_2}{s+\sqrt{A_2^2+b_2^2}} & \frac{-A_2}{s+\sqrt{A_2^2+b_2^2}} \end{bmatrix} \begin{bmatrix} \frac{-A_1}{s+\sqrt{A_1^2+b_1^2}} \\ \frac{-s-b_1}{s+\sqrt{A_1^2+b_1^2}} \end{bmatrix} \right\|_\infty = \left\| \frac{(A_2-A_1)s+(A_2b_1-A_1b_2)}{s^2+(c_1+c_2)s+c_1c_2} \right\|_\infty \tag{4.26}$$

where $c_1 = \sqrt{A_1^2 + b_1^2}$ and $c_2 = \sqrt{A_2^2 + b_2^2}$.

Let $A_1 = b_1 = d_1$ and $A_2 = b_2 = d_2$ in order to set the static gain to one and substitute in (4.26):

$$\delta_\nu(P_1, P_2) = \left\| \frac{(A_2-A_1)s+(A_2b_1-A_1b_2)}{s^2+(c_1+c_2)s+c_1c_2} \right\|_\infty = \left\| \frac{(d_2-d_1)s}{s^2+\sqrt{2}(d_1+d_2)s+2d_1d_2} \right\|_\infty \tag{4.27}$$

From the definition of H_∞ norm it follows that:

$$\left\| \frac{(d_2-d_1)s}{s^2+\sqrt{2}(d_1+d_2)s+2d_1d_2} \right\|_\infty = \max_\omega \left| \frac{(d_2-d_1)i\omega}{-\omega^2+\sqrt{2}(d_1+d_2)i\omega+2d_1d_2} \right| \tag{4.28}$$

In (4.28) the transfer function has two real poles, which can be shown by simply solving the quadratic formula to obtain:

$$p_{1,2} = \frac{-\sqrt{2}(d_1+d_2) \pm \sqrt{2(d_1+d_2)^2 - 8d_1d_2}}{2} =$$
$$\frac{-\sqrt{2}(d_1+d_2) \pm \sqrt{2d_1^2 + 4d_1d_2 + 2d_2^2 - 8d_1d_2}}{2} =$$
$$\frac{-\sqrt{2}(d_1+d_2) \pm \sqrt{2d_1^2 - 4d_1d_2 + 2d_2^2}}{2} = \frac{-\sqrt{2}(d_1+d_2) \pm \sqrt{2(d_1-d_2)^2}}{2} =$$
$$\frac{-\sqrt{2}(d_1+d_2) \pm \sqrt{2}(d_1-d_2)}{2} = \begin{cases} -\sqrt{2}d_1 \\ -\sqrt{2}d_2 \end{cases}$$

I.e. the Bode magnitude plot has exactly one global maximum for positive ω and there is no

local minimum or inflection point.

The calculation of the maximum in (4.28) is a long and standard process, therefore only the basic steps are outlined here. Let the frequency function of (4.28) be denoted by $M(\omega)$.

1. Calculate the absolute value of $M(\omega)$.
   (a) Expand $M(\omega)$ by the complex conjugate of its denominator.
   (b) Separate the real and imaginary parts.
   (c) Calculate $\sqrt{Re(M(\omega))^2 + Im(M(\omega))^2}$
2. Since the square root is monotonic, $H(\omega) = |M(\omega)|^2$ can be used, without loss of generality.
3. Calculate the ω derivative of $H(\omega)$.
4. Since the transfer function of equation (4.28) has two real poles, it is sufficient to use the equation $\frac{dH(\omega)}{d\omega} = 0$ for the correct result.

The final result is

$$\delta_\nu(P_1, P_2) = \frac{1}{\sqrt{2}} \left| \frac{d_2 - d_1}{d_1 + d_2} \right| = \left| \frac{1}{\sqrt{2}} \frac{b_2 - b_1}{b_1 + b_2} \right| \tag{4.29}$$

where we applied $d_1 = b_1$ and $d_2 = b_2$.

To see the correlation of (4.29) with the hyperbolic distance, we substitute the discrete poles of the system in the formula of the pseudo-hyperbolic distance in eq. (3.3). In order to connect the discrete representation with the continuous one we investigate the limit of the distance with sampling time T approaching zero. Hence:

$$\left| \lim_{T \to 0} \frac{e^{b_1 T} - e^{b_2 T}}{1 - e^{b_1 T} e^{b_2 T}} \right| = \left| \lim_{T \to 0} \frac{b_1 e^{b_1 T} - b_2 e^{b_2 T}}{-(b_1 + b_2) e^{(b_1 + b_2) T}} \right| = \left| \frac{b_2 - b_1}{b_1 + b_2} \right| \tag{4.30}$$

When comparing (4.29) and (4.30) it can be seen that the only difference between the ν-gap metric and the pseudo hyperbolic distance is the scalar coefficient $\frac{1}{\sqrt{2}}$.

4.3 Relation of H_∞ norm with hyperbolic geometry

Similar argument can be applied to the correspondence of the H_∞ norm and pseudo hyperbolic distance. In order to see this, we compute the H_∞ norm of the difference of the stable systems $P_1(s)$ and $P_2(s)$ as:

$$\left\| \frac{A_1}{s + b_1} - \frac{A_2}{s + b_2} \right\|_\infty = \left\| \frac{(A_2 - A_1)s + (A_2 b_1 - A_1 b_2)}{s^2 + (b_1 + b_2)s + b_1 b_2} \right\|_\infty \tag{4.31}$$

Again, let $A_1 = b_1 = d_1$ and $A_2 = b_2 = d_2$ then we get:

$$\left\| \frac{A_1}{s+b_1} - \frac{A_2}{s+b_2} \right\|_\infty = \left\| \frac{(d_2 - d_1)s}{s^2 + (d_1+d_2)s + d_1 d_2} \right\|_\infty \tag{4.32}$$

Note that, the obtained formula has the same structure as equation (4.27), hence the same reasoning can be applied. The final result is:

$$\left\| \frac{A_1}{s+b_1} - \frac{A_2}{s+b_2} \right\|_\infty = \left| \frac{b_2 - b_1}{b_1 + b_2} \right| \tag{4.33}$$

Therefore, it can be concluded from (4.33) and (4.30) that the H_∞ norm of the difference of $P_1(s)$, $P_2(s)$ is equivalent with the pseudo hyperbolic distance as the sample time approaches zero. □

4.4 Numerical example

Let $P_1(s)$ and $P_2(s)$ be two continuous time LTI SISO systems with the transfer function:

$$P_1(s) = \frac{0.3}{s+0.3}, \quad P_2(s) = \frac{p}{s+p} \tag{4.34}$$

where the pole p is the element of the interval $[0.01, 1]$.
Compute the

- H_∞ norm of $\|P_1(s) - P_2(s)\|_\infty$
- $\nu - gap$ metric times $\sqrt{2}$ of $P_1(s)$, $P_2(s)$
- pseudo-hyperbolic distance of the zero-order-hold equvivalent of the poles -0.3 and $-p$

for the whole interval of p with different sample time. The following figures show the results.

4.4 Numerical example

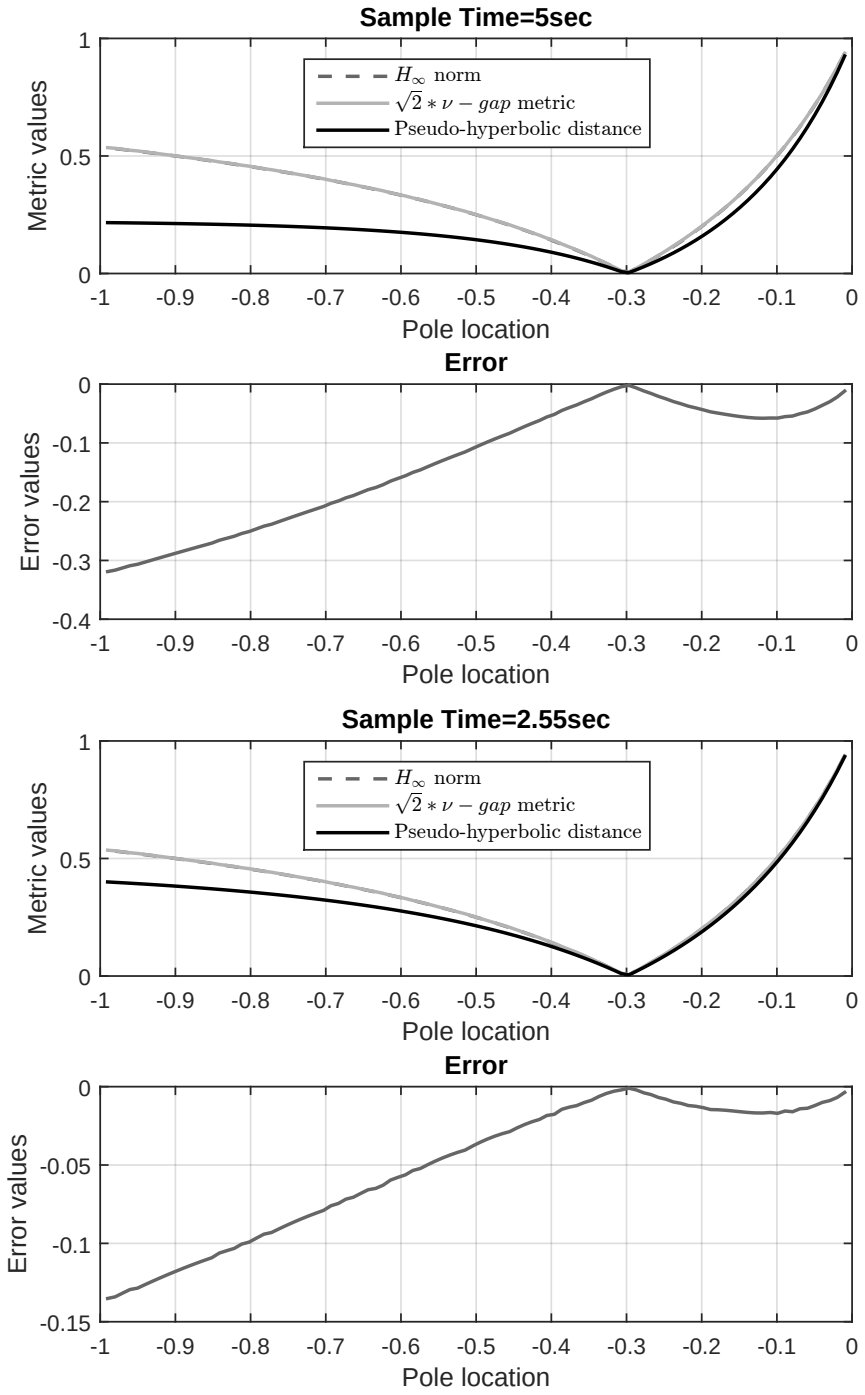

The figures clearly show that as the sample time is approaching zero the pseudo-hyperbolic distance becomes exactly the same quantity as H_∞ norm or $\nu - gap$ metric if the discussed assumptions hold. The H_∞ norm and the $sqrt2 * \nu - gap$ metric are the top of each other as expected. The error is calculated with respect to $sqrt2 * \nu - gap$. In the third figure, where the sample time is 0.1 sec, the error is due to the numeric error.

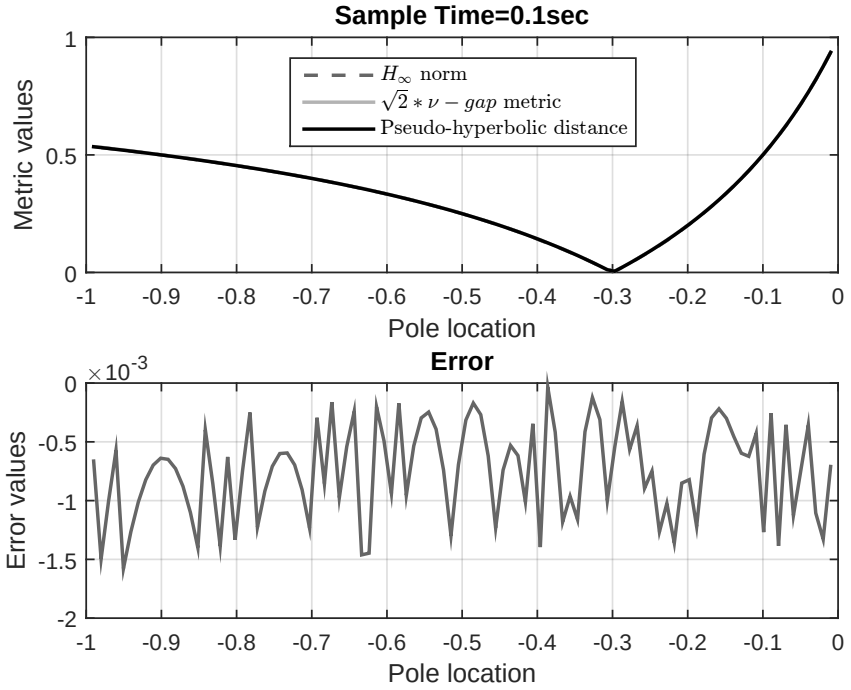

4.5 Application in reduction of linear parameter varying system

4.5.1 Introduction

The discovered connection can be viewed as the hyperbolic distance representing dynamic similarities from a specific point of view between two first order systems. In higher order systems the connection between the hyperbolic distance and the dynamic similarities can be exploited if two systems are compared pole-by-pole. So for example a linear parameter varying (LPV) system can be examined at two distinct frozen parameter values and the systems at those distinct parameter values can be compared pole-by-pole based on hyperbolic distance. More details about LPV systems can be found in [54], [55], [56]. In the following a summary is given about the application of hyperbolic distance in LPV reduction framework that was published in [LPG+17] [GLP+16].

4.5.2 Problem formulation

A continuous-time LPV system can be given in a state-space form as follows

$$G(\rho): \begin{array}{c} \dot{x}(t) = A(\rho(t))x(t) + B(\rho(t))u(t) \\ y(t) = C(\rho(t))x(t) + D(\rho(t))u(t), \end{array} \tag{4.35}$$

where $\rho : \mathbb{R}_+ \to \mathbb{R}$ denotes the time varying scalar scheduling parameter, $x : \mathbb{R}_+ \to \mathbb{R}^{n_x}$, $u : \mathbb{R}_+ \to \mathbb{R}^{n_u}$ and $y : \mathbb{R}_+ \to \mathbb{R}^{n_y}$, are respectively the state, input and output. The matrix functions $A : \mathbb{R} \to \mathbb{R}^{n_x \times n_x}$, $B : \mathbb{R} \to \mathbb{R}^{n_x \times n_u}$, $C : \mathbb{R} \to \mathbb{R}^{n_y \times n_x}$, $D : \mathbb{R} \to \mathbb{R}^{n_y \times n_u}$ are continuous functions of ρ. We assume that both ρ, $\dot{\rho}$ and $\ddot{\rho}$ are bounded.

In order to perform the numerical computations, the LPV system (4.35) is evaluated over a parameter grid $\Gamma = \{\rho_1 = \rho_{min}, \rho_2, \ldots, \rho_N = \rho_{max}\}$, $\rho_1 < \rho_2 < \ldots < \rho_N$ and the set of LTI systems, obtained at the grid points. This grid-based representation is often directly generated by trimming a nonlinear system at different operating points [57].

The aim of the model reduction is to find $G_{red}(\rho, \dot{\rho}, \{\ddot{\rho}\})$ of order $n_x^{red} \ll n_x$ to be used for designing a model based controller for (4.35). Therefore, the input-output behavior of the full order model has to be preserved as much as possible.

4.5.3 Summary of the reduction algorithm

The proposed model reduction algorithm is based on a similar representation as modal description but this is applied for LPV systems. The modal form for LTI systems can be represented by the block-diagonal structure of the system matrix in state space form, where each block corresponds to an eigenvalue. In order to extend this idea for the LPV system, a diagonalizable system matrix is necessary. So as a firs step the eigendecomposition of the sequence of matrices is computed. The result are the eigenvalues and eigenvectors at every gridpoint. After this point the problem is that the correspondence of the eigenvalues are not assured and one has to reconstruct the correct ordering of the eigenvalues over the parameter domain. For this purpose, a graph-theoretic solution is proposed in [GLP+16]. The problem is reformulated as a minimum cost perfect-matching problem over bipartite graphs (see [58], [59]) using pseudo-hyperbolic metric between the eigenvalues. At this point the usage of pseudo-hyperbolic metric is adequate because only one eigenvalue is compared to an other one, therefore, from the discussion above it follows that it carries information about the dynamic similarities.

The next step is to ensure smooth interpolation of the resulting system over the entire parameter domain. For this it is necessary to correct the eigenvector systems since the parameter-varying eigenspace can contain arbitrary sign changes. The problem is translated into a complex Procrustes-problem (see [60], [61], [62]) that generates an optimal transformation using Frobenius norm which renders the eigenvectors as close to each other as possible.

After smoothing, the states are grouped into smaller sets by using hierarchical clustering ([63], [64]). The main idea is to divide the system into smaller subsystems by selecting dynamically similar modes together then this smaller set can be reduced as an LPV system. For this purpose, a similarity measure is defined to compare parameter-varying modes by using the pseudo-hyperbolic metric [GLP+16]. At each step of the clustering, those two data objects are

merged, where the distance is the smallest. This is repeated until all modes are merged into a single cluster.

For each subsystem, a quadratic controllability and observability Gramians are computed respectively. The corresponding Lyapunov inequalities are constructed as finite number of LMI constraints by gridding over the admissible parameter domain. The proposed iterative optimization is solved in [65] where the parameter-varying singular values, along with the balancing transformations, are constructed. The parameter-varying transformation introduces an affine dependency in the reduced blocks.

4.6 Conclusion

As it is demonstrated, hyperbolic geometry has intrinsic relations with LTI system theory that can be seen from the presented fact that for a special setup some important quantities in control engineering are identical with the hyperbolic distance. More precisely we can take $P_1(s)$ and $P_2(s)$ as two first order continuous time LTI SISO systems and $H_1(z)$ and $H_2(z)$ as the discrete zero-order-hold equivalent of $P_1(s)$, $P_2(s)$. If we set the static gains equal to 1 and if the sampling time approaches zero, the ν-gap metric of continuous systems and the H_∞ norm of the difference of the continuous systems become equivalent metrics to the pseudo-hyperbolic distance of the poles of the discrete systems.

This finding offers a technique to analyze dynamic similarities between poles that essentially determines the dynamics of a LTI system based on a geometric approach. As it is presented, pole based comparison between LTI systems can be applied for LPV model reduction.

The fact that the hyperbolic distance takes two complex numbers as an input parameter seems to constrain the technique to pole-by-pole comparison but as the intuitive example in section 4.1 suggests the method may work on higher order systems but this extension requires further investigation in the future.

New scientific results:

Thesis 1. *Let $P_1(s)$ and $P_2(s)$ are two first order continuous time LTI SISO systems and let $G_1(z)$ and $G_2(z)$ are the discrete zero-order hold equivalent of $P_1(s)$, $P_2(s)$ with an appropriate sampling time. Then, if the static gains are equal to one and the sampling time is approaching zero:*

- *the ν-gap metric of continuous systems and the pseudo-hyperbolic distance of the poles of the discrete systems are equivalent metrics*

4.6 Conclusion

- *the H_∞ norm of the difference of the continuous systems and the pseudo-hyperbolic distance of the poles of the discrete systems are equivalent*

Corresponding publications: [GPLS17]

Chapter 5

Parametric LTI interpolation based on hyperbolic lines

5.1 Introduction

Ordinary differential equations are a powerful tool for modeling dynamic systems. However, accurate models often involve a large number of equations, primarily aiding in understanding complex physical phenomena. When used for simulation, control design, or vibration optimization, these models can be computationally inefficient, demanding significant execution time and memory. To overcome this challenge, model order reduction techniques have been developed, creating reduced-order models that approximate the input-output behavior of large-scale systems with far fewer equations. Additionally, in engineering applications, system dynamics often depend on parameters such as material properties, geometry, or configuration. In such cases, parametric model order reduction (pMOR) [5] is necessary to account for these variations efficiently.

Generating and reducing large-scale models can be highly resource-intensive. For instance, a complex computational fluid dynamics (CFD) simulation [66, 67] may take days to evaluate at a single value of the parameter. Similarly, optimizing a mechanical structure for vibration using the finite element method (FEM) often requires model evaluations at every step, even for systems with thousands of states. The primary objective of pMOR is to generate a reduced model that remains accurate for any parameter value, eliminating the need to repeat the modeling and reduction process.

Typically, high-dimensional models that depend on parameters are only available at specific parameter values. As a result, most pMOR techniques leverage interpolation. The general approach of interpolation-based methods follows a two-step process: first, the high-dimensional models at selected parameter values are reduced independently. Then, reduced models for other

parameter values are generated through interpolation using the existing reduced models ([6,7]); see Figure 5.1.

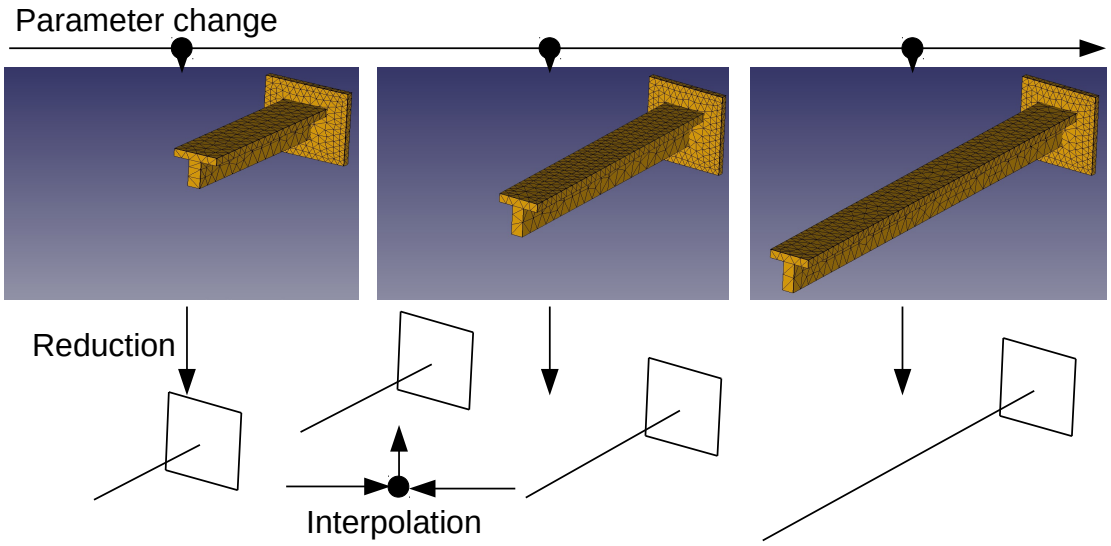

Figure 5.1: Basic process of pMOR

The figure represents a cantilever beam with varying lengths, treated as a parametric system. In this setup, reduced-order models are generated for different beam lengths. Once these reduced models are obtained, interpolation is performed between them to efficiently approximate the system's behavior for new, unseen lengths—without needing to run a full simulation each time.

Because the behavior of the complex system at the desired parameter value is not directly known, additional prior information must be integrated into the interpolation algorithm. This ensures that the interpolated models closely capture the original behavior of the system beyond the initially available models. For instance, if the original system is known to be stable across the entire valid parameter domain, the interpolated system should also maintain stability.

Another crucial aspect is ensuring that the interpolated model behaves similarly to the original high-order system. Since interpolation relies on information from a given set of reduced models, the parameter domain must be sampled densely enough to capture the system's behavior accurately. More specifically, the combination of known models and a priori knowledge of the original system provides sufficient information to construct an interpolated model that closely resembles the original system from an application-specific perspective.

In most parametric LTI model interpolation, system evaluations are performed at selected parameter values, which serve as anchor points for interpolation. However, selecting these values is a non-trivial task. Poor choices can lead to significant errors, especially in regions with rapid system variation.

5.1 Introduction

To improve accuracy, samples should capture key changes in system behavior. Rather than distributing points uniformly, methods like adaptive sampling, sensitivity analysis, are used to place samples where they are most informative [68, 69]. These techniques proposes an automated adaptive sampling strategy for parametric model order reduction (pMOR) using matrix interpolation, where sampling points are chosen based on subspace distances to efficiently generate reduced models. The downside of this methods are that it is not evident how subspace distances translate to system behavior. In this regard the paper present a novel sampling criteria that links the criteria to the pole locations which can be interpreted easily by a trained user as system behavior.

An effective application of such algorithms is optimizing drone structures. Enhancing unmanned aerial vehicle (UAV) design to minimize vibration improves flight stability, sensor accuracy, and component lifespan. In fixed-wing UAVs, it also helps mitigate flutter [70]. Drones are widely used in aerial surveying [71] and agriculture [72], but structural advancements can further enhance efficiency and durability. For multirotors, reducing frame resonance and motor-induced vibrations is as important as minimizing weight. Topology optimization [73, 74] refines arm and hub structures to achieve an optimal stiffness-to-weight ratio. Fixed-wing UAVs prioritize reducing aeroelastic effects and engine-induced vibrations by optimizing wing and fuselage structure. Finite element analysis (FEA) and CFD provide accurate vibration predictions but require significant computational resources.

In the case of a scalar parameter, the poles of the parametric LTI system move along a root locus or trajectory. However, for sampled systems, only discrete points along these loci are known. The key idea was to replace the unknown continuous trajectories with artificial ones between the sampled points, enabling interpolation along these constructed paths. It was shown that using hyperbolic lines as interpolating paths is particularly advantageous, as they preserve stability when the system is stable for all parameter values. Moreover, the interpolated system remains close to the original samples in the H_∞ norm and, in certain cases, retains the minimum-phase property.

In this chapter two parametric LTI interpolation methods are presented. Accordingly, the chapter is organized into two main parts. In each part the problem is formulated, the corresponding algorithm is described and analyzed, and the discussion is closed with a numerical example.

The first part presents a stability-preserving interpolation technique for which a specific error bound can be calculated. The second part extends the approach to also guarantee minimum-phase properties besides the features of the first method.

Finally, to support the intended vibration-related applications and the numerical examples, a new sampling criterion is presented alongside a new structure-preserving reduction method for

beam-like structures. This part explains how a Bernoulli (Euler–Bernoulli) beam description can be used to obtain reduced parametric LTI models with the required structure for the interpolation framework.

5.2 Stability preserving parametric LTI interpolation with guaranteed bounds

5.2.1 Problem formulation

In this section, the following single input single output (SISO) discrete time linear time-invariant system (LTI) is considered:

$$G(\lambda) : \begin{cases} x_{t+1} = A(\lambda)x_t + B(\lambda)u_t \\ y_t = C(\lambda)x_t \end{cases} \tag{5.1}$$

where $A(\lambda) \in \mathbb{R}^{n\times n}$, $B(\lambda) \in \mathbb{R}^{n\times 1}$, $C(\lambda) \in \mathbb{R}^{1\times n}$ are parameter dependent matrices with the scalar parameter $\lambda \in \mathbb{R}$. The input and the output is $u_t \in \mathbb{R}$ and $y_t \in \mathbb{R}$ respectively. The state variable is $x_t \in \mathbb{R}^n$. It is important to note that the main difference between LPV and parametric LTI systems is that the parameter does not depend on time in the case of parametric LTI.

The followings are assumed on $G(\lambda)$:

1. it is stable for every λ
2. it has no repeated poles
3. for fixed λ let $H_\lambda(z) = C(\lambda)\left(zI - A(\lambda)\right)^{-1} B(\lambda)$ be the transfer function of $G(\lambda)$ with the partial fractional expansion

$$H_\lambda(z) = \frac{r_1(\lambda)}{z - p_1(\lambda)} + \frac{r_2(\lambda)}{z - p_2(\lambda)} + \ldots + \frac{r_n(\lambda)}{z - p_n(\lambda)} \tag{5.2}$$

let $p_i(\lambda)$ and $r_i(\lambda)$, $i = 1 \ldots n$ be the poles and the residuals, respectively.

It is assumed that the described model $G(\lambda)$ cannot be (or practically cannot be) evaluated at an arbitrary λ instead, it is known at k given points of λ that is $G_i = G(\lambda_i)$ $i = 1 \ldots k$. This assumption means that the behavior of the model $G(\lambda)$ is not known if $\lambda \neq \lambda_i$, $i = 1 \ldots k$. For large scale systems it is a general problem since the dependency of λ in $G(\lambda)$ is rarely known in closed form.

5.2 Stability preserving parametric LTI interpolation with guaranteed bounds

Since there is a scalar parameter $\lambda \in \mathbb{R}$ it is important to note that there is a natural ordering of the models e.g. one can say that the adjacent known models of $G(\lambda)$ ($\lambda_i \leq \lambda \leq \lambda_{i+1}$) are G_i, G_{i+1}. This ordering is used in the following.

It is worth to note that the requirement to have no repeated pole just slightly decreases the generality. In practice to eliminate the repeated poles some perturbation can be added to the original model without affecting the behavior significantly.

Existing methods guarantee stability but other important premises are not addressed. In this section one more crucial a priori assumption is incorporated into the interpolation method. One can assume that samples from the domain of the parameter are taken so the model $G(\lambda)$ ($\lambda_i \leq \lambda \leq \lambda_{i+1}$) does not "deviate" arbitrary from the adjacent known models G_i, G_{i+1}. In other words, this assumption says that the real model does not behave arbitrary when the parameter is between known models. Without this assumption any interpolation method could give an inconsistent result. One way to formally state this assumption is the following: the known systems G_i ($i = 1 \ldots k$) are distributed in a way that for every i a scalar valued $\hat{f}$ function exists that satisfies:

$$\begin{aligned} &\|G(\lambda) - G_i\| \leq \hat{f}(G_{i+1}, G_i) \\ &\|G(\lambda) - G_{i+1}\| \leq \hat{f}(G_{i+1}, G_i) \quad \lambda_i \leq \lambda \leq \lambda_{i+1} \end{aligned} \tag{5.3}$$

where $\hat{f}$ depends only on the known G_{i+1} and G_i and double bar means an application specific system norm.

Inequality (5.3) means that the function $\hat{f}$ gives an upper bound on the norm of the difference between a neighboring model and the interpolated model. In practice it is hard to verify that this assumption holds or not but it is an essential requirement that the known models have to relate to the interpolated model.

The interpolation algorithm introduced in this section is stability preserving and follows the assumption posed in (5.3) with respect to the H_∞ norm. So in Section 5.3.5 it is shown that an f function exists for the proposed interpolation method in a form:

$$\begin{aligned} &\left\|\hat{G}(\lambda) - G_i\right\|_\infty \leq f(G_{i+1}, G_i) \\ &\left\|\hat{G}(\lambda) - G_{i+1}\right\|_\infty \leq f(G_{i+1}, G_i) \quad \lambda_i \leq \lambda \leq \lambda_{i+1} \end{aligned} \tag{5.4}$$

where $\hat{G}(\lambda)$ is the interpolated model. It is worth to mention that the existence of $\hat{f}$ in (5.3) is assumed so it depends on the properties of the interpolation method whether f in (5.4) can be constructed or not.

5.2.1.1 Notations

In Section 5.3.1 the algorithm is described in details and as it is shown $\hat{G}(\lambda)$ $\lambda_i \leq \lambda \leq \lambda_{i+1}$ is determined by G_{i+1}, G_i and λ so only the adjacent models and the parameter is used.

The known models G_{i+1} and G_i are changed to G_2 and G_1 respectively. So for example the j^{th} pole of the G_{i+1} model is p_{j2} the j^{th} residual of G_i is r_{j1}.

The parameter λ is changed to ρ in a way that as λ goes from λ_i to λ_{i+1} ρ goes from zero to one. The correspondence between λ and ρ is as follows:

$$\lambda = (1-\rho)\lambda_i + \rho\lambda_{i+1} \quad \rho \in \{0,1\} \tag{5.5}$$

So the interpolated model is noted by $\hat{G}(\rho)$ for the parameter interval $\lambda_i \leq \lambda \leq \lambda_{i+1}$. The j^{th} pole and residual of $\hat{G}(\rho)$ are $p_j(\rho)$ and $r_j(\rho)$

5.3 Problem Formulation

In this paper, MIMO discrete time linear time-invariant systems are considered. Usually the underlying phenomena which are examined are inherently continuous systems but they can be sufficiently approximated with discrete time systems and all the discussion is carried out with the assumption that the real system is modeled with a discrete system using appropriate sampling. Formally, let an element of the transfer function matrix be a generic transfer function [75]:

$$H(z,\zeta) = \frac{\sum_{k=0}^{m} b_k(\zeta) z^{-k}}{1 + \sum_{k=1}^{n} a_k(\zeta) z^{-k}} \tag{5.6}$$

where:

- $\zeta \in \mathbb{R}$ is the parameter,
- $H(z,\zeta)$ is the transfer function at a certain ζ value,
- z is the complex variable of the function.
- $\{b_k(\zeta)\}$ are the numerator coefficients, where $b_k(\zeta) \in \mathbb{R}$,
- $\{a_k(\zeta)\}$ are the denominator coefficients, where $a_k(\zeta) \in \mathbb{R}$,
- m is the order of the numerator,
- n is the order of the denominator.

5.3 Problem Formulation

The following assumptions are made on $H(z, \zeta)$:

- the transfer function remains stable for all ζ ,
- it does not have any repeated poles,
- $m < n$, ensuring a proper transfer function,
- $\{b_k(\zeta)\}$ and $\{a_k(\zeta)\}$ are continuous function of ζ.
- the sampling frequency is chosen to be high enough to ensure that all poles are mapped to the right-hand side of the complex plane, while still remaining within the unit circle.

It is further assumed that for an element of the transfer function matrix that is $H(z, \zeta)$ there is a partial fractional expansion,

$$H(z, \zeta) = \frac{r_1(\zeta)}{z - p_1(\zeta)} + \frac{r_2(\zeta)}{z - p_2(\zeta)} + \ldots + \frac{r_n(\zeta)}{z - p_n(\zeta)} \tag{5.7}$$

where $p_i(\zeta)$ and $r_i(\zeta)$, for $i = 1, \ldots, n$, represent the poles and residues.

The model $H(z, \zeta)$ is assumed to be difficult or impractical to evaluate for arbitrary values of ζ. Instead, it is only available at k specific points, given by $G_i = H(z, \zeta_i)$ for $i = 1, \ldots, k$. Consequently, the behavior of $H(z, \zeta)$ remains unknown for any ζ other than these given points.

Given that ζ is a scalar parameter, it is important to note that the models have a natural ordering. For instance, one can identify adjacent known models of $H(z, \zeta)$ $\zeta_i \leq \zeta \leq \zeta_{i+1}$ as G_i and G_{i+1}. This ordering will be utilized in the following discussion.

This paper presents an interpolation algorithm that preserves stability and ensures that the deviation of the interpolated model from the known adjacent models remains within a guaranteed upper bound in terms of the H_∞ norm. Formally, there exists a function f associated with the proposed interpolation method such that:

$$\begin{aligned} &\|G(\zeta) - G_i\|_\infty \leq f(G_{i+1}, G_i) \\ &\|G(\zeta) - G_{i+1}\|_\infty \leq f(G_{i+1}, G_i), \quad \zeta_i \leq \zeta \leq \zeta_{i+1} \end{aligned} \tag{5.8}$$

where $G(\zeta)$ is the interpolated model. The derivation of f is presented in Section 5.7.

The proposed method is beneficial when it is known a priori that the given system remains stable for all parameter values and that the unknown function $H(z, \zeta)$, within the range $\zeta_i \leq \zeta \leq \zeta_{i+1}$, exhibits a behavior "similar" to G_i and G_{i+1}. Such conditions frequently arise in practical applications. For instance, while the dynamics of an airplane vary with airspeed, it is known that the system remains stable within a certain speed range, and these dynamics change gradually. Similarly, geometrical modifications in a mechanical component often (though not

always) result in predictable changes in its dynamic behavior. If the dynamics of the system are known for specific configurations, physical considerations suggest that other configurations will not exhibit arbitrary deviations.

Discussion on Assumptions

The requirement that $H(z, \zeta)$ remains stable for all ζ is very reasonable. In practical engineering, most systems are designed to operate stably across a range of parameter values. Many physical systems—such as electrical circuits, mechanical structures, and control systems—can be modeled this way, and stability under parametric variation is often a core design goal.

The assumption that $H(z, \zeta)$ has no repeated poles is moderately restrictive but still often realistic. In practice, repeated poles are uncommon in physical systems due to inherent damping and parameter variability. While idealized or overly simplified models may include repeated poles, most real-world systems do not. If this assumption is not met, the system may exhibit more complex transient behavior and be more sensitive to small changes in parameters, which complicates both analysis and implementation.

The condition $m < n$, ensuring a proper transfer function, is very standard and reflects the fact that real systems are causal and physically realizable. Nearly all real-world dynamic systems—across domains such as electronics, mechanics, and thermal processes—satisfy this assumption.

Lastly, the assumption that each element of $H(z, \zeta)$ admits a partial fraction expansion is common and reasonable. Most linear time-invariant systems with rational transfer functions can be expressed this way. If this assumption does not hold, it may indicate that the system is not described by a rational function, which limits the use of standard analytical and numerical tools in engineering practice.

Overall, these assumptions are not overly restrictive and align well with the characteristics of many real-world systems. They ensure that the model remains both mathematically tractable and physically meaningful.

Notations

Section 5.6 provides a detailed description of the algorithm. As demonstrated, $G(\zeta)$ for $\zeta_i \leq \zeta \leq \zeta_{i+1}$ is determined solely by G_{i+1}, G_i, and ζ, meaning that only the adjacent models and the parameter ζ are utilized.

For convenience, the known models G_{i+1} and G_i are relabeled as G_2 and G_1, respectively. Accordingly, the j^{th} pole of the G_{i+1} model is denoted as p_{j2}, while the j^{th} residual of G_i is represented as r_{j1}.

Additionally, the parameter ζ is transformed into ρ such that as ζ varies from ζ_i to ζ_{i+1}, ρ transitions from zero to one. The relationship between ζ and ρ is given by:

$$\zeta = (1-\rho)\zeta_i + \rho\zeta_{i+1}, \quad \rho \in \{0,1\}, \quad i \in \{1,2,3,...\} \tag{5.9}$$

Thus, the interpolated model is represented as $G(\rho)$ over the parameter range $\zeta_i \leq \zeta \leq \zeta_{i+1}$. The j^{th} pole and residual of $G(\rho)$ are denoted as $p_j(\rho)$ and $r_j(\rho)$, respectively.

5.3.1 Algorithm

The presented algorithm shows the interpolation between two adjacent models G_1 and G_2. In this section the algorithm is outlined and the properties of the method are analyzed in the following sections. Only the SISO case is discussed but the extension to MIMO systems is straightforward since the interpolation is element-wise.

The basic idea is that the poles of the model move along certain trajectories on the complex plane as the parameter changes but the model is known at certain points, therefore only samples of the pole trajectories are known. Hence an interpolation strategy can be that the original trajectories are substituted by artificial trajectories that connect the known points to each other. It is a key point that the chosen type of artificial trajectory satisfies the properties that are known a priori about the system e.g. stability (see Section 5.2.1). Hyperbolic lines are proposed to be used as artificial trajectories between known samples because this choice is stability preserving and has a guaranteed upper bounded estimation on the deviation from the known models. So the i^{th} pole of the interpolated system $p_i(\rho)$ is on the hyperbolic line that connects the i^{th} pole of G_1, G_2. The detailed discussion on the properies of this method is presented in Section 5.3.5.

In the followings, the steps of the algorithm are detailed.

5.3.2 Step 1: compute the poles and the residuals of G_1,G_2.

This step is straightforward since we assumed in Section 5.2.1 that the system has a partial fraction decomposition.

5.3.3 Step 2: pair the poles of G_1,G_2.

As the parameter ρ starts from zero to one the i^{th} pole $p_i(\rho)$ of the model $G(\rho)$ travels along a certain trajectory on the complex plane. If a pole of G_1 and a pole of G_2 is on the same trajectory, one can say that these two poles correspond to each other. As it is assumed there are no multiple poles, therefore, these trajectories never cross each other at the same parameter value so the trajectories are unambiguous.

The problem is that the correspondence of the poles in G_1 and G_2 has to be restored since it is not known after step 1.

Therefore, the poles have to be paired. The best pairing of the poles in G_1 and G_2 has to be determined and the problem can be formulated as a graph theory problem.

As it is proposed in [GLP+16] the hyperbolic distance can be used. Consider the set of poles of G_1 $\bar{p}_1 = \{p_{11}, \ldots, p_{n1}\}$ and the set of poles of G_2 $\bar{p}_2 = \{p_{12}, \ldots, p_{n2}\}$. Let $F(\bar{p}_1, \bar{p}_2)$ be a complete bipartite graph with the vertex set $\bar{p}_1$ and $\bar{p}_2$. The edge set is defined as $E = \{(p_{i1}, p_{j2}) \mid \forall(i, j) \text{ pairs}\}$. Let c_{ij} be the cost of the edge (p_{i1}, p_{j2}) that is the hyperbolic distance between the two poles p_{i1}, p_{j2}. In order to find the corresponding poles one has to determine a subset of the edges in a way that every vertex has exactly one pair and the sum of the costs of the edges are minimal. Kuhn-Munkres algorithm can solve this matching problem in polynomial time [76].

It is worth to mention that the presented pairing requires further investigation since for some examples it cannot find the correct corresponding poles. It is also important that even if the pairing is not perfect the interpolation method still guarantees an upper bound. It follows from the presented results in section 5.3.5. The upper bound estimation depends on the pairing and if the pairing is wrong, the upper bound estimate may become a higher value.

5.3.4 Step 3: construct the interpolated transfer function

A hyperbolic line has to be placed between the paired poles p_{i1} and p_{i2}. The interpolated pole $p_i(\rho)$ lies on that curve. In order to calculate the position of $p_i(\rho)$ the hyperbolic line between p_{i1} and p_{i2} have to be parametrized by ρ. The parametrization is carried out as follows: ρw_i is a line segment that starts from zero and ends at w_i as ρ changes from zero to one where $w_i \in \mathbb{D}$ is an appropriately chosen constant. This segment can be considered as a hyperbolic line segment (and it is on an Euclidian line segment as well) and it can be transformed into a hyperbolic line that connects p_{i1} and p_{i2} as ρ goes from zero to one. This transformation can be a congruent transformation that is always a Möbius transformation on a hyperbolic plane [20]. It is a standard computation to find the coefficient for the proper Möbius transformation [20] so without derivation:

$$p_i(\rho) = \frac{p_{i1} - \rho w_i}{1 - \rho w_i \overline{p_{i1}}} \tag{5.10}$$

The value of w_i is:

$$w_i = \frac{p_{i1} - p_{i2}}{1 - p_{i2}\overline{p_{i1}}} \tag{5.11}$$

It is easy to verify that $p_i(\rho)$ is on the hyperbolic line that connects p_{i1} and p_{i2} as ρ goes from zero to one.

To prove this one can substitute zero and one into the function $p_i(\rho)$

$$p_i(0) = p_{i1}$$

$$\begin{aligned} p_i(1) &= \frac{p_{i1} - \frac{p_{i1}-p_{i2}}{1-p_{i2}\overline{p_{i1}}}}{1 - \frac{p_{i1}-p_{i2}}{1-p_{i2}\overline{p_{i1}}}\overline{p_{i1}}} = \frac{\frac{p_{i1}-p_{i2}p_{i1}\overline{p_{i1}}-p_{i1}+p_{i2}}{1-p_{i2}\overline{p_{i1}}}}{\frac{1-p_{i2}\overline{p_{i1}}-\overline{p_{i1}}p_{i1}+\overline{p_{i1}}p_{i2}}{1-p_{i2}\overline{p_{i1}}}} = \frac{p_{i1} - p_{i2}p_{i1}\overline{p_{i1}} - p_{i1} + p_{i2}}{1 - p_{i2}\overline{p_{i1}} - \overline{p_{i1}}p_{i1} + \overline{p_{i1}}p_{i2}} \\ &= \frac{p_{i2} - p_{i2}p_{i1}\overline{p_{i1}}}{1 - p_{i1}\overline{p_{i1}}} = \frac{p_{i2}(1 - p_{i1}\overline{p_{i1}})}{1 - p_{i1}\overline{p_{i1}}} = p_{i2} \end{aligned} \tag{5.12}$$

so the result is p_{i1} and p_{i2} respectively. ρw_i is a hyperbolic line and a Möbius transformation, which is an isometry on the Poincaré disk model, acts on it so the result is also a hyperbolic line. So $p_i(\rho)$ is on a hyperbolic line that contains p_{i1} and p_{i2}. A hyperbolic line is fully determined by two points, therefore, $p_i(\rho)$ fulfills the requirements.

Remarks:
The general formula for all isometric transformation of the Poincaré disk model is (see [20]):

$$w = \frac{\alpha z + \beta}{\overline{\beta} z + \overline{\alpha}} \quad \alpha, \beta \in \mathbb{C},\ 0 \prec |\beta| \prec |\alpha| \,.$$

The equation (5.10) does not obviously fit in the general formula of isometric transformations. The following argument shows that (5.10) is an element of the set of isometric transformations. One can write:

$$\frac{p_{i1} - \rho w_i}{1 - \rho w_i \overline{p_{i1}}} = -\frac{\rho w_i - p_{i1}}{-\overline{p_{i1}}\rho w_i + 1} = \frac{i}{-i}\frac{\rho w_i - p_{i1}}{-\overline{p_{i1}}\rho w_i + 1} = \frac{i\rho w_i - i p_{i1}}{i\overline{p_{i1}}\rho w_i - i} \tag{5.13}$$

so with the choice of $z = \rho w_i$, $\alpha = i$ and $\beta = -i p_{i1}$ the expression in (5.13) is obviously the element of the isometries of the Poincaré disk model.

The residuals $r_i(\rho)$ are interpolated linearly so $r_i(\rho) = (1-\rho)r_{i1} + \rho r_{i2}$. This interpolation strategy of the residuals, as it is shown in the following section, fulfills the requirements that are set in Section 5.2.1, but the choice of the function $r_i(\rho)$ requires further investigation since the properties of the interpolation could be improved by selecting an other strategy.

Finally the formula for the interpolated transfer function is:

$$\hat{H}_\rho(z) = \sum_{i=1}^{n} \frac{r_i(\rho)}{z - p_i(\rho)} = \sum_{i=1}^{n} \frac{(1-\rho)r_{i1} + \rho r_{i2}}{z - \frac{p_{i1}-\rho w_i}{1-\rho w_i \overline{p_{i1}}}} \tag{5.14}$$

If a state space realization is required, it can be constructed from the transfer function. The realization problems are not discussed in this work.

5.3.5 Boundedness and stability

The stability of the interpolated system is a trivial result of its construction. The hyperbolic line lies within the unit circle so do the poles of the interpolated system which means that the system $\hat{G}(\rho)$ is stable.

The rest of the section is devoted to the construction of the function f in (5.4). As the first step it is shown that a uniform bound can be given on the deviation of $\hat{G}(\rho)$ from G_1 in the form

$$\left\|\hat{G}(\rho) - G_1\right\|_\infty \leq g_1(G_1, G_2). \tag{5.15}$$

The deviation of $\hat{G}(\rho)$ from G_2 can be calculated analogously. So the proposed method guarantees that the interpolated system does not deviate arbitrarily from the adjacent sample points in term of the H_∞ norm.

As it is assumed, the systems $\hat{G}(\rho)$ and G_1 have partial fraction decomposition:

$$\left\|\hat{G}(\rho) - G_1\right\|_\infty = \left\|\sum_{i=1}^{n} \left(P_i(\rho) - P_{i1}\right)\right\|_\infty, \tag{5.16}$$

where

$$P_i(\rho) = \frac{r_i(\rho)}{z - p_i(\rho)}, \quad P_{i1} = \frac{r_{i1}}{z - p_{i1}}.$$

Exploiting the subadditivity of the H_∞ norm from (5.66):

$$\left\|\hat{G}(\rho) - G_1\right\|_\infty \leq \sum_{i=1}^{n} \|P_i(\rho) - P_{i1}\|_\infty. \tag{5.17}$$

In the followings an upper bound is given on $\|P_i(\rho) - P_{i1}\|_\infty$.

$$\begin{aligned} \|P_i(\rho) - P_{i1}\|_\infty = \left\|\frac{r_i(\rho)}{z - p_i(\rho)} - \frac{r_{i1}}{z - p_{i1}}\right\|_\infty \leq \\ |r_i(\rho)| \left\|\frac{1}{z - p_i(\rho)}\right\|_\infty + \left\|\frac{r_{i1}}{z - p_{i1}}\right\|_\infty. \end{aligned} \tag{5.18}$$

Compute an upper bound term by term in (5.68). The last term can be calculated exactly since it is a first order system:

$$\left\|\frac{r_{i1}}{z - p_{i1}}\right\|_\infty = \max_{z=e^{i\omega}} \left|\frac{r_{i1}}{z - p_{i1}}\right| = \left|\frac{r_{i1}}{\frac{p_{i1}}{|p_{i1}|} - p_{i1}}\right|. \tag{5.19}$$

The residual $r_i(\rho)$ in the first term is interpolated linearly so:

$$|r_i(\rho)| = |(1-\rho)r_{i1} + \rho r_{i2}| \leq \max\{|r_{i1}|, |r_{i2}|\}. \tag{5.20}$$

The term $\frac{1}{z-p_i(\rho)}$ in (5.68) is also a first order system as the last term but it depends on ρ. As the first step one can write:

$$\left\|\frac{1}{z-p_i(\rho)}\right\|_\infty = \left|\frac{1}{\frac{p_i(\rho)}{|p_i(\rho)|} - p_i(\rho)}\right| = \left|\frac{|p_i(\rho)|}{p_i(\rho)(1-|p_i(\rho)|)}\right| =$$
$$\frac{|p_i(\rho)|}{|p_i(\rho)|}\left|\frac{1}{1-|p_i(\rho)|}\right| = \left|\frac{1}{1-|p_i(\rho)|}\right| = \left|\frac{1}{1-\left|\frac{p_{i1}-\rho w_i}{1-\rho w_i\overline{p_{i1}}}\right|}\right|. \tag{5.21}$$

Since $\left|\frac{p_{i1}-\rho w_i}{1-\rho w_i\overline{p_{i1}}}\right| \leq 1$ it is obvious that:

$$\max_\rho \left|\frac{1}{1-\left|\frac{p_{i1}-\rho w_i}{1-\rho w_i\overline{p_{i1}}}\right|}\right| = \left|\frac{1}{1-\max\limits_\rho\left|\frac{p_{i1}-\rho w_i}{1-\rho w_i\overline{p_{i1}}}\right|}\right|. \tag{5.22}$$

A geometric argument is applied to determine the maximum of $\left|\frac{p_{i1}-\rho w_i}{1-\rho w_i\overline{p_{i1}}}\right|$: ρw_i is a line segment that starts from zero and ends at w_i. From the equation (3.3) the expression $\left|\frac{p_{i1}-\rho w_i}{1-\rho w_i\overline{p_{i1}}}\right|$ is a pseudo-hyperbolic distance between a point of the hyperbolic line segment determined by ρw_i and p_{i1}. The maximum distance between the points of the line segment and a point occurs between one of the endpoints of the line segment and the point. So the maximum at (5.74) occurs if $\rho = 0$ or $\rho = 1$. As it is discussed in Section 5.3.1 the value of $\frac{p_{i1}-\rho w_i}{1-\rho w_i\overline{p_{i1}}}$ at $\rho = 0$ and $\rho = 1$ are p_{i1} and p_{i2} respectively so:

$$\left\|\frac{1}{z-p_i(\rho)}\right\|_\infty \leq \max\left\{\left|\frac{1}{1-|p_{i1}|}\right|, \left|\frac{1}{1-|p_{i2}|}\right|\right\}. \tag{5.23}$$

The upper bound on the deviation is:

$$\left\|\hat{G}(\rho) - G_1\right\|_\infty \leq g_1(G_1, G_2) = \sum_{i=1}^{n}\Bigg(\max\{|r_{i1}|, |r_{i2}|\}\cdot$$
$$\max\left\{\left|\frac{1}{1-|p_{i1}|}\right|, \left|\frac{1}{1-|p_{i2}|}\right|\right\} + \left|\frac{r_{i1}}{\frac{p_{i1}}{|p_{i1}|} - p_{i1}}\right|\Bigg). \tag{5.24}$$

When the deviation is taken from G_2 then:

$$\|G(\rho) - G_2\|_\infty \leq g_2(G_1, G_2) = \sum_{i=1}^{n} \Bigg(\max\{|r_{i1}|, |r_{i2}|\} \cdot \max\left\{ \left| \frac{1}{1-|p_{i1}|} \right|, \left| \frac{1}{1-|p_{i2}|} \right| \right\} + \left| \frac{r_{i2}}{\frac{p_{i2}}{|p_{i2}|} - p_{i2}} \right| \Bigg). \tag{5.25}$$

So the function f in (5.4) can be constructed as:

$$f(G_1, G_2) = \max\{g_1(G_1, G_2), g_2(G_1, G_2)\}. \tag{5.26}$$

5.3.6 Numerical example

The example is a finite element (FE) model of a 3D cantilever Timoshenko beam [77]. This benchmark problem is created in Matlab environment and it is used in many research studies as a sample model for example [11, 68, 78–80]. In this paper the results are compared with the results in [11] so exactly the same setup is used. The length L of the beam is the free geometric parameter which varies between $L = 0.9m$ and $L = 1.1m$. The model output is the vertical displacement of the tip of the beam, and the input is a vertical force at this point. The dimension of the system is chosen to be $n = 144$ degree of freedom. The parameter space is sampled uniformly to get three local models $\tilde{M}_i$ with $i = 1, 2, 3$ for lengths $L_1 = 0.9m$, $L_1 = 1.0m$, $L_1 = 1.1m$. The local models are reduced using a two-sided Krylov subspace method with reduced order $q = 23$ and expansion points $s_0 = 0$ to obtain three low-order systems $\tilde{G}_i$. Since the proposed method works on discrete time systems the continuous model $\tilde{G}_i$ is transformed into a zero-order-hold equivalent discrete system G_i. The sampling time is set in a way that every pole of the discrete system is on the right complex half-plane, the value is $T_s = 0.00005sec$. The guaranteed upper bound for the interval $L = 0.9 - 1m$ is $f = 0.0575$ and for the interval $L = 1 - 1.1m$ is $f = 0.0641$. The true least upper bound for the interval $L = 0.9 - 1m$ is 0.0119 and for the interval $L = 1 - 1.1m$ is 0.0129. The guaranteed upper bound is in the same magnitude as the least upper bound in this example.

In order to compare the proposed method and the methods in [11], the relative error between the interpolated and directly reduced systems expressed in the H_2-norm is plotted (see Fig. 5.2 and Fig. 5.3) .

H_2-norm is used because it is applied in [11]. The performance of the proposed method is acceptable in H_2 sense as well, though the maximum relative error of the proposed method is greater (0.389) than the error in [11] (0.113) but much better than the reference system in [11].

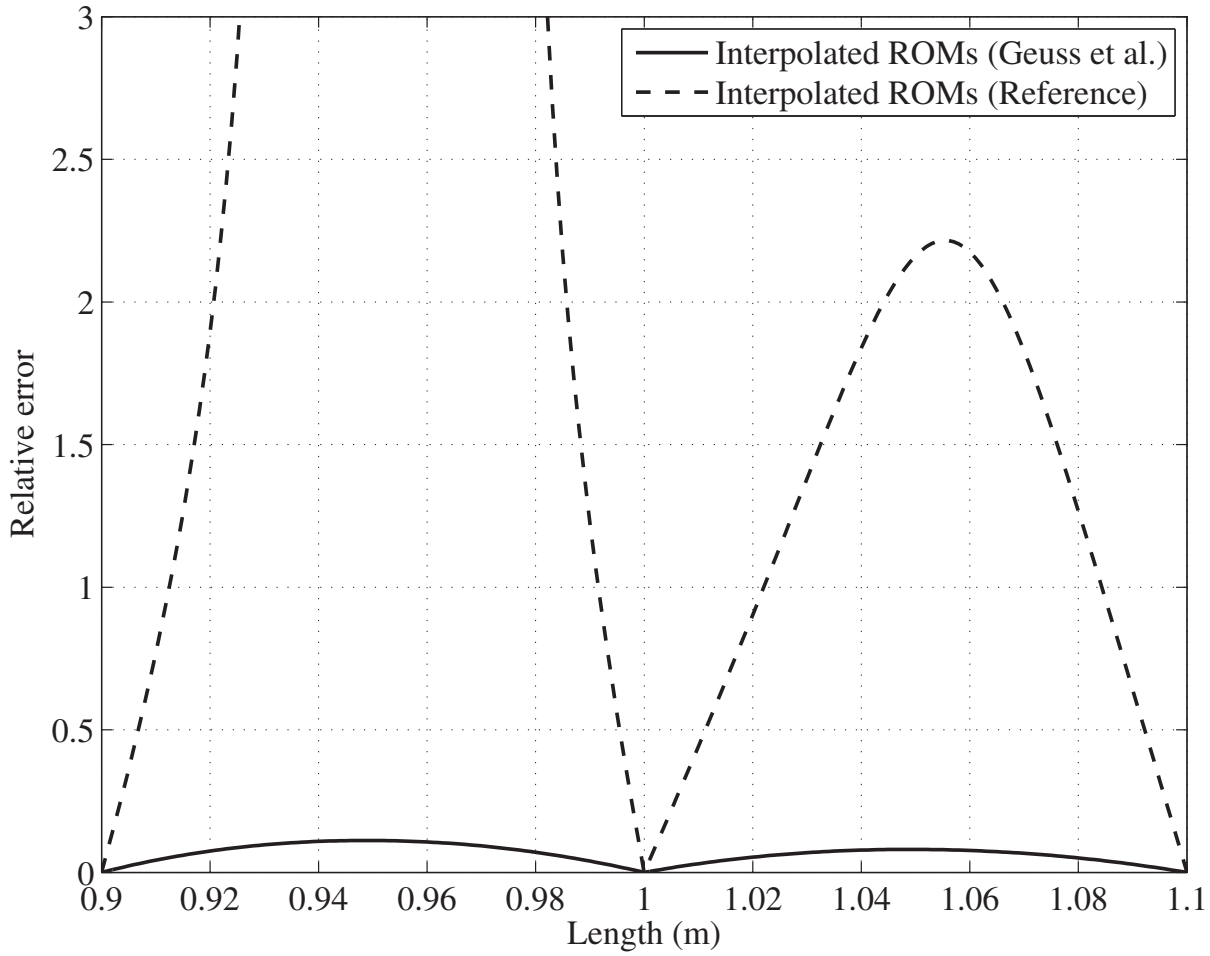

Figure 5.2: Relative error of interpolated models expressed in the H_2-norm for the cantilever beam. Result is generated with the methods in [11]. The figure is taken from [11]

5.4 Minimal phase preserving parametric LTI interpolation with guaranteed bounds

This section shares the same structure and has similar content as section 5.2 and certain parts seem to be repeated, however, due to the numerous minor differences it was advantageous to re-express certain descriptions with the necessary modifications instead of referencing back to section 5.2 multiple times. However, in some cases, when it was not confusing we used referencing instead of repetition.

5.4.1 Problem formulation

The problem formulation is similar to the one in Section 5.2.1 but it needs to be reformulated since the focus is on minimal phase systems. The following single input single output (SISO) discrete

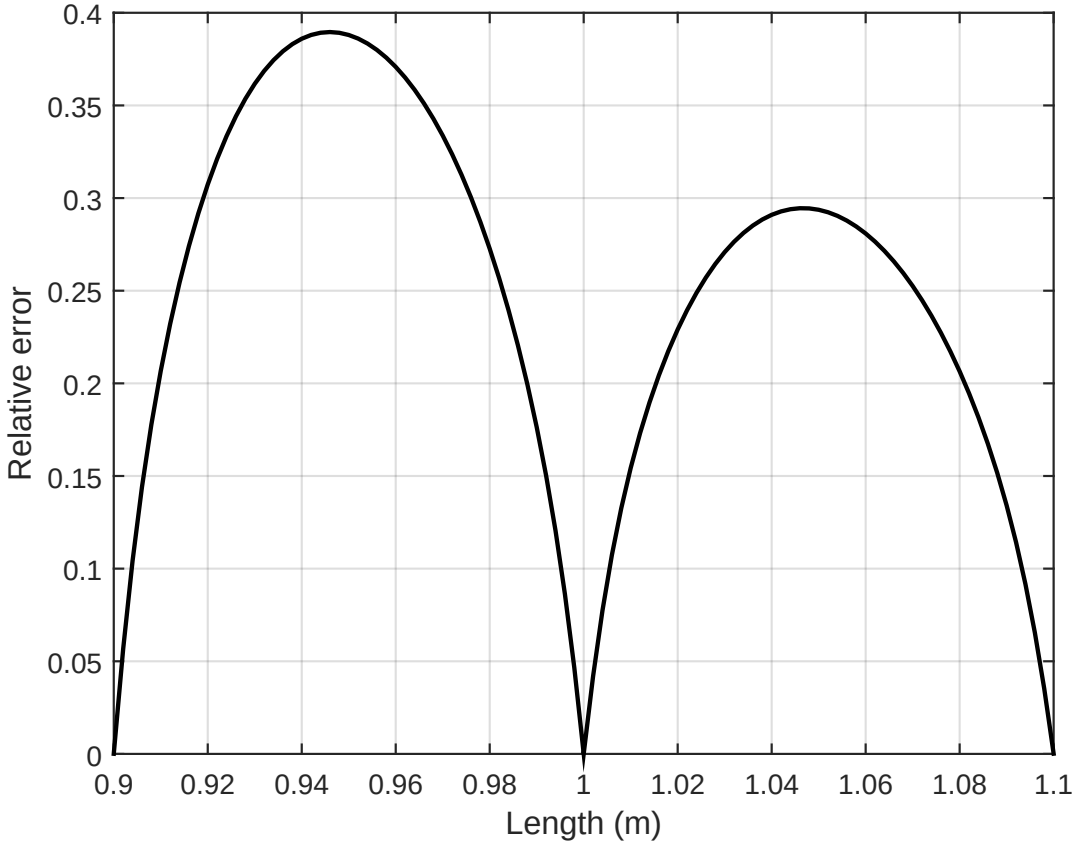

Figure 5.3: Relative error of interpolated models expressed in the H_2-norm for the cantilever beam. Result is generated by the proposed method.

time linear time-invariant system (LTI) is considered(as MIMO extension is straightforward by element-wise application):

$$G(\zeta) : \begin{cases} x_{t+1} = A(\zeta)x_t + B(\zeta)u_t \\ y_t = C(\zeta)x_t \end{cases} \tag{5.27}$$

where $A(\zeta) \in \mathbb{R}^{n\times n}$, $B(\zeta) \in \mathbb{R}^{n\times 1}$, $C(\zeta) \in \mathbb{R}^{1\times n}$ are parameter dependent matrices with the scalar parameter $\zeta \in \mathbb{R}$. The input and the output is $u_t \in \mathbb{R}$ and $y_t \in \mathbb{R}$ respectively. The state variable is $x_t \in \mathbb{R}^n$. It is important to note that the main difference between LPV and parametric LTI systems is that the parameter does not depend on time in the case of parametric LTI.

The followings are assumed on $G(\zeta)$:

1. it is stable for every ζ
2. it has no repeated poles

3. all the zeros are in the unit disk $\mathbb{D} := \{z \in \mathbb{C} : |z| < 1\}$

4. it has no repeated zeros

5. for fixed ζ let $H_\zeta(z) = C(\zeta)\,(zI - A(\zeta))^{-1}\,B(\zeta)$ be the transfer function of $G(\zeta)$ with the zero-pole-gain model:

$$H_\zeta(z) = k(\zeta) \prod_{i=1}^{m} (z - z_i(\zeta)) \prod_{j=1}^{n} \frac{1}{z - p_j(\zeta)} \tag{5.28}$$

where $p_j(\zeta)$ $j = 1 \dots n$ are the poles and $z_i(\zeta)$ $i = 1 \dots m$ are the zeros and $m < n$.

It is assumed that the described model $G(\zeta)$ cannot be evaluated at an arbitrary ζ (or practically it is hard to evaluate) instead it is known at k given points of ζ that is $G_i = G(\zeta_i)$ $i = 1 \dots k$. This assumption means that the behavior of the model $G(\zeta)$ is not known if $\zeta \neq \zeta_i$, $i = 1 \dots k$.

Since there is a scalar parameter $\zeta \in \mathbb{R}$ it is important to note that there is a natural ordering of the models e.g. one can say that the adjacent known models of $G(\zeta)$ ($\zeta_i \leq \zeta \leq \zeta_{i+1}$) are G_i, G_{i+1}. This ordering is used in what follows.

In this section an interpolation algorithm is proposed that is stability preserving and the deviation of the interpolated model has a guaranteed upper bound from the known adjacent models with respect to H_∞ norm. In a formal way, an f function exists for the proposed interpolation method in a form:

$$\begin{aligned} &\left\|\hat{G}(\zeta) - G_i\right\|_\infty \leq f(G_{i+1}, G_i) \\ &\left\|\hat{G}(\zeta) - G_{i+1}\right\|_\infty \leq f(G_{i+1}, G_i) \quad \zeta_i \leq \zeta \leq \zeta_{i+1} \end{aligned} \tag{5.29}$$

where $\hat{G}(\zeta)$ is the interpolated model. The construction of f is shown in Section 5.4.6. In this section we also assume that the original sampling of the system $G(\zeta)$ fulfills the condition in (5.3).

The proposed method is applicable when it is a priori known that the given system is minimum phase and stable in every parameter value and the unknown $G(\zeta)$ ($\zeta_i \leq \zeta \leq \zeta_{i+1}$) remains "similar" to G_i and G_{i+1}. These conditions appear frequently in practice. For example the dynamics of an airplane changes with airspeed but it is known that it is stable for a certain range of speed and the dynamics changes gradually. Geometrical changes in a mechanical component usually (not every case) cause traceable changes in dynamical behavior so if the dynamics is known at certain setups then it is expected based on physical consideration on the actual component that other setups do not deviate arbitrary.

5.4 Minimal phase preserving parametric LTI interpolation with guaranteed bounds

Existing methods guarantee stability [5] [11] so for a given problem f in (5.29) exists but there is no guarantee that the value of it does not become arbitrarily large. The presented interpolation method guarantees an upper bound on f. Moreover f can be given in a closed form. Furthermore the minimum phase property is also guaranteed.

5.4.1.1 Notations

In Section 5.4.2 the algorithm is described in details and as it will be shown $\hat{G}(\zeta)$ $\zeta_i \leq \zeta \leq \zeta_{i+1}$ is determined by G_{i+1}, G_i and ζ, so only the adjacent models and the parameter are used.

The known models G_{i+1} and G_i are exchanged to G_2 and G_1 respectively. So for example the j^{th} pole of the G_{i+1} model is p_{j2} while the j^{th} zero of G_i is z_{j1}.

The parameter ζ is exchanged to ρ in a way that as ζ goes from ζ_i to ζ_{i+1} then ρ goes from zero to one. The correspondence between ζ and ρ is as follows:

$$\zeta = (1-\rho)\zeta_i + \rho\zeta_{i+1} \quad \rho \in \{0,1\} \tag{5.30}$$

So the interpolated model is denoted by $\hat{G}(\rho)$ for the parameter interval $\zeta_i \leq \zeta \leq \zeta_{i+1}$. The j^{th} pole and zero of $\hat{G}(\rho)$ are $p_j(\rho)$ and $z_j(\rho)$.

5.4.2 Algorithm

The presented algorithm shows the interpolation between two adjacent models G_1 and G_2 the same way as in section 5.3.1.

The basic idea is the same as the one presented in 5.3.1 where the original trajectories are substituted by artificial trajectories of the poles.

Similar considerations can be applied to the zeros of the system. If the zeros of the system are stable and if the interpolated zero is on a hyperbolic line similarly to a pole, the interpolated system is a minimum phase system as the original system. In the following, the transfer function is in the pole-zero-gain form and the interpolation is carried out on hyperbolic lines for poles and zeros as well. The gain of the system is interpolated linearly.

In the following, the steps of the algorithm are detailed.

5.4.3 Step 1: compute the poles-zero form of G_1,G_2.

This step is straightforward since we assumed in Section 5.4.1 that the system has a zero-pole-gain model.

5.4.4 Step 2: pair the poles and zeros of G_1,G_2.

The pairing is done identically as it is discussed in 5.3.1 in step 2 and the pairing of zeros is done using the exact same method.

It is worth to mention that the presented pairing requires further investigation as for coarse sampling on parameter space the method may lead to an incorrect pairing. It is also important that even if the pairing is not perfect the interpolation method still guarantees an upper bound, stability and minimum phase property. It follows from the presented results in section 5.4.6.

5.4.5 Step 3: construct the interpolated transfer function

A hyperbolic line has to be placed between the paired poles p_{i1} and p_{i2}. The interpolated pole $p_i(\rho)$ lies on that curve. In order to calculate the position of $p_i(\rho)$ the hyperbolic line between p_{i1} and p_{i2} has to be parametrized by ρ. The parametrization is carried out as follows: ρw_i is a line segment that starts from zero and ends at w_i as ρ changes from zero to one where $w_i \in \mathbb{D}$ is an appropriately chosen constant. This segment can be considered as a hyperbolic line segment (and it is on an Euclidean line segment as well) and it can be transformed into a hyperbolic line that connects p_{i1} and p_{i2} as ρ goes from zero to one. This transformation can be a congruent transformation that is a Möbius transformation on a hyperbolic plane [20]. It is a standard computation to find the coefficient for the proper Möbius transformation [20] so without derivation:

$$p_i(\rho) = \frac{p_{i1} - \rho w_i}{1 - \rho w_i \overline{p_{i1}}} \tag{5.31}$$

The value of w_i is:

$$w_i = \frac{p_{i1} - p_{i2}}{1 - p_{i2}\overline{p_{i1}}} \tag{5.32}$$

It is easy to verify that $p_i(\rho)$ is on the hyperbolic line that connects p_{i1} and p_{i2} as ρ goes from zero to one.

To prove this it can be substituted by writing 0 and 1 into the function $p_i(\rho)$ and the result is p_{i1} and p_{i2} respectively. ρw_i is a hyperbolic line and a Möbius transformation, which is an isometry on the Poincaré disk model, acts on it so the result is also a hyperbolic line [20]. So $p_i(\rho)$ is on a hyperbolic line that contains p_{i1} and p_{i2}.

The parametrization of the hyperbolic line between two corresponding zeros z_{i1} and z_{i2} is carried out analogously to case of poles so:

$$z_i(\rho) = \frac{z_{i1} - \rho v_i}{1 - \rho v_i \overline{z_{i1}}} \tag{5.33}$$

The value of v_i is:

$$v_i = \frac{z_{i1} - z_{i2}}{1 - z_{i2}\overline{z_{i1}}} \tag{5.34}$$

The gain $k(\rho)$ is interpolated linearly so $k(\rho) = (1-\rho)k_1 + \rho k_2$.

Finally the formula for the interpolated transfer function is:

$$\begin{aligned} \hat{H}_\rho(z) = k(\rho) \prod_{i=1}^{m} (z - z_i(\rho)) \prod_{j=1}^{n} \frac{1}{z - p_j(\rho)} = \\ ((1-\rho)k_1 + \rho k_2) \prod_{i=1}^{m} \left(z - \frac{z_{i1} - \rho v_i}{1 - \rho v_i \overline{z_{i1}}} \right) \prod_{j=1}^{n} \frac{1}{z - \frac{p_{j1} - \rho w_j}{1 - \rho w_j \overline{p_{j1}}}} \end{aligned} \tag{5.35}$$

If the state space realization is required, it can be constructed from the transfer function. The realization problems are not discussed in this paper.

5.4.6 Boundedness and minimal phase

The stability and minimum phase property of the interpolated system is trivial from the construction. The hyperbolic line lies within the unit circle which means the poles and zeros of the interpolated system are also in the unit circle. This exactly means that the system $\hat{G}(\rho)$ is stable and has the minimum phase property.

In the following the construction of the function f in (5.29) for the algorithm is presented.

As the first step it is shown that uniform bound can be given on the deviation of $\hat{G}(\rho)$ from G_1 in the form

$$\left\| \hat{G}(\rho) - G_1 \right\|_\infty \leq g_1(G_1, G_2) \tag{5.36}$$

The deviation of $\hat{G}(\rho)$ from G_2 can be calculated analogously.

$$\begin{aligned} \left\| k(\rho) \prod_{i=1}^{m} (z - z_i(\rho)) \prod_{j=1}^{n} \frac{1}{z - p_i(\rho)} - G_1 \right\|_\infty \leq \\ \left\| k(\rho) \prod_{i=1}^{m} (z - z_i(\rho)) \prod_{j=1}^{n} \frac{1}{z - p_i(\rho)} \right\|_\infty + \|G_1\|_\infty \end{aligned} \tag{5.37}$$

Since the H_∞ norm is sub-multiplicative then:

$$\left\| k(\rho) \prod_{i=1}^{m} (z - z_i(\rho)) \prod_{j=1}^{n} \frac{1}{z - p_i(\rho)} \right\|_\infty \leq$$
$$|k(\rho)| \prod_{i=1}^{m} \|z - z_i(\rho)\|_\infty \prod_{j=1}^{n} \left\| \frac{1}{z - p_i(\rho)} \right\|_\infty \tag{5.38}$$

Compute an upper bound term by term in (5.38). The static gain is interpolated linearly so:

$$|k(\rho)| = |(1-\rho)k_1 + \rho k_2| \leq \max\{|k_1|, |k_2|\} \tag{5.39}$$

The upper bound on interpolated zeros can be expressed as follows:

$$\|z - z_i(\rho)\|_\infty = \max_{\omega,\rho} \left| e^{i\omega} - \frac{z_{i1} - \rho v_i}{1 - \rho v_i \overline{z_{i1}}} \right| \tag{5.40}$$

The difference between $e^{i\omega}$ and $\frac{z_{i1}-\rho v_i}{1-\rho v_i \overline{z_{i1}}}$ as vectors is maximal if they are collinear and directed to the opposite direction. The length of $e^{i\omega}$ is always one so if the terms in (5.40) are collinear as vectors, the result depends only on $\frac{z_{i1}-\rho v_i}{1-\rho v_i \overline{z_{i1}}}$. So the following can be written:

$$\max_{\omega,\rho} \left| e^{i\omega} - \frac{z_{i1} - \rho v_i}{1 - \rho v_i \overline{z_{i1}}} \right| \leq \max_{\rho} \left| e^{i\left(\arg\left(\frac{z_{i1}-\rho v_i}{1-\rho v_i \overline{z_{i1}}}\right)+\pi\right)} - \frac{z_{i1} - \rho v_i}{1 - \rho v_i \overline{z_{i1}}} \right| =$$
$$\max_{\rho} \left| -e^{i\arg(z_i(\rho))} - z_i(\rho) \right| = \max_{\rho} \left| \frac{z_i(\rho)}{|z_i(\rho)|} + z_i(\rho) \right| = \max_{\rho} \left| \frac{z_i(\rho)}{|z_i(\rho)|} (1 + |z_i(\rho)|) \right| =$$
$$\max_{\rho} \left(\left| \frac{z_i(\rho)}{z_i(\rho)} \right| |1 + |z_i(\rho)|| \right) = \max_{\rho} (1 + |z_i(\rho)|) = \max_{\rho} \left(1 + \left| \frac{z_{i1} - \rho v_i}{1 - \rho v_i \overline{z_{i1}}} \right| \right) \tag{5.41}$$

Analogously to (5.74) the upper bound estimate on (5.40) can be expressed as:

$$\|z - z_i(\rho)\|_\infty \leq 1 + \max\{|z_{i1}|, |z_{i2}|\} \tag{5.42}$$

The term $\frac{1}{z-p_i(\rho)}$ in (5.38) is a first order system that depends on ρ. In order to compute the upper bound of it the following steps can be completed:

$$\left\| \frac{1}{z - p_i(\rho)} \right\|_\infty = \left| \frac{1}{\frac{p_i(\rho)}{|p_i(\rho)|} - p_i(\rho)} \right| = \left| \frac{|p_i(\rho)|}{p_i(\rho)(1 - |p_i(\rho)|)} \right| =$$
$$\frac{|p_i(\rho)|}{|p_i(\rho)|} \left| \frac{1}{1 - |p_i(\rho)|} \right| = \left| \frac{1}{1 - |p_i(\rho)|} \right| = \left| \frac{1}{1 - \left| \frac{p_{i1} - \rho w_i}{1 - \rho w_i \overline{p_{i1}}} \right|} \right| \tag{5.43}$$

Since $\left|\frac{p_{i1}-\rho w_i}{1-\rho w_i \overline{p_{i1}}}\right|$ is a pseudo-hyperbolic distance between p_{i1} and ρw_i, it is less than or equal to one [19]. So one can write:

$$\max_{\rho}\left|\frac{1}{1-\left|\frac{p_{i1}-\rho w_i}{1-\rho w_i \overline{p_{i1}}}\right|}\right| = \left|\frac{1}{1-\max\limits_{\rho}\left|\frac{p_{i1}-\rho w_i}{1-\rho w_i \overline{p_{i1}}}\right|}\right| \tag{5.44}$$

The maximum of $\left|\frac{p_{i1}-\rho w_i}{1-\rho w_i \overline{p_{i1}}}\right|$ is analogous to the discussion above so it is equal to $\max\{|p_{i1}|, |p_{i2}|\}$

So the result on g_1:

$$\begin{aligned} &g_1(G_1, G_2) = \\ &\max\{|k_1|, |k_2|\} \prod_{i=1}^{m} (1 + \max\{|z_{i1}|, |z_{i2}|\}) \cdot \\ &\prod_{j=1}^{n} \max\left\{\left|\frac{1}{1-|p_{j1}|}\right|, \left|\frac{1}{1-|p_{j2}|}\right|\right\} + \|G_1\|_\infty \end{aligned} \tag{5.45}$$

g_2 is:

$$\begin{aligned} &g_2(G_1, G_2) = \\ &\max\{|k_1|, |k_2|\} \prod_{i=1}^{m} (1 + \max\{|z_{i1}|, |z_{i2}|\}) \cdot \\ &\prod_{j=1}^{n} \max\left\{\left|\frac{1}{1-|p_{j1}|}\right|, \left|\frac{1}{1-|p_{j2}|}\right|\right\} + \|G_2\|_\infty \end{aligned} \tag{5.46}$$

$f(G_1, G_2)$ is

$$f(G_1, G_2) = \max\{g_1(G_1, G_2), g_2(G_1, G_2)\} \tag{5.47}$$

It is important to note that the derived bound is a qualitative property of the interpolation method. It says no more than the difference between the interpolated model and the neighboring models can not be arbitrary large. However, it is a conservative estimation so a more accurate bound estimation is a subject of further investigation.

5.4.7 Numerical example

In this example a structural optimization of a finite element (FE) model is presented. The eigenfrequencies are optimized for a certain value. This kind of problem occurs basically in every device that vibrates and on some level this optimization problem has to be addressed

during the design phase. A finite element (FE) model of a 3D cantilever Timoshenko beam is applied [77]. This benchmark problem is created in Matlab environment and it is used in many research studies as a sample model, for example [11,68,78–80]. In this paper the following setup is used. The length L of the beam is 2 meters the free geometric parameter is the height h of the beam, the width is 0.01 meters and it is a steel rod (density: 7850 kg/m^3, Young's modulus: 210 GPa, Poisson's ratio: 0.3). The model output is the vertical displacement of the tip of the beam, and the input is a vertical force at this point. The number of elements of the model is chosen to be $N = 100$. The task is to tune the height of the beam so that the first eigenfrequency is set to be 340 rad/sec. As it is usual in practice, we can assume that the searched parameter value is known in a certain range. In this example, the assumed range for height is $h = 0.2m \ldots 0.3m$. The bode diagram at the extremes of the parameter domain is shown in figure 5.4

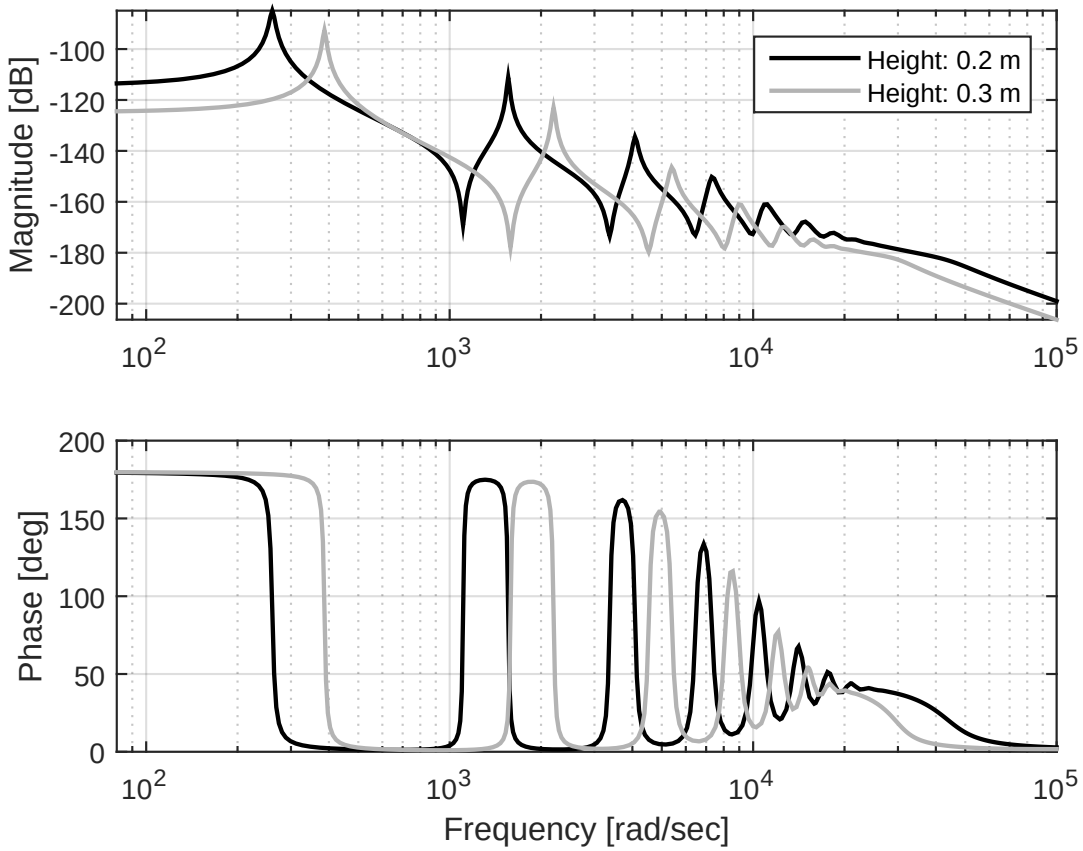

Figure 5.4: Bode diagramm of the beam at height 0.2 m and 0.3 m

The optimization task is convex since the eigenfrequency is monotonic with height. The optimization is solved by golden section search and parabolic interpolation [81,82]. The required time on an Intel Core i7-2600 CPU at 3.4 GHz is 32.11 sec. The result is $h = 0.2627m$

Next the same problem is solved with the interpolation method presented here. First the parameter space is sampled to get local models. The sampling of the parameter space is highly problem specific and it is hard to say general rules. In this example ten uniformly sampled points are taken. Then the local models are reduced using a two-sided Krylov subspace method [83] with reduced order $q = 23$ and expansion points $s_0 = 0$ to obtain the low-order systems $\tilde{G}_i$. Since the proposed method works on discrete time systems the continuous model $\tilde{G}_i$ is transformed into zero-order-hold equivalent discrete system G_i. The sampling time is set in a way that every pole of the discrete system is on the right complex half-plane, the value is $T_s = 0.00001sec$. Then the pole-zero-gain models are computed and the poles and zeros are matched. After the previous steps the interpolated model can be computed at any parameter value. It is important to note that during the optimization only the interpolation needs to be recalculated and the previous steps are not needed. So one can say that there is an off-line phase and an on-line phase. The off-line phase contains the sampling, reduction and matching while the on-line phase contains the computation of the interpolated system.

The optimization is carried out with the same algorithm and the same CPU. The off-line phase takes 5.806 sec and the on-line phase takes 2.431 sec, the resultant height is $h = 0.2591m$ that is less than 1.4 % error.

It is clear that the proposed algorithm significantly reduces the computational effort furthermore it has the advantage that the off-line phase needs to be done only once. So if the optimization task needs to be repeated for a different value, the difference is more pronounced.

5.5 Structure-preserving reduction and sampling for beam-like structures

This section introduces the additional ingredients required to apply the proposed interpolation framework in practice: a sampling criterion and a structure-preserving reduction method for beam-like structures.

Sampling is crucial because the interpolation relies on matching corresponding poles across neighboring parameter samples. If the parameter grid is too coarse, poles can move significantly between samples and the matching problem becomes ambiguous.

Accordingly, a sampling criterion is developed to ensure proper pole matching for a class of second-order LTI systems. To meet this criterion, a practical model order reduction method is introduced that preserves the required structure and is applicable to systems that can be modeled using Bernoulli beam theory (e.g., multicopter rotor arms and fixed-wing aircraft wings). The approach is extended to MIMO systems with a corresponding deviation bound, and the set of

all interpolating trajectories that satisfy the boundedness property is characterized, generalizing beyond hyperbolic lines.

The remainder of this paper is organized as follows. Section 5.3 details the problem formulation and constraints. Section 5.6 presents the proposed algorithm. Section 5.7 proves the boundedness property for the admissible trajectories, and Section 5.8 extends the results to MIMO systems. Section 5.9 provides an example focusing on the proposed structure-preserving reduction method.

5.6 Interpolation Algorithm

The proposed algorithm is designed to interpolate between two adjacent models, G_1 and G_2. This section provides an overview of the algorithm, while its properties are analyzed in subsequent sections.

The fundamental idea is that as the parameter varies, the poles of the model follow specific trajectories in the complex plane. However, since the model is only known at certain discrete points, only sampled positions of these pole trajectories are available. An interpolation approach can therefore involve replacing the original trajectories with artificial ones that connect the known points. A crucial aspect of this strategy is ensuring that the selected artificial trajectories adhere to the system's known a priori properties (see Section 5.3).

In the previous sections, hyperbolic lines were proposed as artificial trajectories connecting known samples. This choice was made because it preserves stability and provides a guaranteed upper bound on the deviation from the known models. In section all the possible trajectories that satisfy this condition are presented paving the way for incorporating a prior knowledge into the root loci if a particular problem is given. For further discussion the hyperbolic line remains as a particular example because in a later section 5.7 it serves as a reference for generalization.

The input data of the algorithm consists of static finite element method (FEM) data related to the structure at the two extreme ends of the parameter range. This means that the FEM model provides information about displacements regarding a certain load that is discussed later, at the minimum and maximum values of a given parameter

5.6.1 Overview of the algorithm

1. Model reduction
   (a) From the FEM data a Bernoulli beam models are generated.
   (b) The beam models are discretized and second order differential equations are generated.

2. The natural frequency sensitivity is evaluated to assess the quality of the system's sampling.
3. The transfer function is generated in partial fractional form
4. The interpolated transfer function is constructed.

The first step is not a standard approach to reduce a high fidelity FEM model. The usual approach is to make a modal analysis in FEM and then using model reduction methods the reduced model is generated. As it will be discussed later the standard model reduction methods are not the suitable tools for the presented interpolation method, because the reduced model has to be in a certain form (details below) and most of the techniques cannot guarantee that. In the following, a detailed algorithm is introduced. The rationale for each step and the reasoning behind the chosen method are provided after the relevant information has been presented. The high level flowchart is in figure 5.5. The steps of the algorithm are detailed, in the followings sections:

5.6.2 Model reduction

5.6.2.1 Creating Bernoulli beam model

Create a high-fidelity finite element model of the structure under investigation. Subject the structure to a pure bending and evaluate the resulting distortion using finite element analysis (FEA) software. Subsequently, calculate the flexural stiffness based on the observed distortion. This process mirrors the approach taken when analyzing a real beam-like structure to determine its structural properties, as described in [84], but here, the physical scenario is replicated within an FEA environment.

The followings are assumed:

- The structure can be modeled by a Bernoulli beam
- Regarding the Bernoulli beam the following is assumed:
  - Cross sections of the beam do not deform in a significant manner under the application of transverse or axial loads and can be assumed as rigid.
  - During deformation, the cross-section of the beam is assumed to remain planar and normal to the deformed axis of the beam.
- There is no bending-torsion coupling.

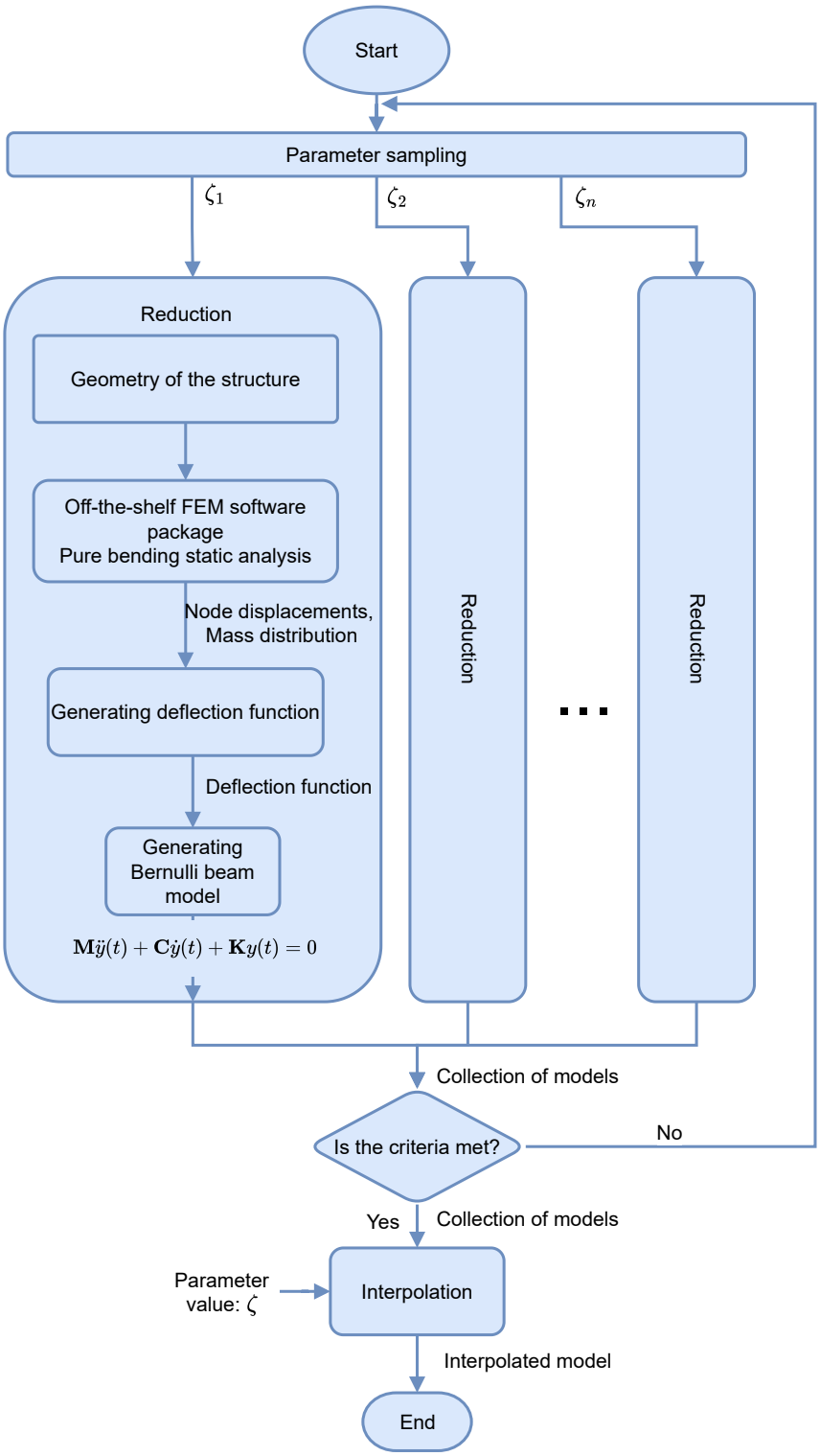

Figure 5.5: Flowchart of the algorithm

- The structure can be modeled as such a beam in which all the principal axes of the cross-sections of the beam are parallel.

- The load is transfered to the structure using a rigid endplate see figure 5.6.
- For flexural stiffness determination pure bending is acting on the structure which are created by equal and opposing forces and the deflections(i.e. node displacements) are readily available from FEA software

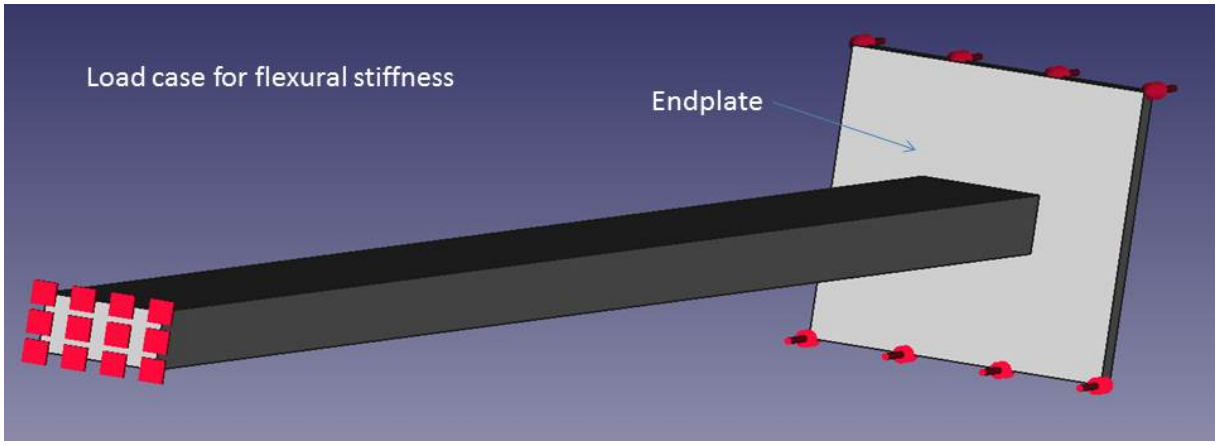

Figure 5.6: Load case

Discussion on the physical meaning and scope of applicability of the assumptions

The structure is modeled as a Bernoulli beam. This theory assumes that transverse shear deformations are negligible, which is appropriate for slender beams where the length is significantly greater than the cross-sectional dimensions. It is particularly suitable when bending dominates the response, and shear effects do not contribute appreciably to the overall deformation.

Within this modeling framework, further assumptions are made regarding the behavior of the beam's cross-sections. First, it is assumed that the cross-sections do not undergo significant deformation under applied loads and can be considered rigid. This means the shape and size of the cross-section remain essentially unchanged during loading, which is a valid assumption for beams made of stiff materials or with geometrically compact sections. Additionally, the cross-sections are assumed to remain planar and orthogonal to the deformed axis of the beam. This condition, central to Euler-Bernoulli theory, implies that no warping or shear distortion occurs and that the beam exhibits mostly pure bending deformation.

Another simplifying assumption is the absence of bending-torsion coupling. Physically, this means that the effects of torsion and bending can be treated independently, and one does not influence the other. This assumption holds when the cross-section is symmetric and loading is applied through the shear center, such that torsional and flexural responses are decoupled.

The model also assumes that all principal axes of the cross-sections remain parallel along the length of the beam. This implies a geometrically uniform or symmetrically varying beam without twist or out-of-plane curvature, ensuring that bending occurs consistently in the defined principal directions.

Finally, the last two assumptions are introduced to suit the subsequent calculations.

Here the used FEA software is Calculix (http://www.calculix.de/) in combination with FreeCad CAD system (https://www.freecadweb.org/). All this software is free.

5.6.2.2 Calculating flexural stiffness

The theory behind this calculation is summarized as follows. Assume that the principal axes of the cross-sections of the beam under investigation are parallel. Choose a coordinate system regarding a beam in a way that the x-axis is parallel with the longitudinal axis of the beam while one of the y or z-axis is parallel with one of the principal axis of the cross-section. For a Bernoulli beam the following equation can be applied [85]:

$$v''(x) = -\frac{M_z(x)}{D(x)} \tag{5.48}$$

where $D(x)$ is the flexural stiffness at the location x, $M_z(x)$ is the bending moment at location x and v is the displacement of the beam. The function $D(x)$ is often referred as $E(x)I(x)$, where $E(x)$ denotes the Young's modulus at position x, and $I(x)$ is the second moment of area at that same point.

We know the displacement of the nodes of the FEM model and we know the bending moment at each cross-section, the aim is to calculate the $D(x)$ flexural stiffness function along the beam.

Next the process of calculating flexural stiffness is presented. The basic approach is that we choose a line segment inside the point cloud of the nodes and every node is projected to that line segment. The line segment represents the neutral line so it has to be chosen accordingly. The starting point of this line segment should be at the clamped end of the structure while the other end should be at the other end of the structure. Now we define a coordinate system that has an x-axis that is collinear with the defined line segment and the origin is at the clamped end of the structure and it is directed to the other end of the projection line. The y axis of this coordinate system is perpendicular to the x axis. In this $x - y$ system we can plot the projected node position versus node displacements and a polynomial can be fitted to this set of data. To determine $D(x)$, the second derivative of the resultant polynomial is computed. It is worth noting that the precise selection of the projection line—ideally aligned with the neutral line—is beyond the current scope and is reserved for future work.

Step-by-step procedure:

5.6 Interpolation Algorithm

1. Translate the origin to the beginning of the projection line. The starting point of the projection line is $\underline{p_1}$ the endpoint is $\underline{p_2}$. Let the i^{th} vector of a node be $\underline{n_i} = [n_{xi}, n_{yi}, n_{zi}]$. Then the i^{th} translated node vector is $\underline{n_{ti}} = \underline{n_i} - \underline{p_1}$.

2. Compute the unit vector of the projection line. Let the unit vector of the projection line be p_u. So:

$$\underline{p_u} = \frac{\underline{p_2} - \underline{p_1}}{\left\|\underline{p_2} - \underline{p_1}\right\|_2} \tag{5.49}$$

3. Project the nodes to the projection line. Let the projected nodes be $\underline{n_p}$, then:

$$\underline{n_p} = \underline{\underline{n}}\,\underline{p_u} \tag{5.50}$$

   where $\underline{\underline{n}}$ matrix contains the coordinates of the nodes.

4. Delete all the nodes that are outside the line segment. Every element of $\underline{n_p}$ is omitted if the element value is less than zero or greater than $\left\|\underline{p_2} - \underline{p_1}\right\|_2$.

5. Compute the scalar displacements. There is a displacement vector associated with each node. In a bending load case there is only one direction where the displacement is significant so in order to avoid the introduction of a new coordinate frame the length of the displacement vector is used. Let $\underline{\underline{d}}$ be the matrix of the coordinates of the displacements. The i^{th} scalar displacement is $d_{si} = \left\|\underline{d_i}\right\|_2$

6. Fit a polynomial to the $\underline{n_p} \rightarrow \underline{d_s}$ data set. Since one end of the beam is clamped the displacement and the first derivative of the displacement function at the clamping are zero because it is the boundary condition for clamped constrain. Therefore, the zero order and first order term in the fitted polynomial have to be zero. So the fitting is carried out as follows [86]:

$$\underbrace{\begin{bmatrix} n_{p1}^k & n_{p1}^{k-1} & \dots & n_{p1}^2 \\ n_{p2}^k & n_{p2}^{k-1} & \dots & n_{p2}^2 \\ \vdots & \vdots & \ddots & \vdots \\ n_{pN}^k & n_{pN}^{k-1} & \dots & n_{pN}^2 \end{bmatrix}}_{\underline{\underline{M}}} \underbrace{\begin{bmatrix} a_n \\ a_{n-1} \\ \vdots \\ a_2 \end{bmatrix}}_{\underline{\Theta}} = \begin{bmatrix} d_{s1} \\ d_{s2} \\ \vdots \\ d_{sN} \end{bmatrix} \tag{5.51}$$

   where n_{pj}^k refer to the k-th power of the x-coordinate of the j-th projected point and $a_n ... a_2$ are the coefficients of the polynomials.

So the least-squares approximation of the polynomial parameters $\underline{\Theta}$ are:

$$\underline{\Theta} = \underline{\underline{M}}^{+} \underline{d_s} \tag{5.52}$$

where "+" means pseudo-inverse that gives the least squares regression of the data [86].

7. Differentiate the polynomial twice in order to get v''.

5.6.2.3 Note on more realistic modeling

The main limitation of the above-described method is that it cannot handle bending-torsion coupling. One way to deal with this is that in the bending case and the torsion case ruled surface fitting is carried out. Since the approximating ruled surface is distorted and bent, a general method of ruled surface fitting should be applied, as in [87]. Bending-torsion coupling is significant in beam-like structures that are non-symmetric, composite, or curved. For example slender curved beams or structures with off-axis material properties.

In such cases, bending in one direction causes twisting (torsion) and vice versa, due to geometry or material anisotropy.

Ruled surface fitting involves approximating a complex, often distorted or bent surface using a surface generated by sweeping a straight line along a spatial curve. This is useful for modeling deformations in beams, especially when they twist and bend, as it provides a geometrically intuitive way to approximate the shape changes.

5.6.3 Transfer function approximation of Bernoulli beam

At this point, we have a differential equation that represents the Bernoulli beam model of the structure. A finite element model is generated from that model in the form [85]:

$$\mathbf{M}\ddot{y}(t) + \mathbf{C}\dot{y}(t) + \mathbf{K}y(t) = 0 \tag{5.53}$$

- $\mathbf{M}, \mathbf{C}, \mathbf{K} \in \mathbb{R}^{N \times N}$ are the mass, damping, and stiffness matrices, respectively,
- $y(t) \in \mathbb{R}^N$ is the vector of generalised coordinates
- $t \in \mathbb{R}^+$ denotes time.

It is important to note that this finite element model is a reduced version. Creating a finite element model from the Bernoulli beam model is a standard textbook exercise [88–90], so it is not detailed here. Note that for damping, we will use Rayleigh damping but any diagonalizable damping is sufficient.

The important factor here is that the new model can contain the interpolation parameter ρ, which is not possible using ordinary FEM model. These parameters can be used to calculate the sensitivity of the natural frequency and by extension the sensitivity of the poles of the system. This is very important because if we can calculate the sensitivity of the poles regarding the parameters then the sampling density of the interpolation parameter can be checked. For now, the process of sensitivity analysis is presented, and its importance will be discussed in the next steps of the algorithm.

The sensitivity analysis is based on [91] the details can be found there. As it is shown in [91]:

$$\lambda_{i,\zeta} = \lambda_i \frac{\mathbf{u}_i^T \left(\mathbf{K}_\zeta - \lambda_i^2 \mathbf{M}_\zeta + i\lambda_i \mathbf{C}_\zeta\right) \mathbf{u}_i}{\mathbf{u}_i^T \left(\zeta_i^2 \mathbf{M} + \mathbf{K}\right) \mathbf{u}_i} \tag{5.54}$$

where:

- $\lambda_{i,\zeta} = \frac{\partial \lambda_i}{\partial \zeta}$ is the derivative of the i-th eigenvalue with respect to ζ,
- λ_i is the i-th natural frequency,
- $\mathbf{M}_\zeta, \mathbf{C}_\zeta, \mathbf{K}_\zeta$ are the derivative of the $\mathbf{M}, \mathbf{C}, \mathbf{K}$ with respect to ζ,
- $\mathbf{u}_i$ are the mode shapes at specific parameter value.

At this point it is obvious why it is important to have a model that contains the interpolation parameter. The matrices $\mathbf{M}_\zeta, \mathbf{C}_\zeta, \mathbf{K}_\zeta$ cannot be calculated otherwise.

Next using this result we show that a criterion can be given to the sampling of the interpolating parameter. If the criterion is met then the sampling is good enough if it is not then finer sampling is required.

If $G_1 = G_i$ corresponds to ζ_i and $G_2 = G_{i+1}$ corresponds to ζ_{i+1} and take the j-th pole p_{j1} of the system G_1 at ζ_i and the same pole p_{j2} of the system G_1 at ζ_{i+1} then it is easy to see that the position of the interpolated pole $p_{j\zeta}$ is in a circle:

$$p_{j\zeta} \in \{p_{j1} + t|(\zeta - \zeta_i)\lambda_{j,\zeta}|e^{i\theta} : \quad \forall t \in [0,1] \; and \; \forall \theta \in [0, 2\pi) \; and \; \zeta_i \leq \zeta \leq \zeta_{i+1}\} \tag{5.55}$$

and similarly if we take the estimation from the other end of the interpolating parameter:

$$p_{j\zeta} \in \{p_{j2} + t|(\zeta_{i+1} - \zeta)\lambda_{j,\zeta}|e^{i\theta} : \quad \forall t \in [0,1] \; and \; \forall \theta \in [0, 2\pi) \; and \; \zeta_i \leq \zeta \leq \zeta_{i+1}\} \tag{5.56}$$

Let the circle around p_{j1} when $\zeta = \zeta_{i+1}$ be C_{j1} and the circle around p_{j2} when $\zeta = \zeta_i$ be

C_{j2}. So:

$$C_{j1} = \{p_{j1} + t|(\zeta_{i+1} - \zeta_i)\lambda_{j,\zeta_i}|e^{i\theta} : \quad \forall t \in [0,1] \; and \; \forall \theta \in [0, 2\pi)\}$$
$$C_{j2} = \{p_{j2} + t|(\zeta_{i+1} - \zeta_i)\lambda_{j,\zeta_{i+1}}|e^{i\theta} : \quad \forall t \in [0,1] \; and \; \forall \theta \in [0, 2\pi)\}$$

Let:

$$\mathcal{D} = \{D_j = C_{j1} \cup C_{j2} : j = 1, 2, 3...n\}, \tag{5.57}$$

where n is the number of poles. Each D_j can either be connected or disjoint, depending solely on the properties of C_{j1} and C_{j2}. From now on we say D_j is connected meaning C_{j1} and C_{j2} are overlapping.

Let:

$$\mathcal{S} = \bigcup_{j=1}^{n} D_j \tag{5.58}$$

Notice that if all D_j are connected, then $\mathcal{S}$ can contain at most n disconnected regions. These regions are the D_j, and they are formed by overlapping circles.

Now, we describe the sampling criteria of the system. As it is stated before the interpolated poles must lie on an artificial trajectory between the end positions that are the samples of the system under examination. But it has to be known which pole corresponds to which pole. In 5.2, pole matching was used based on their hyperbolic distance but it has no guarantee that the poles matched correctly. This is primarily due to the absence of an estimation for the fineness of sampling across the parameter range. Assuming that every D_j is connected for any sampling, we can define the criterion:

Criterion 1. *If the set $\mathcal{S}$ on the complex plane contains exactly n disjoint subsets then the pole matching problem is perfectly solved and the interpolating parameter sampling is sufficient, where n is the number of poles.*

In other words, if every D_j is connected and the sets satisfy $D_j \cap D_i = \emptyset$ for all $i \neq j$ (i.e., each compound set D_j, formed by a pair of circles, is disjoint from all others), then the sampling is fine enough.

In the following, we prove that if the circles C_{j1} and C_{j2} overlap for every sampling (i.e., all the D_j are connected), then there exists a sampling that generates exactly n disjoint regions on $\mathcal{S}$.

Proof. Let p_{j1} and p_{j2} denote the j-th pole at ζ_i and ζ_{i+1}, respectively. Let $\lambda_{j,1}$ and $\lambda_{j,2}$ be the sensitivities of the j-th pole at ζ_i and ζ_{i+1}.

Given that:

- the roots of a polynomial change continuously as its coefficients vary continuously,

- the sensitivity of the poles (see equation 5.54) is a continuous function of ζ,
- the diameters of the circles C_{j1} and C_{j2} are continuous functions of ζ, based on equations 5.55 and 5.56,

the following limits hold:

$$\lim_{\zeta \to \zeta_i} p_{j\zeta} = p_{j1}, \qquad \lim_{\zeta \to \zeta_i} \lambda_{j\zeta} = \lambda_{j1}.$$

Here, ζ approaches ζ_i from the direction of ζ_{i+1}.

The limit represents finer sampling, as increasingly finer discretization causes the poles and their sensitivities to become progressively closer.

Based on the limits above and equation 5.55, the diameter of the circles C_{j1} and C_{j2} tends to zero as ζ approaches ζ_i. Since no two poles can occupy the same location, there must exist a sampling such that all connected D regions are disjoined from each other.

□

It follows that the regions $D_j, j = 1, 2, 3...n$, formed by the union of overlapping circles corresponding to the same pole across sampled values of ζ, vary continuously as well. Therefore, under sufficiently fine sampling, each D_j remains connected, and disjointness between different D regions can be maintained, ensuring reliable pole matching.

Note that it does not matter whether we use hyperbolic or Euclidean geometry, since they have the same topology [19].

The intuition behind this is that the sensitivity of the poles determines their possible locations as the parameter varies from its initial to final value. Each pole must remain within a certain region—specifically, within a defined circle C_{j1} at the starting value and within another circle C_{j2} at the ending value of the parameter. This overlap indicates that the two different estimates are consistent. We assume the model does not vary so drastically that the region D_j becomes disconnected. If all the overlapping pairs of circles are disjoint, then we have identified the correct pole matching. If this criterion is met, then the sampling of the system is sufficient; otherwise, the sampling needs to be finer.

5.6.4 Compute the poles and the residuals of G_1,G_2.

This step is straightforward, given the assumption in Section 5.3 that the system admits a partial fraction decomposition.

5.6.5 Construct the interpolated transfer function

As stated in 5.2, the formula for the interpolated transfer function assuming hyperbolic line between each corresponding pole and linear interpolation between residuals is:

$$H_\rho(z) = \sum_{i=1}^{n} \frac{r_i(\rho)}{z - p_i(\rho)} \tag{5.59}$$

where

$$p_i(\rho) = \frac{p_{i1} - \rho w_i}{1 - \rho w_i \overline{p_{i1}}} \tag{5.60}$$

$$r_i(\rho) = (1 - \rho) r_{i1} + \rho r_{i2} \tag{5.61}$$

and

$$w_i = \frac{p_{i1} - p_{i2}}{1 - p_{i2} \overline{p_{i1}}}. \tag{5.62}$$

In 5.60, the parameter ρ varies from 0 to 1. The formula used represents a parametrization of a hyperbolic line, for which we need to compute w_i (see [20]). We can interpret it in a way that ρw_i is a straight line not just in the hyperbolic sense but also in the Euclidean sense and that it is transformed using a congruent transformation to become the pole trajectory. This kind of transformation is always a Möbius transformation on the hyperbolic plane [20].

If we assume a general trajectory $t(\rho)$ then we can also use the same transformation so we can write:

$$p_i(\rho) = \frac{p_{i1} - t(\rho) w_i}{1 - t(\rho) w_i \overline{p_{i1}}} \tag{5.63}$$

The relevance of this type of construction is shown in the next section.

5.7 Boundedness and Stability

In earlier work, hyperbolic lines were proposed as artificial trajectories between known samples, owing to their stability-preserving nature and the existence of a guaranteed upper bound on the deviation from the known models. Since hyperbolic lines lie entirely within the unit circle, the poles of the interpolated system also remain inside the unit circle, ensuring system stability. In 5.2, these stability properties and deviation bounds are derived specifically for hyperbolic lines. Here, we extend the proof to cover all trajectories that satisfy the same bound.

The hyperbolic line, as an artificial pole trajectory has favorable properties like stability preservation and uniform boundedness but never represents the behavior of the model and cannot be adapted to different situations. It is reasonable to assume that the places of the poles follow some pattern as the parameter changes and that is not a hyperbolic line. The interpolation

method should be able to handle this additional information. In this section, the goal is to find a set of trajectories that have the same properties as the hyperbolic line. Using a larger set of trajectories enables techniques that adapt to specific pole trajectories.

5.7.1 Set of bounded trajectories

The hyperbolic line is stability preserving and satisfy the following deviation bound:

$$\begin{aligned} \|G(\rho) - G_1\|_\infty &\leq f(G_1, G_2) = \max\{g_1(G_1, G_2), g_2(G_1, G_2)\} \\ \|G(\rho) - G_2\|_\infty &\leq f(G_1, G_2) = \max\{g_1(G_1, G_2), g_2(G_1, G_2)\} \end{aligned} \tag{5.64}$$

where

$$\begin{aligned} g_1(G_1, G_2) &= \sum_{i=1}^{n} \left(\max\{|r_{i1}|, |r_{i2}|\} \max\left\{ \left| \frac{1}{1-|p_{i1}|} \right|, \left| \frac{1}{1-|p_{i2}|} \right| \right\} + \left| \frac{r_{i1}}{\frac{p_{i1}}{|p_{i1}|} - p_{i1}} \right| \right) \\ g_2(G_1, G_2) &= \sum_{i=1}^{n} \left(\max\{|r_{i1}|, |r_{i2}|\} \max\left\{ \left| \frac{1}{1-|p_{i1}|} \right|, \left| \frac{1}{1-|p_{i2}|} \right| \right\} + \left| \frac{r_{i2}}{\frac{p_{i2}}{|p_{i2}|} - p_{i2}} \right| \right) \end{aligned} \tag{5.65}$$

The detailed derivation can be found in 5.2. In order to create a self-contained derivation the first steps of the original derivation in 5.2 are repeated.

The rest of the section is devoted to the construction of a set that contains all the trajectories that satisfy eq. 5.64.

As assumed the systems $G(\rho)$ and G_1 have a partial fraction decomposition:

$$\|G(\rho) - G_1\|_\infty = \left\| \sum_{i=1}^{n} (P_i(\rho) - P_{i1}) \right\|_\infty \tag{5.66}$$

where

$$P_i(\rho) = \frac{r_i(\rho)}{z - p_i(\rho)}, \quad P_{i1} = \frac{r_{i1}}{z - p_{i1}}$$

Exploiting the subadditivity of the H_∞ norm from (5.66):

$$\|G(\rho) - G_1\|_\infty \leq \sum_{i=1}^{n} \|P_i(\rho) - P_{i1}\|_\infty \tag{5.67}$$

In the following, an upper bound is given on $\|P_i(\rho) - P_{i1}\|_\infty$.

$$\|P_i(\rho) - P_{i1}\|_\infty = \left\| \frac{r_i(\rho)}{z - p_i(\rho)} - \frac{r_{i1}}{z - p_{i1}} \right\|_\infty \leq$$
$$|r_i(\rho)| \left\| \frac{1}{z - p_i(\rho)} \right\|_\infty + \left\| \frac{r_{i1}}{z - p_{i1}} \right\|_\infty \tag{5.68}$$

Compute an upper bound term-by-term in (5.68). The last term can be calculated exactly since it is a first order system:

$$\left\| \frac{r_{i1}}{z - p_{i1}} \right\|_\infty = \max_{z=e^{i\omega}} \left| \frac{r_{i1}}{z - p_{i1}} \right| = \left| \frac{r_{i1}}{\frac{p_{i1}}{|p_{i1}|} - p_{i1}} \right| \tag{5.69}$$

The residual $r_i(\rho)$ in the first term is interpolated linearly:

$$|r_i(\rho)| = |(1 - \rho) r_{i1} + \rho r_{i2}| \leq \max\{|r_{i1}|, |r_{i2}|\} \tag{5.70}$$

The second term in (5.68) is also a first order system like the last term but it depends on ρ. As the first step one can write:

$$\left\| \frac{1}{z - p_i(\rho)} \right\|_\infty = \left| \frac{1}{\frac{p_i(\rho)}{|p_i(\rho)|} - p_i(\rho)} \right| = \left| \frac{|p_i(\rho)|}{p_i(\rho)(1 - |p_i(\rho)|)} \right| = \frac{|p_i(\rho)|}{|p_i(\rho)| \, |(1 - |p_i(\rho)|)|} =$$
$$\frac{|p_i(\rho)|}{|p_i(\rho)|} \left| \frac{1}{1 - |p_i(\rho)|} \right| = \left| \frac{1}{1 - |p_i(\rho)|} \right| = \left| \frac{1}{1 - \left| \frac{p_{i1} - \rho w_i}{1 - \rho w_i \overline{p_{i1}}} \right|} \right| \tag{5.71}$$

The expression

$$\left| \frac{p_{i1} - \rho w_i}{1 - \rho w_i \overline{p_{i1}}} \right| \leq 1 \tag{5.72}$$

is less than or equal to one because it represents the pseudo-hyperbolic distance between the complex numbers p_{i1} and ρw_i in the unit disk $\mathbb{D}$. Pseudo-hyperbolic distance is always less than or equal to one [19]. It is equal to one when one of the point is on the unit circle which cannot happen since we assumed stable systems.

In order to construct an upper bound the maximum of the expression

$$\max_\rho \left| \frac{1}{1 - \left| \frac{p_{i1} - \rho w_i}{1 - \rho w_i \overline{p_{i1}}} \right|} \right| \tag{5.73}$$

is needed. Since we discussed that the inner part $\left| \frac{p_{i1} - \rho w_i}{1 - \rho w_i \overline{p_{i1}}} \right|$ is less than one we can move the

maximum operation inside the expression:

$$\max_{\rho} \left| \frac{1}{1 - \left| \frac{p_{i1} - \rho w_i}{1 - \rho w_i \overline{p_{i1}}} \right|} \right| = \left| \frac{1}{1 - \max_{\rho} \left| \frac{p_{i1} - \rho w_i}{1 - \rho w_i \overline{p_{i1}}} \right|} \right| \tag{5.74}$$

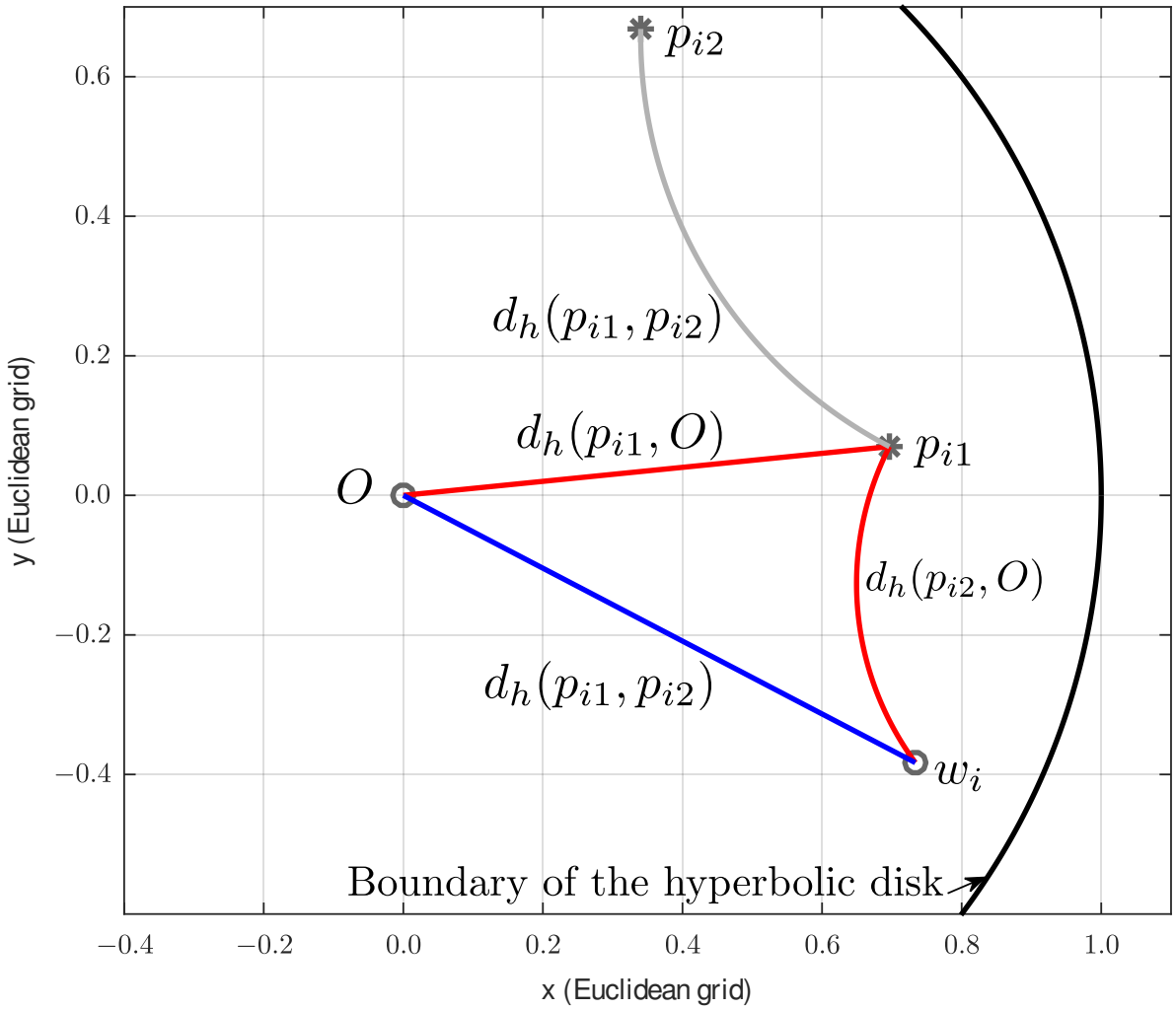

Figure 5.7: Geometric representation of the derivation of the upper bound

A geometric approach is used to find the maximum of $\left| \frac{p_{i1} - \rho w_i}{1 - \rho w_i \overline{p_{i1}}} \right|$ (see Figure 5.7). The term ρw_i traces a line segment from zero to w_i (blue line), while p_{i1} is a fixed point in the complex plane. The expression $\left| \frac{p_{i1} - \rho w_i}{1 - \rho w_i \overline{p_{i1}}} \right|$ represents the pseudo-hyperbolic distance between p_{i1} and any point along the segment defined by ρw_i. A key geometric property states that the maximum distance between a fixed point and a point on a line segment occurs at one of the endpoints of the segment (these are depicted as a red line segment). Therefore, the maximum in (5.74) is

reached when ρ takes either of its extreme values, $\rho = 0$ or $\rho = 1$. As discussed in Section 5.6, the values of $\frac{p_{i1}-\rho w_i}{1-\rho w_i \overline{p_{i1}}}$ at $\rho = 0$ and $\rho = 1$ are p_{i1} and p_{i2} respectively:

$$\left\| \frac{1}{z - p_i(\rho)} \right\|_\infty \leq \max \left\{ \left| \frac{1}{1 - |p_{i1}|} \right|, \left| \frac{1}{1 - |p_{i2}|} \right| \right\} \tag{5.75}$$

It is worth noting that the result in (5.75) is connected to the choice of $w_i = \frac{p_{i1}-p_{i2}}{1-p_{i2}\overline{p_{i1}}}$. w_i is a point with the property that the hyperbolic distance of w_i from the origin equals the hyperbolic distance between p_{i1} and p_{i2} and the hyperbolic distance of w_i from p_{i1} is equal to the hyperbolic distance between p_{i2} and the origin. The distance of w_i from the origin is a direct consequence of the definition of w_i.

After this, we can notice that the boundedness of the hyperbolic pole trajectory follows from the fact that the distance from a point to a line segment is maximal at one of the endpoints of the line segment see Figure 5.7.

In general, there is a set of curves that satisfy the condition that one of the endpoints is the furthest point from a given point in the plane. For example, see Figure 5.8. The furthest point on the line segment $\overline{w_i O}$ from p_{i1} is w_i in this example. The bound is determined by the furthest point, so every curve that starts from the origin O and ends at w_i with no point on that curve having a distance from p_{i1} which is greater than $d_h(p_{i1}, w_i)$ gives the same bound. The geometric constraint is that any candidate curve must lie in the hyperbolic circle around p_{i1} with radius $d_h(p_{i1}, w_i)$ and must start from origin and end at w_i.

It is obvious that the actual pole trajectory is obtained after the chosen $w_i O$ trajectory inside the boundary circle is transformed by equation (5.63).

5.8 MIMO extension

Let $H_\rho(z)$ be a transfer matrix. Each element of the matrix can be interpolated as a SISO system. For each element, there is an H_∞ upper bound estimate thus using the Gerschgorin theorem one can show that an upper bound estimate exists for the original system.

5.8.1 Maximal singular value estimation using Gerschgorin theorem

Estimate the greatest singular value $\bar{\sigma}(A)$ of the matrix $A \in \mathbb{C}^{n\times m}$ using the Gerschgorin theorem. According to the Gershgorin Circle Theorem [92], every eigenvalue λ of a matrix $A = [a_{ij}] \in \mathbb{C}^{n\times n}$ lies within at least one disk $D(a_{ii}, R_i)$, where $R_i = \sum_{j\neq i} |a_{ij}|$. Consider the matrix A^*A, where A^* is the complex conjugate transpose of A since this matrix is positive

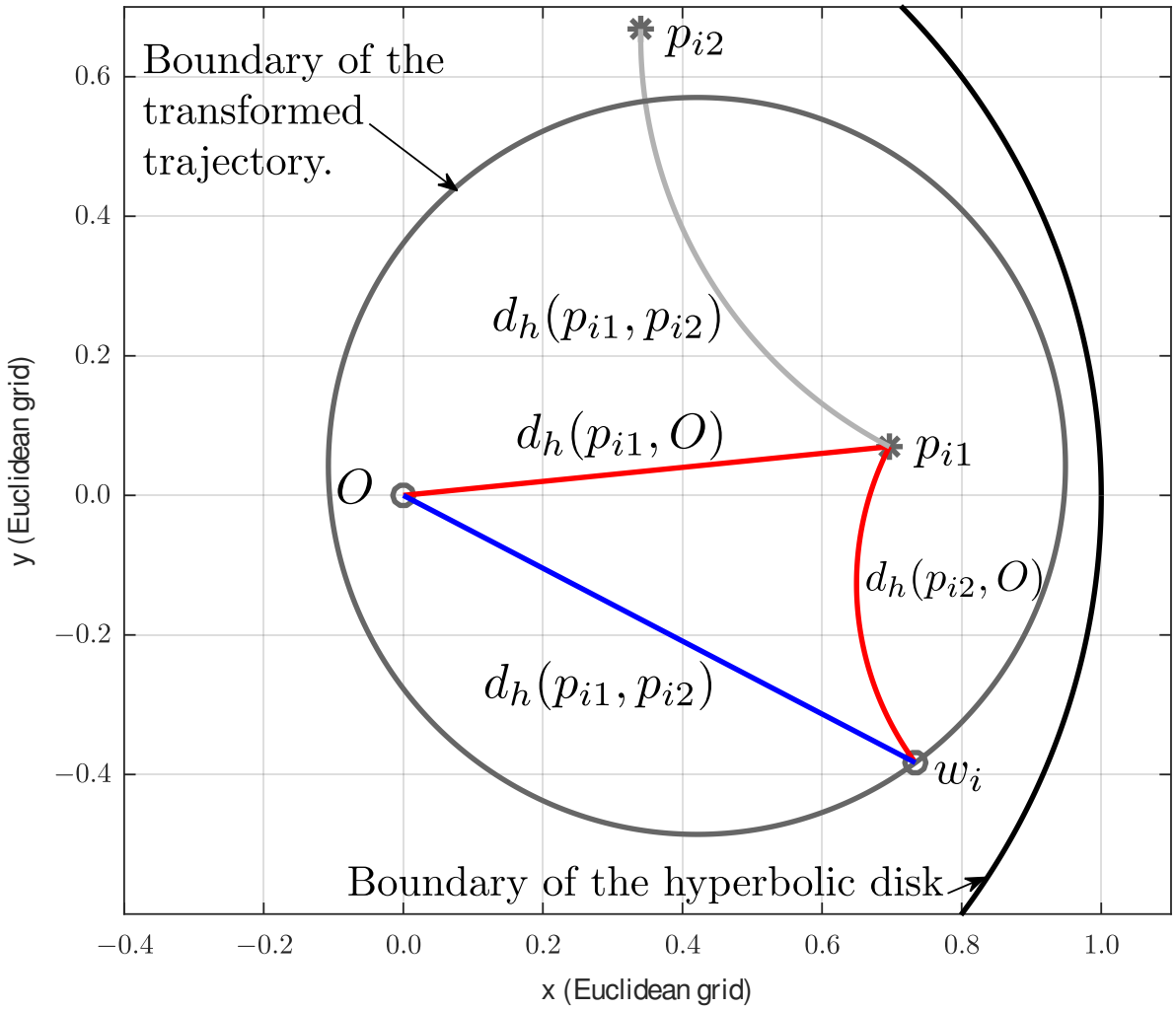

Figure 5.8: Basic geometric objects on Poincaré disk model of hyperbolic geometry

semi-definite, all its eigenvalues are real. Thus, by definition $\bar{\sigma}(A) = \sqrt{\lambda_{\max}(A^*A)}$ where $\lambda_{\max}$ is the largest eigenvalue of A^*A.

Gerschgorin theorem provides an estimate on the location of the eigenvalues so one can apply it to A^*A. Let a_{ij} be an element of A^*A and let the quantity R_i be $R_i = \sum_{j \neq i} |a_{ij}|$ sum of all non-diagonal elements in a row. A circle with center a_{ii} and radius R_i is called Gerschgorin circle D_i. According to Gerschgorin theorem the eigenvalues of A^*A lie in one of the Gerschgorin circles. Since all the eigenvalues of A^*A are real, the estimate of $\bar{\sigma}(A)$ is the largest point where a Gerschgorin circle intersects the real line.

Let $A \in \mathbb{C}^{n \times m}$ be a matrix. For the largest singular value $\bar{\sigma}$ of A the following holds:

$$\bar{\sigma}(A) \leq \sqrt{\max\{D_i \cap \mathbb{R}, i = 1 \ldots rank(A^*A)\}} = \sqrt{\max\{R_i + a_{ii}, i = 1 \ldots rank(A^*A)\}} \quad (5.76)$$

where D_i is the i^{th} Gerschgorin circle of A^*A, R_i is the radius of the i^{th} Gerschgorin circle and

a_{ii} is the i^{th} diagonal element of A^*A.

The inequality in (5.76) follows directly from the Gerschgorin theorem. The equality is true because the diagonal elements of A^*A are positive reals so the center points of the Gerschgorin circles lie on the real line so the greatest value where one of the Gerschgorin circles intersects the real line is $\max\{R_i + a_{ii}, i = 1 \dots rank(A^*A)\}$ It also means that

$$\bar{\sigma}(A) \leq \sqrt{\max\left\{\sum_{j=1}^{m} \left|a_{ij}\right|, i = 1 \dots m\right\}} \tag{5.77}$$

where a_{ij} is an element of A^*A.

5.8.2 Construction of upper bound for MIMO system

In this section, it is shown that the function f in (5.106) exists for a MIMO model if each element of the transfer matrix is interpolated piecewise as a SISO system. Thus, it is shown that a uniform bound can be given on the deviation of MIMO models $G(\rho)$ from G_1 in the form:

$$\|G(\rho) - G_1\|_\infty \leq g_1(G_1, G_2) \tag{5.78}$$

The deviation of $G(\rho)$ from G_2 can be calculated analogously.

Let the transfer matrix of the system $G(\rho) - G_1$ be $M_\rho(z)$. The problem is to find an upper bound estimate on the H_∞ norm of $M_\rho(z)$ that depends only on G_1 and G_2.

The H_∞ norm of $M_\rho(z)$ at a given parameter ρ is given by [93]:

$$\|G(\rho) - G_1\|_\infty = \left\|M_\rho(z)\right\|_\infty = \operatorname*{ess\,sup}_{\omega\in\mathbb{R}} \bar{\sigma}\left(M_\rho(e^{i\omega})\right) \tag{5.79}$$

where $\bar{\sigma}\left(M_\rho(e^{i\omega})\right)$ is the maximal singular value of the matrix $M_\rho(e^{i\omega})$ at a given ω. Every member of the studied class of systems (see Section 5.3) reaches its maximum on the unit circle, therefore there is no need for the essential supremum, simply a maximum can be used.

$$\|G(\rho) - G_1\|_\infty = \left\|M_\rho(z)\right\|_\infty = \max_{\omega\in\mathbb{R}} \bar{\sigma}\left(M_\rho(e^{i\omega})\right) \tag{5.80}$$

The upper bound of the H_∞ norm of $M_\rho(z)$ is

$$\left\|M_\rho(z)\right\|_\infty \leq \max_{\rho} \left\|M_\rho(z)\right\|_\infty = \max_{\rho} \max_{\omega\in\mathbb{R}} \bar{\sigma}\left(M_\rho(e^{i\omega})\right) \tag{5.81}$$

Let ω_0 and ρ_0 be the discrete frequency and parameter value where the maximal singular value of the matrix $M_\rho(e^{i\omega})$ reaches its maximum. Let $m_{ij} \in \mathbb{C}$ be an element of the matrix

$M_{\rho_0}(e^{i\omega_0})$. Compute the Gerschgorin estimate $\bar{\sigma}'$ of the maximal singular value $\bar{\sigma}$ of $M_{\rho_0}(e^{i\omega_0})$. As the first step, the elements of $M^*_{\rho_0}(e^{i\omega_0})M_{\rho_0}(e^{i\omega_0})$ need to be expressed. Let m'_{ij} be an element of $M^*_{\rho_0}(e^{i\omega_0})M_{\rho_0}(e^{i\omega_0}) \in \mathbb{C}^{n\times n}$ then:

$$m'_{ij} = \sum_{k=1}^{n} \overline{m_{ki}} m_{kj} \tag{5.82}$$

where bar means complex conjugate. So the Gerschgorin estimate $\bar{\sigma}'$ according to (5.77) is:

$$\bar{\sigma}' = \sqrt{\max\left\{\sum_{j=1}^{n}\left|m'_{ij}\right|, i = 1\ldots n\right\}} = \sqrt{\max\left\{\sum_{j=1}^{n}\left|\sum_{k=1}^{n}\overline{m_{ki}}m_{kj}\right|, i = 1\ldots n\right\}} \tag{5.83}$$

we can move the absolute value operation inside the summa and apply to each factors

$$\bar{\sigma}' = \sqrt{\max\left\{\sum_{j=1}^{n}\sum_{k=1}^{n}\left|\overline{m_{ki}}\right|\left|m_{kj}\right|, i = 1\ldots n\right\}}. \tag{5.84}$$

The value of $\bar{\sigma}'$ is the Gersgorin estimate for $\max_\rho \max_{\omega\in\mathbb{R}} \bar{\sigma}\left(M_\rho(e^{i\omega})\right)$. According to equation 5.77, this estimate is greater than the upper bound of the H_∞ norm of $M_\rho(z)$, that is:

$$\max_{\rho}\max_{\omega\in\mathbb{R}} \bar{\sigma}\left(M_\rho(e^{i\omega})\right) \le \bar{\sigma}'. \tag{5.85}$$

Notice that $\left|m_{ij}\right|$ is a value on the magnitude curve of a SISO transfer function at ω_0 and ρ_0 on the unit circle. The transfer function is $G(\rho_0)_{ij} - G_{1ij}$, following the definition of $M_\rho(z)$. The maximum of the magnitude curve of a SISO transfer function is equal to its H_∞ norm. Therefore, $\left|m_{ij}\right|$ cannot exceed $\left\|G(\rho_0)_{ij} - G_{1ij}\right\|_\infty$

$$\left|m_{ij}\right| \le \left\|G(\rho_0)_{ij} - G_{1ij}\right\|_\infty \le f_{1ij}(G_{1ij}, G_{2ij}) \tag{5.86}$$

where the function f_1 is the upper bound estimate for a SISO system according to Section 5.7. The second inequality follows from the existence of the upper bound for SISO systems (see Section 5.7). Thus, from (5.84) and (5.86) the following is true:

$$\bar{\sigma}' = \sqrt{\max\left\{\sum_{j=1}^{n}\sum_{k=1}^{n}\left|\overline{m_{ki}}\right|\left|m_{kj}\right|, i = 1\ldots n\right\}} \le \sqrt{\max\left\{\sum_{j=1}^{n}\sum_{k=1}^{n} f_{1ki}f_{1kj}, i = 1\ldots n\right\}} = \bar{\sigma}'' \tag{5.87}$$

Thus, the upper bound for a MIMO system exists and an estimate of it is $\bar{\sigma}''$ since

$$\|G(\rho) - G_1\|_\infty = \left\|M_\rho(z)\right\|_\infty \leq \max_{\rho} \max_{\omega \in \mathbb{R}} \bar{\sigma}\left(M_\rho(e^{i\omega})\right) \leq \bar{\sigma}' \leq \bar{\sigma}'' \tag{5.88}$$

5.9 Example

The interpolation and the usefulness in the optimization of this method are well documented in the previous sections. The example focuses on the construction of the Bernoulli beam model from FEM data.

We choose the simplest example in order to be able to verify the result using analytic calculations. Consider the massless cantilever beam that has a mass at the end (see Figure 5.9). This example is actually the building block of the lumped-mass FEM model of a Bernoulli beam therefore it can be easily extended to more complex cases.

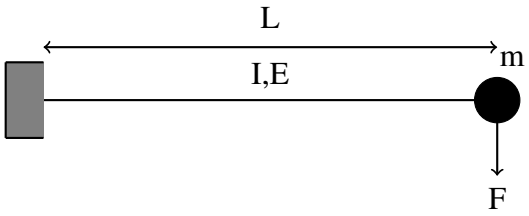

Figure 5.9: Cantilever beam with end mass

The beam is an aluminum rod with a rectangular cross-section of 20 mm × 40 mm, with the following parameters:

- $L = 1$ m
- $I = 26666\ mm^4$
- $E = 70$ GPa
- $m = 1$ kg

The applied load is a 0.1 Nm pure bending moment along the entire span. The unloaded nodes are projected onto the projection line (see Figure 5.10), then the corresponding displacement is carried to the next step.

In the next step, a polynomial is fitted to the projected data. Since the cross-section of the beam and the Young's modulus of the material remain constant throughout, the solution to the Bernoulli equation is a quadratic polynomial [89]; therefore, a quadratic function is selected for the fitting process. However, in more general cases, the order of the polynomial must be selected

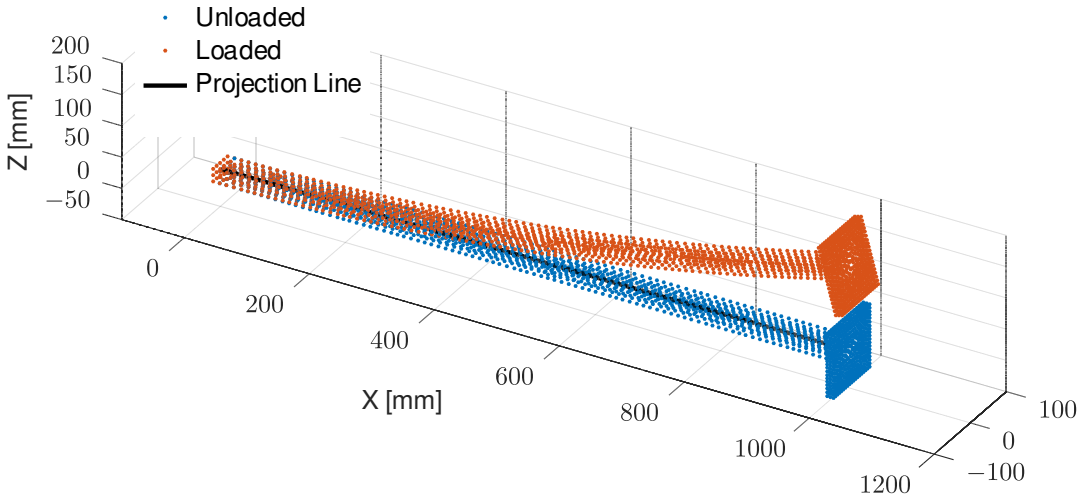

Figure 5.10: Loaded beam (The deformation is not to scale)

carefully to obtain an acceptable result while avoiding overfitting. A higher-order polynomial may provide a closer fit to the data points, but it could also introduce artificial oscillations that do not reflect the true behavior of the system. Conversely, a lower-order polynomial might fail to capture important features.

In Figure 5.11, the node data and the fitted polynomial are nearly indistinguishable due to the accuracy of the polynomial fit. To provide insight into the deviation between the fitted polynomial and the original data, an additional plot displaying the error between these two datasets is included.

Since the fitted polynomial is a quadratic polynomial, its second derivative is a constant value given by $v'' = -5.3327 \times 10^{-5}$. Using equation (5.48), the stiffness can be calculated as $IE_{FEM} = 1875.2$ N/m. The theoretical calculation gives $IE = 26666 \times 10^{-12} \times 70 \times 10^{9} = 1866.6$ N/m, resulting in an error of less than one percent.

We now derive the transfer function of the beam, where the input is a force applied perpendicular to the tip, and the output is the resulting deflection of the beam.

The cantilever beam is modeled as a spring-mass-damper system with Rayleigh damping. The stiffness of a massless cantilever beam with modulus E, moment of inertia I, and length L is [85]:

$$k = \frac{3EI}{L^3} \tag{5.89}$$

Rayleigh damping is defined as [77]:

$$c = \alpha m + \beta k \tag{5.90}$$

where α is the mass-proportional damping coefficient, and β is the stiffness-proportional

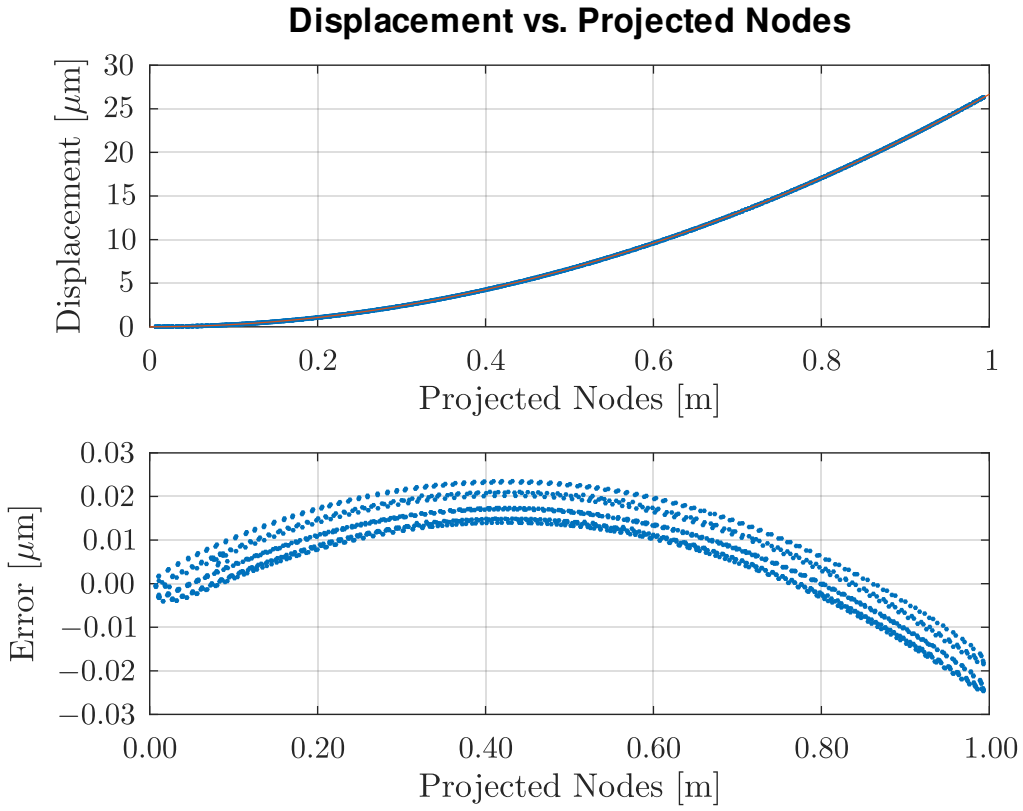

Figure 5.11: Polynomial fit for projected node data

damping coefficient.

The equation of motion for the mass m at the tip is:

$$m\ddot{x}(t) + c\dot{x}(t) + kx(t) = F(t) \tag{5.91}$$

Substituting $c = \alpha m + \beta k$:

$$m\ddot{x}(t) + (\alpha m + \beta k)\dot{x}(t) + kx(t) = F(t) \tag{5.92}$$

Taking the Laplace transform (assuming zero initial conditions):

$$ms^2X(s) + (\alpha m + \beta k)sX(s) + kX(s) = F(s) \tag{5.93}$$

Factoring $X(s)$:

$$X(s)\left[ms^2 + (\alpha m + \beta k)s + k\right] = F(s) \tag{5.94}$$

The transfer function is:

$$G(s) = \frac{X(s)}{F(s)} = \frac{1}{ms^2 + (\alpha m + \beta k)s + k} \tag{5.95}$$

After this point the result expressed in 5.2 and 5.4 applies.

5.10 Conclusion

This chapter proposed interpolation methods for parametric SISO LTI systems with a scalar parameter that preserve stability and provide computable H_∞ bounds on the deviation between the interpolated and sampled models. An extension was also given that preserves the minimum-phase property.

The core idea is to replace the unknown pole/zero trajectories of the original parametric system by artificial trajectories constructed between neighboring samples. The choice of these trajectories is decisive: it must preserve stability while enabling explicit deviation bounds. Hyperbolic lines satisfy these requirements, and the framework is further generalized by characterizing the class of admissible trajectories for which the boundedness proof remains valid, enabling an extension to MIMO settings.

To support vibration-oriented applications, a structure-preserving reduction procedure for beam-like structures was presented: starting from static FEM data, a reduced parametric second-order model consistent with Bernoulli (Euler–Bernoulli) beam theory is obtained, which keeps the mass–damping–stiffness structure required by the interpolation framework. A sampling criterion was also introduced to make pole correspondence between neighboring parameter samples unambiguous.

Future work focuses on improving accuracy and reducing conservatism (in particular for MIMO singular-value bounds), refining residue interpolation beyond linear rules, extending the approach to vector-valued parameters and higher-order sensitivity information, and analyzing error propagation due to polynomial fitting; incorporating Timoshenko beam models.

New scientific results:

Thesis 2. First part: *A stability preserving interpolation method is proposed for parametric SISO LTI system with a scalar parameter. The transfer function $\hat{H}_\rho(z)$ of the interpolated model is calculated by:*

$$\hat{H}_\rho(z) = \sum_{j=1}^{n} \frac{r_j(\rho)}{z - p_j(\rho)} = \sum_{j=1}^{n} \frac{(1-\rho)r_{ji} + \rho r_{ji+1}}{z - \frac{p_{ji} - \rho w_j}{1 - \rho w_j \overline{p_{ji}}}}. \tag{5.96}$$

where

$$\rho = \frac{\zeta - \zeta_i}{\zeta_{i+1} - \zeta_i} \quad \zeta_i \leq \zeta \leq \zeta_{i+1} \tag{5.97}$$

and

$$w_j = \frac{p_{ji} - p_{ji+1}}{1 - p_{ji+1}\overline{p_{ji}}}. \tag{5.98}$$

It is also proven that the deviation of the interpolated model $\hat{G}(\zeta)$ from the adjacent known models G_{i+1} and G_i is bounded in H_∞ sense by the function f that is:

$$\begin{aligned} \left\|\hat{G}(\zeta) - G_i\right\|_\infty &\leq f(G_i, G_{i+1}) \\ \left\|\hat{G}(\zeta) - G_{i+1}\right\|_\infty &\leq f(G_i, G_{i+1}) \quad \zeta_i \leq \zeta \leq \zeta_{i+1} \end{aligned} \tag{5.99}$$

where

$$f(G_i, G_{i+1}) = \max\{g_1(G_i, G_{i+1}), g_2(G_i, G_{i+1})\}. \tag{5.100}$$

where

$$g_1(G_i, G_{i+1}) = \sum_{j=1}^{n} \left(\max\{|r_{ji}|, |r_{ji+1}|\} \cdot \max\left\{ \left| \frac{1}{1 - |p_{ji}|} \right|, \left| \frac{1}{1 - |p_{ji+1}|} \right| \right\} + \left| \frac{r_{ji}}{\frac{p_{ji}}{|p_{ji}|} - p_{ji}} \right| \right) \tag{5.101}$$

$$g_2(G_i, G_{i+1}) = \sum_{j=1}^{n} \left(\max\{|r_{ji}|, |r_{ji+1}|\} \cdot \max\left\{ \left| \frac{1}{1 - |p_{ji}|} \right|, \left| \frac{1}{1 - |p_{ji+1}|} \right| \right\} + \left| \frac{r_{ji+1}}{\frac{p_{ji+1}}{|p_{ji+1}|} - p_{ji+1}} \right| \right) \tag{5.102}$$

Second part: *A stability and minimum phase preserving interpolation method is proposed for parametric SISO LTI system with a scalar parameter. The transfer function $\hat{H}_\rho(z)$ of the interpolated model is calculated by:*

$$\hat{H}_\rho(z) = ((1-\rho)k_1 + \rho k_2) \prod_{i=1}^{m} \left(z - \frac{z_{i1} - \rho v_i}{1 - \rho v_i \overline{z_{i1}}} \right) \prod_{j=1}^{n} \frac{1}{z - \frac{p_{j1} - \rho w_j}{1 - \rho w_j \overline{p_{j1}}}} \tag{5.103}$$

where

$$\rho = \frac{\zeta - \zeta_i}{\zeta_{i+1} - \zeta_i} \quad \zeta_i \leq \zeta \leq \zeta_{i+1} \tag{5.104}$$

and

$$w_j = \frac{p_{ji} - p_{ji+1}}{1 - p_{ji+1}\overline{p_{ji}}} \quad , v_i = \frac{z_{i1} - z_{i2}}{1 - z_{i2}\overline{z_{i1}}}. \tag{5.105}$$

It is also proven that the deviation of the interpolated model $\hat{G}(\zeta)$ from the adjacent known models G_{i+1} and G_i is bounded in H_∞ sense by the function f that is:

$$\begin{aligned} \left\|\hat{G}(\zeta) - G_i\right\|_\infty &\leq f(G_i, G_{i+1}) \\ \left\|\hat{G}(\zeta) - G_{i+1}\right\|_\infty &\leq f(G_i, G_{i+1}) \quad \zeta_i \leq \zeta \leq \zeta_{i+1} \end{aligned} \tag{5.106}$$

where

$$f(G_i, G_{i+1}) = \max\{g_1(G_i, G_{i+1}), g_2(G_i, G_{i+1})\}. \tag{5.107}$$

where

$$\begin{aligned} g_1(G_1, G_2) = &\max\{|k_1|, |k_2|\} \prod_{i=1}^{m} (1 + \max\{|z_{i1}|, |z_{i2}|\}) \cdot \\ &\prod_{j=1}^{n} \max\left\{\left|\frac{1}{1 - |p_{j1}|}\right|, \left|\frac{1}{1 - |p_{j2}|}\right|\right\} + \|G_1\|_\infty \end{aligned} \tag{5.108}$$

$$\begin{aligned} g_2(G_1, G_2) = &\max\{|k_1|, |k_2|\} \prod_{i=1}^{m} (1 + \max\{|z_{i1}|, |z_{i2}|\}) \cdot \\ &\prod_{j=1}^{n} \max\left\{\left|\frac{1}{1 - |p_{j1}|}\right|, \left|\frac{1}{1 - |p_{j2}|}\right|\right\} + \|G_2\|_\infty \end{aligned} \tag{5.109}$$

Corresponding publications: [GSS17], [GS18]

Thesis 3. *A structure-preserving reduction method and a sampling criterion are proposed for beam-like structures in order to make the pole matching problem unambiguous, which is a prerequisite for the interpolation framework. First, a practical reduction procedure is given that starts from static FEM data and constructs a parametric second-order model consistent with Bernoulli (Euler–Bernoulli) beam theory. The resulting reduced dynamics are kept in the second-order form*

$$\mathbf{M}\ddot{y}(t) + \mathbf{C}\dot{y}(t) + \mathbf{K}y(t) = 0, \tag{5.110}$$

which preserves the physically meaningful mass–damping–stiffness structure needed by the subsequent analysis.

Second, a sampling criterion is introduced to ensure correct pole correspondence between neighboring parameter samples. Using the sensitivity of the eigenvalues/natural frequencies with respect to the parameter the possible locations of each pole between two samples are bounded by circles around the end-point poles. The sampling is declared sufficient if these pole-specific regions remain separated.

5.10 Conclusion

Third, the interpolation framework is extended to MIMO systems, and the class of admissible pole trajectories that preserve the boundedness property is characterized, generalizing the approach beyond hyperbolic lines.

Corresponding publications: [GS25]

Chapter 6

LTI system pole identification based on the Fourier transform of Laguerre-coefficients

6.1 Introduction

The difference between time domain representation and frequency domain representations of signals allows engineers to approach the same signal from different aspects. As a result richer understanding can be achieved about the phenomena that is represented by the signal that is under investigation. Following this idea many representations of signals can be created. The question is if we gain new insight of the phenomena that is under investigation.

In this thesis a new signal transformation is proposed that can be parametrized, therefore, several representations of the signal can be generated. Instead of analyzing the signal in these new transformed domains as it is usually done, the following basic idea is proposed: the difference between representations can be exploited in order to gain new information about the signal. Needless to say that here the signals under investigation are frequency functions of an LTI system and the poles of that system are extracted. It is important to note that here we do not attempt to build a fully functional identification method only the fundamental features of this new approach, which compares transformed signals, are analyzed.

The outline of the basic idea is as follows: Let us denote the Laguerre transform with the parameter b_1 of a frequency function $F \in \mathrm{H}^2$ with $\mathcal{L}_{b1}\{F\}$ of an LTI system G and denote the Fourier transform of $f \in l^2$ with $\mathcal{F}\{f\}$. Let S_1 and S_2 be

$$\left.\begin{aligned} S_1 &= \mathcal{F}\{\mathcal{L}_{b1}\{F\}\} \\ S_2 &= \mathcal{F}\{\mathcal{L}_{b2}\{F\}\} \end{aligned}\right\} \; F \in \mathrm{H}^2 \tag{6.1}$$

It will be shown that once the difference between S_1 and S_2 is depicted then the poles of G can

be calculated analytically.

6.2 Model set and data

The presented method works on the following model set:

- Discrete linear time invariant system.
- Every system under investigation can be expressed as:

$$F(z) = \frac{A_1}{1 - a_1 z} + \frac{A_2}{1 - a_2 z} + \cdots + \frac{A_N}{1 - a_N z}, \tag{6.2}$$

  where N is finite. (Bar means complex conjugate.)
- Stable.
- There are no poles with multiplicity greater than one.

The input data of the identification method is the sampled frequency function of $F(z)$.

6.3 Pole identification using Laguerre coefficients

One can notice that the Laguerre coefficients in (4.18) form a geometrical sequence with quotient

$$q = \frac{\overline{a} - \overline{b}}{1 - \overline{a}b}.$$

The geometrical sequence is convergent if the system is stable and $a \in \mathbb{D}$ [41]. This connection between the Laguerre coefficients and the pole plays a key role in the presented method. For the sake of simplicity we can reformulate (4.18) as

$$A\frac{\sqrt{1 - |b|^2}}{(1 - \overline{a}b)} = fe^{i\delta} \qquad \frac{\overline{a} - \overline{b}}{1 - \overline{a}b} = re^{i\varphi} \tag{6.3}$$

so

$$l_n = fr^n e^{i(n\varphi + \delta)}. \tag{6.4}$$

If we consider the general case

$$F(z) = \frac{A_1}{z - a_1} + \frac{A_2}{z - a_2} + \cdots + \frac{A_N}{z - a_N},$$

the coefficients of Laguerre basis functions parametrized by b can be expressed as

$$\begin{aligned} l_n(b) &= f_1 r_1^n e^{i(n\varphi_1+\delta_1)} + f_2 r_2^n e^{i(n\varphi_2+\delta_2)} + \dots \\ &\quad + f_N r_N^n e^{i(n\varphi_N+\delta_N)} \qquad (n = 0, 1, 2, \dots). \end{aligned} \tag{6.5}$$

Notice that the above equation utilize the property of the model set possessing poles of multiplicity one.

The fact that the Laguerre coefficients are a sum of geometrical sequences is exploited to solve the pole identification problem.

As the first step the equation (6.5) should be reformulated into a vector form

$$\begin{aligned} \begin{bmatrix} l_1(b) \\ l_2(b) \\ \vdots \\ l_j(b) \\ \vdots \end{bmatrix} &= \begin{bmatrix} f_1 r_1 e^{i(\varphi_1+\delta_1)} \\ f_1 r_1^2 e^{i(2\varphi_1+\delta_1)} \\ \vdots \\ f_1 r_1^j e^{i(j\varphi_1+\delta_1)} \\ \vdots \end{bmatrix} + \begin{bmatrix} f_2 r_2 e^{i(\varphi_2+\delta_2)} \\ f_2 r_2^2 e^{i(2\varphi_2+\delta_2)} \\ \vdots \\ f_2 r_2^j e^{i(j\varphi_2+\delta_2)} \\ \vdots \end{bmatrix} + \dots \\ &\quad + \begin{bmatrix} f_{N-1} r_{N-1} e^{i(\varphi_{N-1}+\delta_{N-1})} \\ f_{N-1} r_{N-1}^2 e^{i(2\varphi_{N-1}+\delta_{N-1})} \\ \vdots \\ f_{N-1} r_{N-1}^j e^{i(j\varphi_{N-1}+\delta_{N-1})} \\ \vdots \end{bmatrix} + \begin{bmatrix} f_N r_N e^{i(\varphi_N+\delta_N)} \\ f_N r_N^2 e^{i(2\varphi_N+\delta_N)} \\ \vdots \\ f_N r_N^j e^{i(j\varphi_N+\delta_N)} \\ \vdots \end{bmatrix}. \end{aligned} \tag{6.6}$$

It is obvious that the pole identification problem can be interpreted as the solution of the system of equations (6.6). The general solution solves the system identification problem as the residues are also unknown variables. This mehod focuses on the pole identification with a partial solution of (6.6).

Before we discuss the proposed solution some observation should be taken. It is easy to see that the left side is known while the right side is unknown entirely; the number of variables and the number of poles are unknown, but finite according to our assumption. The number of the equations are infinite and it can be extended because every term in the equations belongs to a particular Laguerre parameter b. Therefore, we can choose different parameters and get the same number of systems of equations as many parameters b were chosen (see Fig.6.1). The ability to get different systems of equations with different Laguerre parameters is exploited in the presented method.

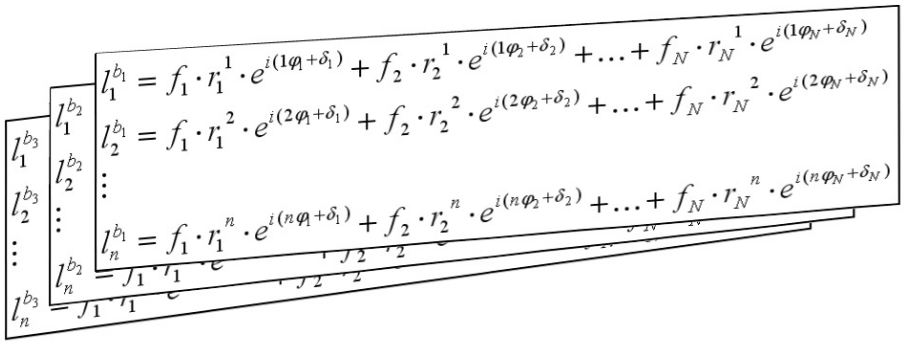

Figure 6.1: Extended set of system of equation

6.3.1 Partial solution of the system of equations generated by Laguerre coefficients

It is obvious that each column-vector at the right side of (6.6) is a geometric sequence with a complex quotient and the absolute value of the quotient is less then one because we assumed stability i.e. the series is convergent. We can consider this kind of geometric sequence as a discrete complex signal with an important feature namely it is oscillating (excluding some special cases). So the series of the Laguerre–coefficients is the *sum of oscillating signals*. We can take the discrete Fourier transform of the Laguerre–coefficients $(l_1, l_2 \ldots, l_n, \ldots)$ to obtain the components of the periodic contents in separated form. The components have $\varphi_1, \varphi_2, \ldots, \varphi_N$ frequencies so the result of the discrete Fourier transform contains local maxima at those frequencies. The discrete Fourier transform obviously exists as a convergent geometric sequence has a discrete Fourier transform. Hence, the finite sum of convergent geometric sequences has a discrete Fourier transform as well.

The frequencies of the peak values of the discrete Fourier transform $(\varphi_1, \varphi_2, \ldots, \varphi_N)$ are the arguments of the quotients of each geometric sequence. These arguments are functions of the Laguerre parameter b. Therefore, for example the first argument can be expressed according to (6.3) as:

$$\varphi_1(b_1) = arg(r_1 e^{i\varphi_1}) = arg\left(\frac{\overline{a_1} - \overline{b_1}}{1 - \overline{a_1} b_1}\right), \tag{6.7}$$

where a_1 is the first pole of the system and b_1 is the given Laguerre parameter.

At this point the peak values of the Fourier transform of the Laguerre coefficients and the pole are connected with the equation (6.7), from this relationship the pole can not be reconstructed because the place of the pole contains two parameters and only one of them is determined by the argument of the quotient. To overcome this problem another Laguerre parameter can be applied that generates a new system of equations like (6.6). So one can determine a pole by solving the

next system of equations:

$$\left.\begin{aligned}\varphi_1(b_1) &= arg\left(\tfrac{\overline{a_1}-\overline{b_1}}{1-\overline{a_1}b_1}\right)\\ \varphi_2(b_2) &= arg\left(\tfrac{\overline{a_1}-\overline{b_2}}{1-\overline{a_1}b_2}\right)\end{aligned}\right\}\rightarrow a_1 \tag{6.8}$$

The system of equations (6.8) can be applied on every pole, therefore, the pole identification problem can be solved. In the next section the analytic solution of (6.8) is presented.

6.3.2 Analytic solution of the system of equations that addresses the identification problem

The solution can be divided into two parts. The first one analyzes one equation of (6.8). The second part aims to solve the system of equations using the previously described analysis.

Take the following equation:

$$\varphi = arg\left(\frac{\overline{z}-\overline{b}}{1-\overline{z}b}\right) \tag{6.9}$$

where $z, b \in \mathbb{D}$, $\varphi \in \mathbb{R}$ and b, φ are constant.

It is shown next that this equation is an equation of an arc on the complex plane. It is trivial that the following equation

$$\varphi = arg\,(\overline{z}) \tag{6.10}$$

is an equation of a half-line on the complex plane since $\overline{z} = re^{i\varphi}$ satisfies (6.10) where $r \in \mathbb{R}^+$.

The term

$$\frac{\overline{z}-\overline{b}}{1-\overline{z}b} \tag{6.11}$$

is an argument transformation for the function (6.10). This means that those $\overline{z}$ are the solution of (6.9) that become a half-line in the form $re^{i\varphi}$ after the transformation (6.11). The transformation (6.11) is a Möbius transformation, therefore, the set of solutions is an arc [20]. It is also true that this arc can be considered a hyperbolic half-line on the Poincaré disk model becasue of the following: the general formula for all isometric transformation of the Poincaré disk model is:

$$w = \frac{\alpha z + \beta}{\overline{\beta} z + \overline{\alpha}} \quad \alpha, \beta \in \mathbb{C},\ |\beta|^2 - |\alpha|^2 = 1.$$

and with the choice of $\alpha = 1$ and $\beta = -\overline{b}$ the (6.11) takes the form of an isometric transformation

$$\frac{\overline{z}-\overline{b}}{1-\overline{z}b} = \frac{\overline{z}-\overline{b}}{-b\overline{z}+1}. \tag{6.12}$$

The solution of (6.10) is an origin crossing half-line and any isometric transformation on the

6.3 Pole identification using Laguerre coefficients

Poincaré disk transforms it into a hyperbolic line, therefore, the solution of (6.9) is a hyperbolic half-line.

In the following a parametrization of the arc that satisfies (6.9) is given. The parametrization is regarded on the whole circle that contains that arc. We can write:

$$re^{i\varphi} = \frac{\overline{z} - \overline{b}}{1 - \overline{z}b} \tag{6.13}$$

Then $\overline{z}$ can be expressed:

$$\frac{re^{i\varphi} + \overline{b}}{1 + re^{i\varphi}b} = \overline{z} \tag{6.14}$$

Some modification is required to express $\overline{z}$ in the form of the isometric transformation of the Poincaré disk model, so:

$$\overline{z} = \frac{re^{i\varphi} + \overline{b}}{1 + re^{i\varphi}b} = \frac{e^{-\frac{\varphi}{2}}}{e^{-\frac{\varphi}{2}}} \frac{re^{i\varphi} + \overline{b}}{1 + re^{i\varphi}b} = \frac{e^{\frac{\varphi}{2}}r + e^{-\frac{\varphi}{2}}\overline{b}}{e^{\frac{\varphi}{2}}rb + e^{-\frac{\varphi}{2}}} \tag{6.15}$$

Equation (6.15) is in the form of the general isometric transformation of the Poincaré disk model with $\alpha = e^{\frac{\varphi}{2}}$ and $\beta = e^{-\frac{\varphi}{2}}\overline{b}$.

In the following, we use the above described parametrization to solve the system of equation (6.8). Since in (6.8) the free variable is $\overline{a_1}$ we can write that up to the valid domain of (6.9) the following is true:

$$\left.\begin{aligned} \varphi_1(b_1) &= arg\left(\tfrac{\overline{a_1}-\overline{b_1}}{1-\overline{a_1}b_1}\right) \\ \varphi_2(b_2) &= arg\left(\tfrac{\overline{a_1}-\overline{b_2}}{1-\overline{a_1}b_2}\right) \end{aligned}\right\} \Leftrightarrow \left\{\begin{aligned} \overline{a_1} &= \tfrac{\alpha_1 r_1+\beta_1}{\overline{\beta_1} r_1+\overline{\alpha_1}} \\ \overline{a_1} &= \tfrac{\alpha_2 r_2+\beta_2}{\overline{\beta_2} r_2+\overline{\alpha_2}} \end{aligned}\right. \tag{6.16}$$

In (6.16) the first and second equations are equations of circles and we have to find the intersections of those circles, therefore, we can write:

$$\begin{aligned} \frac{\alpha_1 r_1 + \beta_1}{\overline{\beta_1} r_1 + \overline{\alpha_1}} &= \frac{\alpha_2 r_2 + \beta_2}{\overline{\beta_2} r_2 + \overline{\alpha_2}} \\ (\alpha_1 r_1 + \beta_1)\left(\overline{\beta_2} r_2 + \overline{\alpha_2}\right) &= (\alpha_2 r_2 + \beta_2)\left(\overline{\beta_1} r_1 + \overline{\alpha_1}\right) \\ \alpha_1\overline{\beta_2} r_1 r_2 + \beta_1\overline{\beta_2} r_2 + \alpha_1\overline{\alpha_2} r_1 + \beta_1\overline{\alpha_2} &= \alpha_2\overline{\beta_1} r_1 r_2 + \beta_2\overline{\beta_1} r_1 + \alpha_2\overline{\alpha_1} r_2 + \beta_2\overline{\alpha_1} \end{aligned} \tag{6.17}$$

6.3 Pole identification using Laguerre coefficients

Let

$$
\begin{aligned}
a_1 &= a_{r1} + ia_{i1} = \alpha_1\overline{\beta_2} \\
b_1 &= b_{r1} + ib_{i1} = \beta_1\overline{\beta_2} \\
c_1 &= c_{r1} + ic_{i1} = \alpha_1\overline{\alpha_2} \\
d_1 &= d_{r1} + id_{i1} = \beta_1\overline{\alpha_2} \\
a_2 &= a_{r2} + ia_{i2} = \alpha_2\overline{\beta_1} \\
b_2 &= b_{r2} + ib_{i2} = \beta_2\overline{\beta_1} \\
c_2 &= c_{r2} + ic_{i2} = \alpha_2\overline{\alpha_1} \\
d_2 &= d_{r2} + id_{i2} = \beta_2\overline{\alpha_1},
\end{aligned}
$$

then:

$$
\begin{aligned}
&(a_{r1}r_1r_2 + b_{r1}r_2 + c_{r1}r_1 + d_{r1}) + i\,(a_{i1}r_1r_2 + b_{i1}r_2 + c_{i1}r_1 + d_{i1}) = \\
&(a_{r2}r_1r_2 + b_{r2}r_1 + c_{r2}r_2 + d_{r2}) + i\,(a_{i2}r_1r_2 + b_{i2}r_1 + c_{i2}r_2 + d_{i2}) \\
&((a_{r1} - a_{r2})\,r_1r_2 + (b_{r1} - c_{r2})\,r_2 + (c_{r1} - b_{r2})\,r_1 + (d_{r1} - d_{r2})) + \\
&i\,((a_{i1} - a_{i2})\,r_1r_2 + (b_{i1} - c_{i2})\,r_2 + (c_{i1} - b_{i2})\,r_1 + (d_{i1} - d_{i2})) = 0.
\end{aligned} \tag{6.18}
$$

So we can split the equation into the real and the imaginary part and we can solve it as a system of equations. In order to simplify the notation let:

$$
\begin{aligned}
a_3 &= a_{r1} - a_{r2} \\
b_3 &= b_{r1} - c_{r2} \\
c_3 &= c_{r1} - b_{r2} \\
d_3 &= d_{r1} - d_{r2} \\
a_4 &= a_{i1} - a_{i2} \\
b_4 &= b_{i1} - c_{i2} \\
c_4 &= c_{i1} - b_{i2} \\
d_4 &= d_{i1} - d_{i2}
\end{aligned}
$$

so:

$$
\left.
\begin{aligned}
a_3r_1r_2 + b_3r_2 + c_3r_1 + d_3 = 0 \\
a_4r_1r_2 + b_4r_2 + c_4r_1 + d_4 = 0
\end{aligned}
\right\} \tag{6.19}
$$

6.3 Pole identification using Laguerre coefficients

If $a_3 \neq 0$ and $a_4 \neq 0$ then:

$$\left.\begin{aligned} r_1 r_2 + \tfrac{b_3}{a_3} r_2 + \tfrac{c_3}{a_3} r_1 + \tfrac{d_3}{a_3} = 0 \\ r_1 r_2 + \tfrac{b_4}{a_4} r_2 + \tfrac{c_4}{a_4} r_1 + \tfrac{d_4}{a_4} = 0 \end{aligned}\right\} \tag{6.20}$$

Now we can subtract the two equations from each other:

$$\left(\frac{b_3}{a_3} - \frac{b_4}{a_4}\right) r_2 + \left(\frac{c_3}{a_3} - \frac{c_4}{a_4}\right) r_1 + \left(\frac{d_3}{a_3} - \frac{d_4}{a_4}\right) = 0. \tag{6.21}$$

Let:

$$\begin{aligned} b_5 &= -\left(\frac{b_3}{a_3} - \frac{b_4}{a_4}\right) \\ c_5 &= \frac{c_3}{a_3} - \frac{c_4}{a_4} \\ d_5 &= \frac{d_3}{a_3} - \frac{d_4}{a_4} \end{aligned}$$

then if $b_5 \neq 0$

$$r_2 = \frac{c_5}{b_5} r_1 + \frac{d_5}{b_5}. \tag{6.22}$$

Let

$$\begin{aligned} c_6 &= \frac{c_5}{b_5} \\ d_6 &= \frac{d_5}{b_5} \end{aligned}$$

now we can substitute the expression of r_2 back to (6.19):

$$a_3 r_1 \left(c_6 r_1 + d_6\right) + b_3 \left(c_6 r_1 + d_6\right) + c_3 r_1 + d_3 = a_3 c_6 r_1^2 + \left(a_3 d_6 + b_3 c_6 + c_3\right) r_1 + \left(b_3 d_6 + d_3\right) = 0 \tag{6.23}$$

We can simply solve (6.23) with the quadratic formula and if the input parameters (i.e. φ_1,φ_2,b_1,b_2) are valid we get two distinct real solutions s_1 and s_2. One of the solutions is in the unit circle since it represents the intersection of two hyperbolic lines. Let us say that s_1 is that solution. So we can substitute s_1 into one of the equations of (6.16) and we get the pole:

$$a_1 = \frac{\overline{\alpha_2} s_1 + \overline{\beta_2}}{\beta_2 s_1 + \alpha_2} \tag{6.24}$$

6.4 Numerical example

In this section the pixel dynamics of the TFT based indoor positioning system is identified with the proposed method. The basic idea of the TFT based positioning system is shortly summarized in the following [Gőz15], [Gőz10].

6.4.1 Operation principle of TFT based positioning

In order to describe the main idea behind the TFT technology based indoor positioning method, let us recall the main concept of camera based positioning first. For this, consider a pinhole camera model and a point light source moving in front of the camera. (See Figure 6.2). The direction of the light source relative to the camera can be characterized by the angle of arrival, which is the angle between the optical axis and the line connecting the light source with its 2D image on the camera screen Figure 6.2. The angle of arrival can be determined from the position of the image and the distance between the screen and the hole. In this setup the position of the hole is fixed, while the location of detection (i.e. the position of the image on the screen) changes according to the actual position of the light source. Now let the functions be switched: let the location of detection be fixed at the center of the screen and allow the hole to move. Then, the angle of arrival can be determined as follows: move the hole until the sensor is able to detect the light source, then compute the angle by using the position of the hole and the distance between the hole and the screen (see Figure 6.3). Therefore, the algorithm is as simple as in the previous case. At the same time, this slight conceptual modification has a significant advantage: a pinhole camera with movable hole can be realized with simple elements, which results in significant reduction in the cost and complexity of the positioning system.

The front panel of the pinhole camera can be constructed from a TFT unit. A regular TFT display can be disassembled to a TFT unit and a backlight panel as shown in Figure 6.4. If one uses only black and white colors in the image plane, the TFT unit can be interpreted as a special window that can be transparent or opaque according to the image displayed. Thus, by leaving only a small transparent patch and driving every other pixel of the TFT unit into the opaque state a hole can be formed, which is also moveable as the patch can be placed anywhere on the TFT.

The point light source can be a light emitting diode (LED) while the detector, which is placed in the center of the image plane behind the TFT unit, can be any light sensitive element, e.g. a photodiode. If the patch tracks the LED (marker), the instrument can maintain continuous direction measurements frame by frame that are displayed on the TFT panel. To simplify the marker tracking task four independent photodiodes are used according to Figure 6.5. The photodiodes form a square shaped array where a photodiode is placed on each corner of the square. This sensor array is rotated 45 degrees relative to the TFT pixel grid. This arrangement

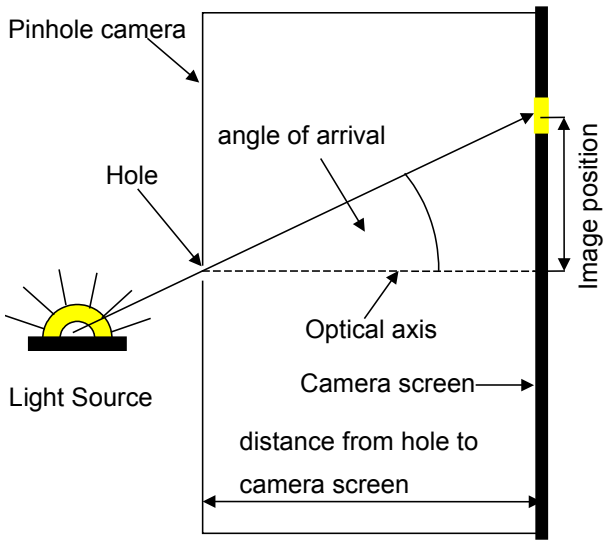

Figure 6.2: Angle of arrival determination with simple pinhole camera

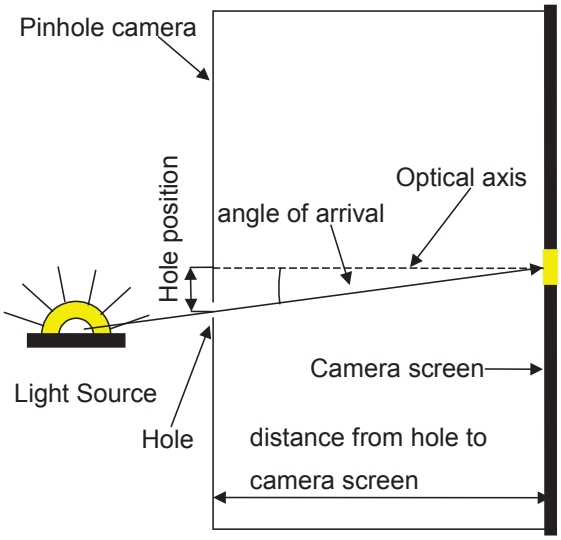

Figure 6.3: Angle of arrival determination with modified movable hole pinhole camera

allows to determine the heading of the marker. The fifth photodiode in the middle of the sensor array measures the absolute value of the luminous intensity of the LED.

The position of a marker can be determined at least from two measurements made by sensors positioned far enough from each other. Multiple marker detection is also possible, because on the same TFT image multiple pinhole camera can be created simultaneously by using multiple patches. Figure 6.6 shows the scheme of the positioning system.

The continuous operation requires exact knowledge of the LEDs. Searching the LEDs is required in two cases: for the initialization of the system and when the device loses the marker.

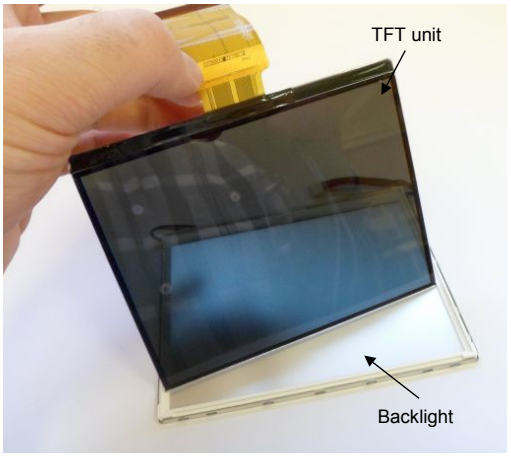

Figure 6.4: Disassembled TFT module

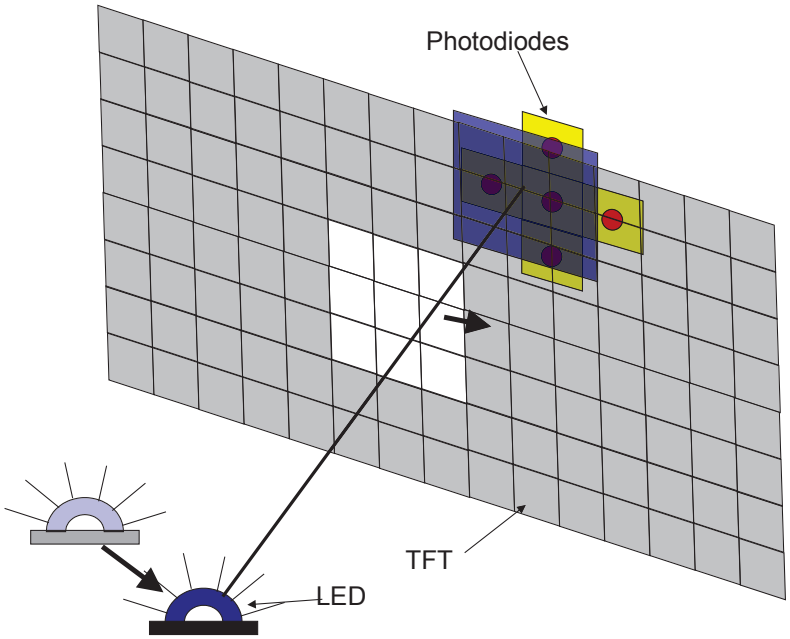

Figure 6.5: The LED tracking

Searching algorithms and the corresponding problems are not discussed here as it does not add anything to the understanding of the basic operation principle. The proposed device itself measures angle of arrival so in order to get 3D measurements, the principle of stereo-camera reconstruction should be used. This is discussed in details in [94, 95].

This positioning system has some potential advantages. It is well known [96] that reliable link can be established between the LED marker and the sensing element, which makes this system very insensitive to ambient light even if the ambient light changes rapidly. Since the number of sensing elements is small, the computational requirements are negligible compared to

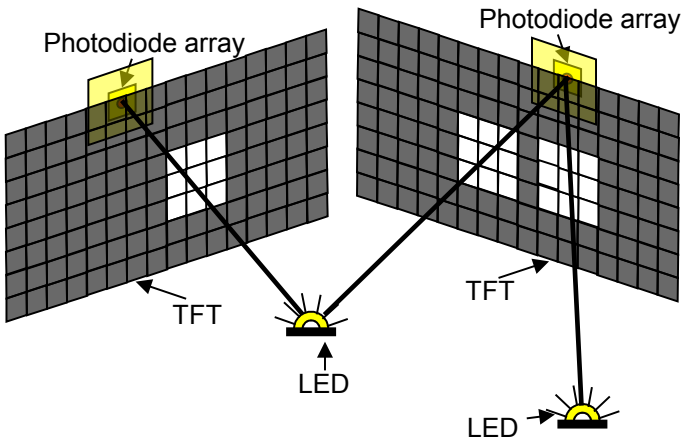

Figure 6.6: Theoretical scheme of the positioning system

image processing. Moreover, every part of the system is available on market in mass production so the price of the system is low.

6.4.2 Identification of pixel dynamics

The response of the pixel is very important from the aspect of positioning system because the marker tracking control has to be designed according to the pixel dynamics. The full dynamical model of the positioning system is presented in [Gőz15] here only the pixel dynamics are considered that can be modeled as a first order system and all the signals are taken from the simulation generated in [Gőz15] so the result can be compared to the correct value.

The presented example is a first order system with the transfer function:

$$F(z) = \frac{1}{z - 0.82}.$$

Measurement noise acts on the output. Since the input data of the method is the sampled frequency function of the system the applied input signal is multisine with 256 components. The output with the additive white noise can be seen in Fig. 6.7.

The peak to peak amplitude of the signal is about two hundred while the peak to peak amplitude of the noise is about fifty, of course the dimension of the amplitude is irrelevant.

The algorithm of the identification procedure is the following:

1. Choose a Laguerre parameter b_1.
2. Apply the multisine input.
3. Compute the frequency function.
4. Compute the Laguerre–coefficients .

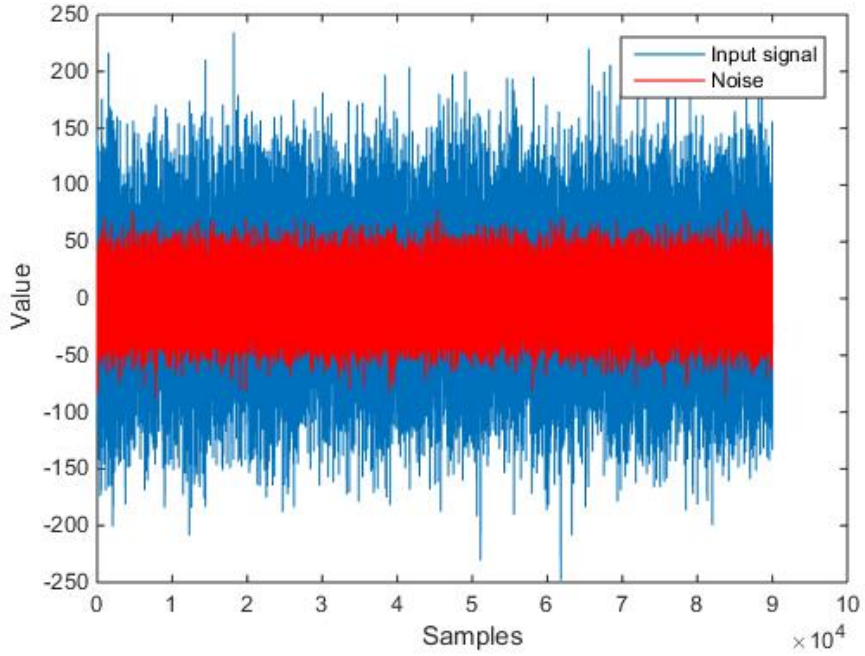

Figure 6.7: Output signal with noise

5. Compute the Fourier transform of the Laguerre–coefficients .
6. Determine $\varphi_1(b_1)$, $\varphi_2(b_1)$.
7. Repeat step 1–6 with b_2.
8. Solve the system of equations (6.8) with respect to each pole.

This example uses $b_1 = 0.8750 + 0.2843i$, $b_2 = 0.2 + 0.5i$. Fig. 6.8 shows the absolute value of the Fourier transform of the Laguerre–coefficients without noise. As it can be seen the number of peaks is equal to the number of poles and because of the finite number of Laguerre–coefficients spectral leakage appears. The effect of noise can be seen in Fig. 6.9. It is obvious that the peaks corresponding to the poles are significant and the peaks are almost at the same position. The problem is that we have to decide whether the other peaks represent other poles or not. To make a distinction between a pole generated peak and a noise generated peak further analysis is required, such as an iterative pole elimination [39]. In Fig. 6.10 and Fig. 6.11 the noiseless and the noisy case are presented when Laguerre parameter $b_1 = 0.8750 + 0.2843i$.

The identified pole in noisless case is $0.8192 - 0.0094i$ while in the noisy case the pole is $0.8114 + 0.0057i$. It is clear that the spectral leakage and the resolution of the Fourier transformation sets the practical barrier at this stage, but the noise immunity seems good even if the noisy case is not analyzed on a theoretical level.

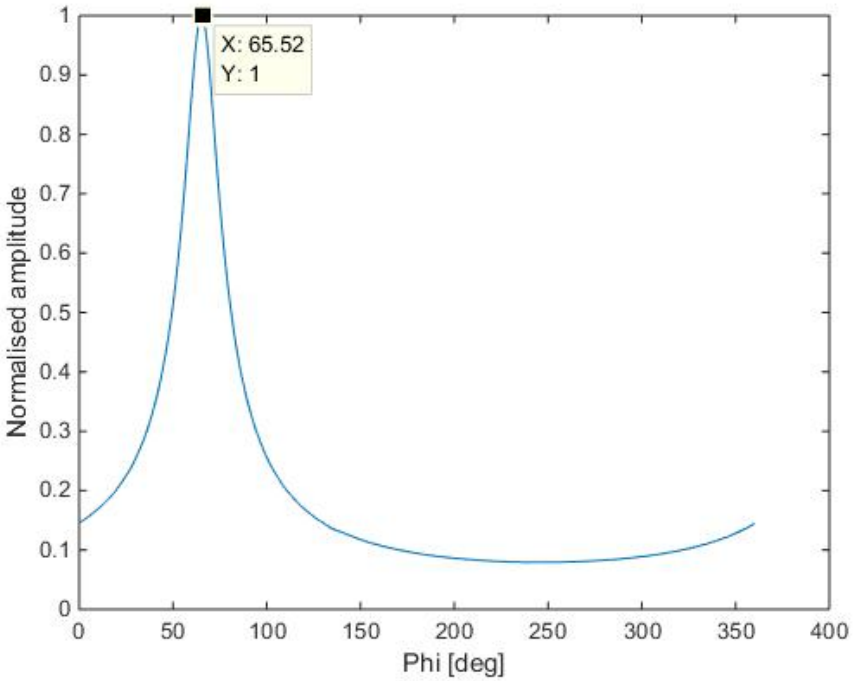

Figure 6.8: Fourier transform of Laguerre–coefficients without noise ($b_2 = 0.2 + 0.5i$)

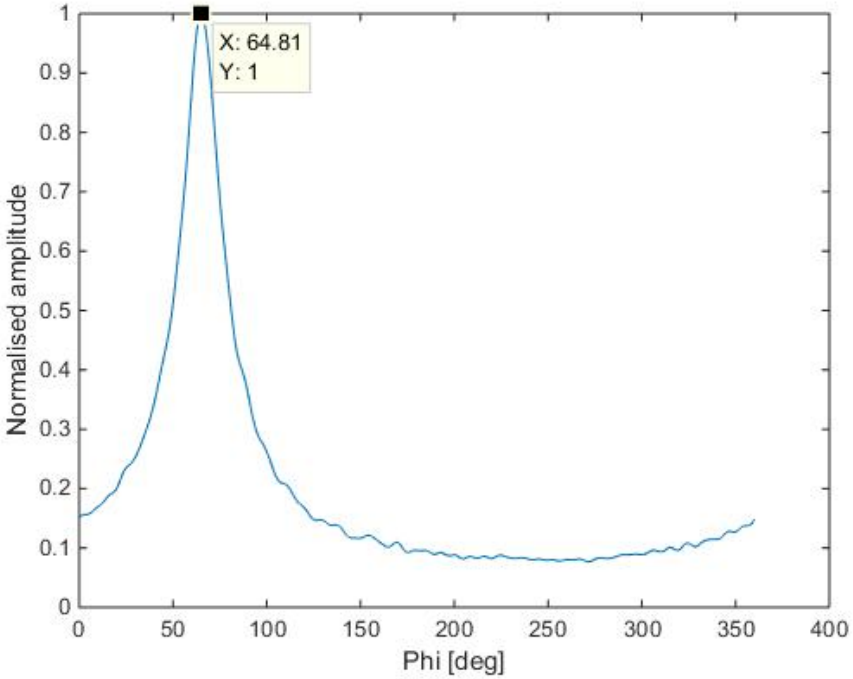

Figure 6.9: Fourier transform of Laguerre–coefficients with noise ($b_2 = 0.2 + 0.5i$)

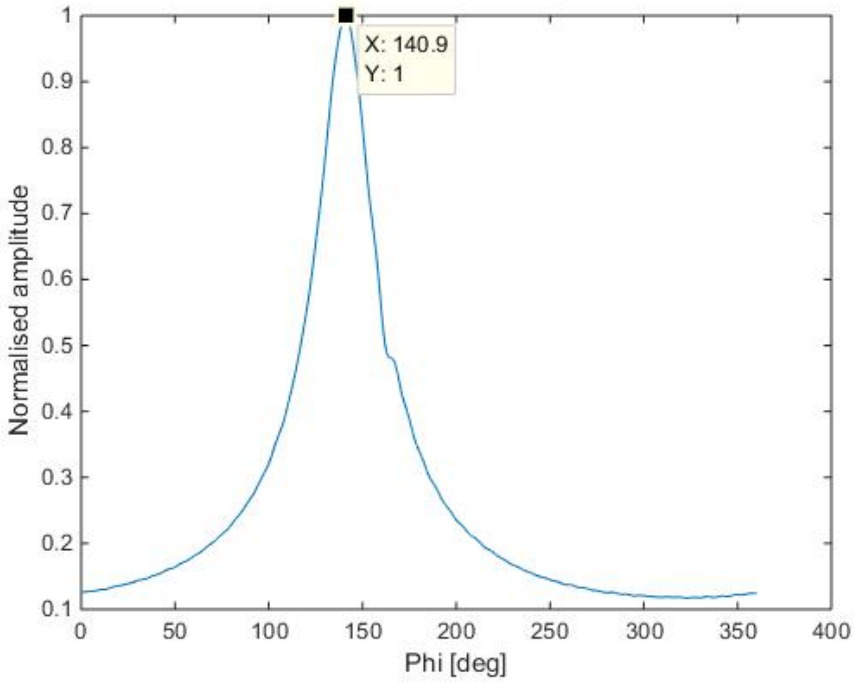

Figure 6.10: Fourier transform of Laguerre–coefficients without noise ($b_1 = 0.8750 + 0.2843i$)

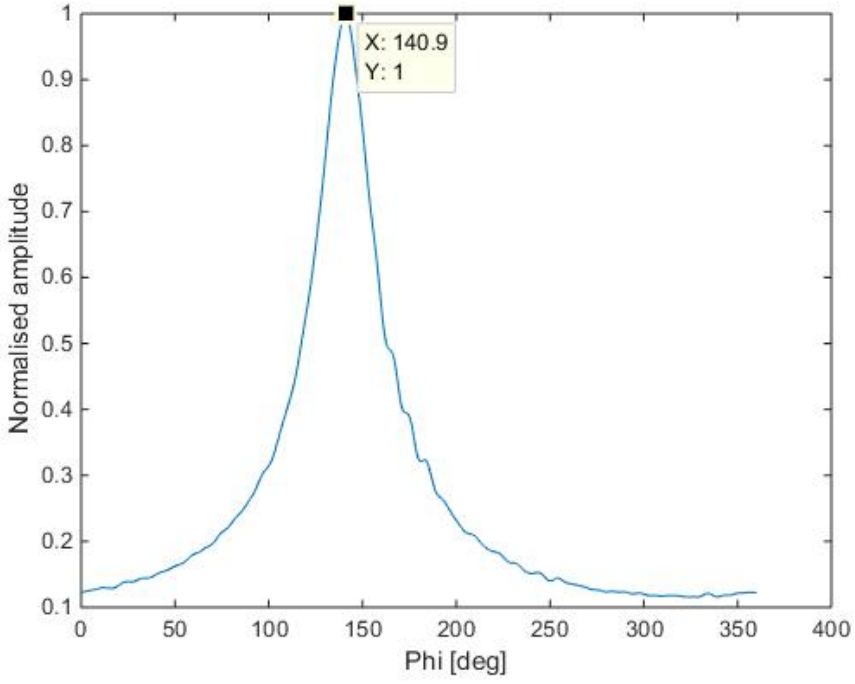

Figure 6.11: Fourier transform of Laguerre–coefficients with noise ($b_1 = 0.8750 + 0.2843i$)

6.5 Conclusion

An outline of a method for identification of system poles elaborated, and the basic properties were analyzed. The method utilizes the Fourier transform of the Laguerre–coefficients of the discrete–time systems represented on the unit disc. Beyond the conceptual clarity example also confirms that it forms an adequate basis for estimating poles of systems as a significant part of an identification process, nevertheless some issues — namely spectral leakage that is the consequence of the finite number of the available Laguerre–coefficients — require further research.

New scientific results:

Thesis 4. *A method for identification of system poles is proposed. The method utilizes the Fourier transform of the Laguerre–coefficients $l_n(b)$ of the discrete–time systems represented on the unit disc. It is shown that the local maximas of the Fourier transform of the Laguerre–coefficients appear at*

$$arg\left(\frac{\overline{a}_j - \overline{b}}{1 - \overline{a}_j b}\right) = \varphi_j(b) \qquad (j = 1, 2, \ldots, N). \tag{6.25}$$

Two equations are constructed similar to (6.7) *with two different Laguerre–parameters (b_1,b_2) so the pole identification problem is shown to be the solution of a system of equations that is:*

$$\left.\begin{aligned} \varphi_j(b_1) &= arg\left(\tfrac{\overline{a}_j - \overline{b}_1}{1-\overline{a}_j b_1}\right) \\ \varphi_j(b_2) &= arg\left(\tfrac{\overline{a}_j - \overline{b}_2}{1-\overline{a}_j b_2}\right) \end{aligned}\right\} \rightarrow a_j \qquad (j = 1, 2, \ldots, N) \tag{6.26}$$

Analytic solution of (6.26) *is given.*

Corresponding publications: [GS15], [Gőz15], [Gőz10]

Chapter 7

Conclusions and future research

In the present work, the hyperbolic geometry applied for various problems in the field of linear time invariant system theory. The research results are concluded in three distinct thesis points. The main results can be summarized as follows:

- Results are reported, connecting the H_∞ norm and ν-gap metric with the hyperbolic distance. Furthermore, the equivalence of (i) the H_∞ norm of the difference of two first order LTI systems, (ii) the ν-gap of these systems and (iii) the hyperbolic distance is also proved, under specified assumptions.

- A stability preserving interpolation method is proposed for parametric SISO LTI systems with a scalar parameter. The proposed method is based on the geometrical interpolation of the poles. The poles travel on a certain trajectory while the scalar parameter changes and samples of these trajectories are known. Since the real trajectories are unknown between samples artificial trajectories are proposed which are hyperbolic lines.

- It is shown that the usage of hyperbolic lines guarantees stability, furthermore, it guarantees an upper bound on the deviation of the interpolated model from the known models in H_∞ sense.

- A stability preserving interpolation method is proposed for parametric SISO LTI systems with a scalar parameter that also guarantees minimum phase property. The parametric SISO LTI system is sampled over a grid of parameter values and the interpolated system is calculated between these samples. The proposed method is based on the geometrical interpolation of the poles and the zeros. The poles and the zeros travel on a particular trajectory while the scalar parameter changes and the samples of these trajectories are known. As the real paths are unknown between samples, artificial trajectories are proposed which are hyperbolic lines.

- It is shown that the usage of hyperbolic lines guarantees stability, minimum phase. Furthermore, it guarantees an upper bound on the deviation of the interpolated model from the known models in H_∞ sense.

- A new method of identification of the poles is proposed for discrete time linear system. The discrete rational transfer function is represented in a rational Laguerre basis. Laguerre coefficients are considered as a sum of oscillating signals that gives us the opportunity to estimate the places of poles of the system by the Fourier trasform of the Laguerre–coefficients.

Further research:

- **Thesis 1:** The calculation of hyperbolic distance is computationally not expensive the applicability of this method possibly can be extended to a larger dimensional system.

- **Thesis 2:** The generalization of the method for MIMO systems and for vector parameter is in the main focus of the further research.

- **Thesis 3:** Overcoming the spectral leakage problem can significantly improve the applicability of the proposed method.

Publications related directly to the thesis

[Gőz10] István Gőzse. Kísérleti légijármű-modellek pozíciójának meghatározása képmegjelenítő módszerrel. In *Repüléstudományi közlemények Konferencia. Szolnok. (Repüléstudományi Közlemények. Különszám)*, Szolnok, Április 2010.

[Gőz15] István Gőzse. Optical indoor positioning system based on TFT technology. *SENSORS*, 16(1):19, 2015.

[GPLS17] István Gőzse, Tamás Péni, Tamás Luspay, and Alexandros Soumelidis. On the correspondence of hyperbolic geometry and system analysis. In *2017 20th World Congress of the International Federation of Automatic Control*, July 2017.

[GS15] István Gőzse and Alexandros Soumelidis. Realizing system poles identification on the unit disc based on the fourier trasform of laguerre-coefficients. In *MED 2015, 23rd Mediterranean Conference on Control and Automation*, pages 861–866. IEEE, Torremolinos, 2015.

[GS18] István Gőzse and Alexandros Soumelidis. A parametric lti interpolation for minimum phase systems with guaranteed stability and bounds. In *2018 Annual American Control Conference (ACC)*, pages 1224–1229, 2018.

[GS25] István Gőzse and Róbert Szabolcsi. Stability-preserving model reduction and interpolation for vibration optimization in beam-like structures. *Applied Sciences*, 15(10), 2025.

[GSS17] István Gőzse, Zoltán Szabó, and Alexandros Soumelidis. A parametric LTI interpolation with guaranteed stability and bounds. In *2017 25th Mediterranean Conference on Control and Automation (MED)*, pages 749–754, July 2017.

Further publications

[BGA+12] József Bokor, Péter Gáspár, Szilárd Aradi, Péter Bauer, Alfréd András Csikós, István Gőzse, Tamás Luspay, A Mihály, Balázs Németh, J Polgár, Alexandros Soumelidis, I Szászi, and Tamás Tettamanti. *Irányítástechnika gyakorlatok*. Typotex K., 2012. <2013>.

[BGS14] Ádám Bakos, István Gőzse, and Alexandros Soumelidis. Design and analysis of a magnetic off-axis rotary position sensing device. In *MED'14, 22nd Mediterranean Conference on Control and Automation*, pages 194–200. IEEE, Palermo, 2014.

[BRG+12] Ádám Bakos, Gergely Regula, István Gőzse, Bálint Vanek, and József Bokor. Smart actuators for mini unmanned aerial vehicles. In Maré Charles, editor, *Proceedings of the fifth International Conference on Recent Advances in Aerospace Actuation Systems and Components*, pages 196–200. k.n., 2012.

[GLP+16] István Gőzse, Tamás Luspay, Tamás Péni, Zoltán Szabó, and Bálint Vanek. Model order reduction of lpv systems based on parameter varying modal decomposition. In *55th IEEE Conference on Decision and Control*, pages 7459–7464. IEEE, Las Vegas, 2016.

[Gőz12] István Gőzse. Automatikus kisméretű koaxiális helikopter fedélzeti elektronikájának fejlesztése. *REPÜLÉSTUDOMÁNYI KÖZLEMÉNYEK*, 24(2):595–606, 2012.

[Gőz15] István Gőzse. Optical indoor positioning system based on TFT technology. *SENSORS*, 16(1):19, 2015.

[GS11] István Gőzse and Alexandros Soumelidis. Indoor position determination using image display method. In Bokor J and Szabo Z, editors, *9th European Workshop on Advanced Control and Diagnosis*, Budapest, 2011. MTA SZTAKI.

[GSV13] István Gőzse, Alexandros Soumelidis, and Bálint Vanek. Realization of an optical indoor positioning system based on TFT technology. In n S, editor, *6th European Conference on Mobile Robots. ECMR 2013*, pages 62–67, Seattle, 2013. IEEE.

Further publications

[LPG+17] Tamás Luspay, Tamás Péni, István Gőzse, Zoltán Szabó, and Bálint Vanek. Model reduction for LPV systems based on approximate modal decomposition. *International Journal for Numerical Methods in Engineering*, 2017.

[LRV+14] Márk Lukátsi, István Réti, Bálint Vanek, Ádám Bakos, József Bokor, and István Gőzse. Mini actuators for safety critical unmanned aerial vehicles avionics. *PERIODICA POLYTECHNICA: TRANSPORTATION ENGINEERING*, 41(1):25–31, 2014.

[RGS12a] Gergely Regula, István Gőzse, and Alexandros Soumelidis. 3D position and attitude estimation using novel marker detection method. In B Morcego, editor, *20th Mediterranean Conference on Control & Automation (MED2012)*, pages 1019–1024, Seattle, 2012. IEEE.

[RGS12b] Gergely Regula, István Gőzse, and Alexandros Soumelidis. Position estimation using novel calibrated indoor positioning system. In IEEE, editor, *IEEE International Instrumentation and Measurement Technology Conference (I2MTC). Proceedings*, pages 1142–1147, Seattle, 2012. IEEE. #Könyv Szerző ismeretlen.

[RLV+13] István Réti, Márk Lukátsi, Bálint Vanek, István Gőzse, Ádám Bakos, and József Bokor. Smart mini actuators for safety critical unmanned aerial vehicles. In n S, editor, *SysTol 2013. 2nd International Conference on Control and Fault-Tolerant Systems October 9-11, 2013, Nice, France*, pages 474–479, Seattle, 2013. IEEE.

[VBG+14] Bálint Vanek, Péter Bauer, István Gőzse, Márk Lukátsi, István Réti, and József Bokor. Safety critical platform for mini uas insertion into the common airspace. In *AIAA Guidance, Navigation and Control Conference*, pages 1–14. AIAA, Washington, 2014.

[ZBP+16] Tamás Zsedrovits, Péter Bauer, Borbála Jani Mátyásné Pencz, Antal Hiba, István Gőzse, Máté Németh, Zoltán Nagy, Bálint Vanek, Ákos Zarándy, and József Bokor. Onboard visual sense and avoid system for small aircraft. *IEEE AEROSPACE AND ELECTRONIC SYSTEMS MAGAZINE*, 31(9):18–27, 2016.

Bibliography

[1] Alexandros Soumelidis, József Bokor, and Ferenc Schipp. Applying hyperbolic wavelet constructions in the identification of signals and systems. In *SYSID 2009. 15th IFAC symposium on system identification. Preprints. Saint-Malo, 2009.*, pages 1334–1339, Saint-Malo, July 2009. IFAC.

[2] Alexandros Soumelidis, József Bokor, and Ferenc Schipp. Modeling and identification in frequency domain with representations on the blaschke group. In A Alexandridis, editor, *Proceedings of the 14th IASTED International Conference on Control and Applications*, pages 161–168, Anaheim; Calgary; Zurich, 2012. Acta Press.

[3] Roland Toth. *Modeling and Identification of Linear Parameter-Varying Systems*. Springer-Verlag Berlin Heidelberg, 2010.

[4] Tomás Oliveira e Silva. A n-width result for the generalized orthonormal basis function model. In *Preprints of the 13th World Congress of the International Federation of Automatic Control*, volume I, pages 375–380, San Francisco, USA, 1996.

[5] M. Geuss and B. Lohmann. Stable - a stability algorithm for parametric model reduction by matrix interpolation. *Mathematical and Computer Modelling of Dynamical Systems*, 22(4):307–322, 2016.

[6] M. Geuss, H. Panzer, and B. Lohmann. On parametric model order reduction by matrix interpolation. In *2013 European Control Conference (ECC)*, pages 3433–3438, July 2013.

[7] David Amsallem and Charbel Farhat. An online method for interpolating linear parametric reduced-order models. *SIAM Journal on Scientific Computing*, 33(5):2169–2198, 2011.

[8] Rudy Eid, Rosa Castañé-Selga, Heiko Panzer, Thomas Wolf, and Boris Lohmann. Stability-preserving parametric model reduction by matrix interpolation. *Mathematical and Computer Modelling of Dynamical Systems*, 17(4):319–335, 2011.

[9] Markus Giftthaler, Thomas Wolf, Heiko Panzer, and Boris Lohmann. Parametric model order reduction of port-hamiltonian systems by matrix interpolation. *Automatisierungstechnik*, 62:619–628, 2014.

[10] Ortwin Farle, Stefan Burgard, and Romanus Dyczij-Edlinger. Passivity preserving parametric model-order reduction for non-affine parameters. *Mathematical and Computer Modelling of Dynamical Systems*, 2011.

[11] M. Geuss, H. K. F. Panzer, T. Wolf, and B. Lohmann. Stability preservation for parametric model order reduction by matrix interpolation. In *2014 European Control Conference (ECC)*, pages 1098–1103, June 2014.

[12] S. Lawrence Marple Jr. and William M. Carey. Digital spectral analysis with applications. *The Journal of the Acoustical Society of America*, 86(5):2043–2043, 1989.

[13] L. Ljung. Issues in system identification. *IEEE Control Systems*, 11(1):25–29, Jan 1991.

[14] L. Keviczky, J. Bokor, and Cs. Banyasz. A new identification method with special parametrization for model structure determination. In *Proceedings of the 5th IFAC Symposium on System Identification*, pages 651–568, Darmstadt, Germany, 1979.

[15] T. McKelvey, H. Akcay, and L. Ljung. Subspace-based multivariable system identification from frequency response data. *IEEE Transactions on Automatic Control*, 41(7):960–979, Jul 1996.

[16] Peter S C Heuberger, Bo, and Paul M J Van den Hof. *Modelling and Identification with Rational Orthogonal Basis Functions*. Springer, Dordrecht, 2006.

[17] T. O. e Silva. Pole selection in GOBF models. In P. S. C. Heuberger, P. M. J. Van den Hof, and B. Wahlberg, editors, *Modelling and Identification with Rational Orthogonal Basis Functions*, chapter 11, pages 297–336. Springer Verlag, 2005.

[18] A. Soumelidis, M. Pap, F. Schipp, and J. Bokor. Frequency domain identification of partial fraction models. In *Proceedings of the15th IFAC World Congress*, page on CD, Barcelona, Spain, June 2002.

[19] A.F. Beardon and D. Minda. The hyperbolic metric and geometric function theory. In *Proceedings of the International Workshop on Quasiconformal Mappings and their Applications*, 2000.

[20] James W Anderson. *Hyperbolic geometry; 2nd ed.* Springer undergraduate mathematics series. Springer, Berlin, 2005.

Bibliography

[21] U.A. Albert. *Analytic Hyperbolic Geometry: Mathematical Foundations And Applications*. World Scientific Publishing Company, 2005.

[22] A.A. Ungar. Einstein's special relativity: Unleashing the power of its hyperbolic geometry. *Computers and Mathematics with Applications*, 49(2):187 – 221, 2005.

[23] Hirokazu Hasegawa, Takeji Hashimoto, and Stephen T. Hyde. Microdomain structures with hyperbolic interfaces in block and graft copolymer systems. *Polymer*, 37(17):3825 – 3833, 1996.

[24] Stephen T Hyde. Bicontinuous structures in lyotropic liquid crystals and crystalline hyperbolic surfaces. *Current Opinion in Solid State and Materials Science*, 1(5):653 – 662, 1996.

[25] D. Krioukov, F. Papadopoulos, M. Kitsak, A. Vahdat, and M. BoguÃ±Ã¡. Hyperbolic Geometry of Complex Networks. *Physical Review E*, 82(036106), Oct 2010.

[26] Marc Barthélemy. Spatial networks. *Physics Reports*, 499(1):1 – 101, 2011.

[27] Kevin Verbeek and Subhash Suri. Metric embedding, hyperbolic space, and social networks. *Computational Geometry*, 59(Supplement C):1 – 12, 2016.

[28] Andrei Müller, Esther Sanabria-Codesal, Alin Moldoveanu, Victor Asavei, and Dan Dascalu. Two compact smith charts: The 3d smith chart and a hyperbolic disc model of the generalized infinite smith chart. *Romanian Journal of Information Science and Technology*, 19(1-2):166–174, 2016.

[29] M. S. Gupta. Escher's art, smith chart, and hyperbolic geometry. *IEEE Microwave Magazine*, 7(5):66–76, Oct 2006.

[30] Jeffery C. Allen and Jr. Dennis M. Healy. Hyperbolic geometry, Nehari's theorem, electric circuits, and analog signal processing. In Daniel N. Rockmore and Jr. Dennis M. Healy, editors, *Modern Signal Processing*, volume 46. Cambridge University Press, 2004.

[31] E.Folke Bolinder. A survey of the use of non-euclidean geometry in electrical engineering. *Journal of the Franklin Institute*, 265(3):169 – 186, 1958.

[32] E. Folke Bolinder, J I-i, and E. Folke Bolinder. Impedance and power transformations by the isometric circle method and non-euclidean hyperbolic geometry. Technical report, MASSACHUSETTS INSTITUE OF TECHNOLOGY, 1957.

[33] P. Khargonekar and A. Tannenbaum. Non-euclidian metrics and the robust stabilization of systems with parameter uncertainty. *IEEE Transactions on Automatic Control*, 30(10):1005–1013, Oct 1985.

[34] Z. Szabó and József Bokor. *Non-Euclidean Geometries in Modeling and Control*. Széchenyi University Press, 2015.

[35] Zoltán Szabó, József Bokor, and Tibor Vámos. A hyperbolic view on robust control. In *Preprints of the 19th IFAC World Congress*, pages 718–723. IFAC, Cape Town, 2014.

[36] R. Toth. *Modeling and Identification of Linear Parameter-Varying Systems*. Springer-Verlag, 2010.

[37] R. Toth. *Modeling and Identification of Linear Parameter-Varying Systems*. Springer-Verlag, 2010.

[38] Roland Tóth, Peter S. C. Heuberger, and Paul M. J. Van den Hof. Asymptotically optimal orthonormal basis functions for lpv system identification. *Automatica*, 45(6):1359–1370, June 2009.

[39] A. Soumelidis, J. Bokor, and F. Schipp. Realizing system poles identification on the unit disc based on Laguerre representations and hyperbolic metrics. In *Mediterranean Conference on Control and Automation (MED)*, pages 1208–1213, June 2013.

[40] A. Soumelidis, F. Schipp, and J. Bokor. Pole Structure Estimation from Laguerre Representations Using Hyperbolic Metrics on the Unit Disc. In *Conference on Decision and Control (CDC) and European Control Conference*, pages 2136–2141, 2011.

[41] Alexandros Soumelidis, Ferenc Schipp, and József Bokor. Pole reconstruction of systems from laguerre basis representations. In WSEAS, editor, *Recent researches in system science. Proceedings of the 15th WSEAS international conference on systems*, pages 172–179, Corfu, 2011. WSEAS.

[42] A. Soumelidis, J. Bokor, and F. Schipp. Realizing system poles identification on the unit disc based on Laguerre representations and hyperbolic metrics. In *Mediterranean Conference on Control and Automation (MED)*, pages 1208–1213, 2013.

[43] A. Soumelidis, J. Bokor, and F. Schipp. Realizing system poles identification on the unit disc based on laguerre representations and hyperbolic metrics. In *Control Automation (MED), 2013 21st Mediterranean Conference on*, pages 1208–1213, June 2013.

[44] Alexandros Soumelidis, József Bokor, and Ferenc Schipp. Applying hyperbolic wavelets in frequency domain identification. In Ferrier Louis, Bernard Alain, Gusikhin Oleg, and Madani Kurosh, editors, *ICINCO 2012. Proceedings of the 9th International Conference on Informatics in Control, Automation and Robotics. Vol. 1.*, pages 532–535. SciTePress, 2012.

[45] Alexandros Soumelidis, Ferenc Schipp, and József Bokor. On hyperbolic wavelets. In Bittanti, Sergio, Cenedese, Angelo, Zampieri, and Sandro, editors, *18th World Congress of the International Federation of Automatic Control*, pages 2309–2314, Washington, 2011. IFAC by Pergamon Press.

[46] A. Soumelidis, J. Bokor, and F. Schipp. Identifying poles from time-domain data using discrete laguerre system. In *Control Automation (MED), 2012 20th Mediterranean Conference on*, pages 1450–1455, July 2012.

[47] Jennifer Przybilla and Matthias Voigt. Model Reduction of Parametric Differential-Algebraic Systems by Balanced Truncation. *Mathematical and Computer Modelling of Dynamical Systems*, 30(1):303–341, December 2024.

[48] Tea Vojković, Pierre Vuillemin, David Quero, and Charles Poussot-Vassal. Parametric reduced-order modeling of aeroelastic systems. *IFAC-PapersOnLine*, 2022.

[49] Manuela Hund, Tim Mitchell, Petar MlinariÄ‡, and Jens Saak. Optimization-based parametric model order reduction via $\mathcal{H}_2 \otimes \mathcal{L}_2$ first-order necessary conditions, 03 2021.

[50] Alessio Moreschini, Joel D. Simard, and Alessandro Astolfi. Data-driven model reduction for port-hamiltonian and network systems in the loewner framework. *Automatica*, 169:111836, 2024.

[51] Walter Rudin. *Real and complex analysis*. McGraw-Hill, New York, St louis, Paris, 1987.

[52] B. Wahlberg. System identification using laguerre models. *IEEE Transactions on Automatic Control*, 36(5):551–562, May 1991.

[53] Glenn Vinnicombe. *Measuring Robustness of Feedback Systems*. PhD thesis, Department of Engineering, University of Cambridge, 1993.

[54] T. Peni and P. Seiler. Computation of lower bounds for the induced $\mathcal{L}_2$-norm of LPV systems. *International Journal of Robust and Nonlinear Control*, 26(4):646–661, 2016.

[55] J. Bokor and G. Balas. Detection filter design for LPV systems–a geometric approach. *Automatica*, 40:511–518, 2004.

[56] H. Pfifer and P. Seiler. Robustness analysis of linear parameter varying systems using integral quadratic constraints. *International Journal of Robust and Nonlinear Control*, 25(15):2843–2864, 2015.

[57] A. Marcos and G. Balas. Development of linear-parameter-varying models for aircraft. *Journal of Guidance, Control and Dynamics*, 27(2):218–228, 2004.

[58] L. Lovasz and M. D. Plummer. *Matching Theory*, volume 29 of *Annals of Discrete Mathematics*. North-Holland Mathematics Studies, 1986.

[59] R. Burkard, M. Dell'Amico, and S. Martello. *Assignment Problems*. SIAM, 2009.

[60] G. H. Golub and Ch. F. Van Loan. *Matrix computations*. Johns Hopkins University Press, 2013.

[61] M. Geuss, H. Panzer, and B. Lohmann. On parametric model order reduction by matrix interpolation. In *European Control Conference*, pages 3433–3438, 2013.

[62] D. Amsallem and Ch. Farhat. An online method for interpolating linear parametric reduced-order models. *SIAM Journal on Scientific Computing*, 33(5):2169–2198, 2011.

[63] Ch. D. Manning and P. Raghavan abd H. Schütze. *Introduction to Information Retrieval*. Cambridge University Press, 2008.

[64] T. Hastie, R. Tibshirani, and J. Friedman. *The Elements of Statistical Learning*. Data Mining, Inference, and Prediction. Springer, 2009.

[65] G. D. Wood. *Control of Parameter-Dependent Mechanical Systems*. PhD thesis, University of Cambridge, 1995.

[66] SiHun Lee, Kijoo Jang, Sangmin Lee, Haeseong Cho, and SangJoon Shin. Parametric model order reduction by machine learning for fluidâ€“structure interaction analysis. *Eng. with Comput.*, 40(1):45â€“60, January 2023.

[67] Duo Zhang, Zhan-Hao Guo, Yi-Qing Ni, Zhengwei Chen, Wai Kei Ao, Amir Bordbar, and Fang-Ru Zhou. Correlation between cargo properties and train overturning safety for a high-speed freight train under strong winds. *Engineering Applications of Computational Fluid Mechanics*, 17, 06 2023.

[68] M. A. Bazaz, S. A. Nahve, M. Nabi, S. Janardhanan, and M. U. Rehman. Adaptive parameter space sampling in matrix interpolatory pmor. In *2015 International Conference on Recent Developments in Control, Automation and Power Engineering (RDCAPE)*, pages 83–89, March 2015.

[69] Maria Cruz Varona, Mashuq un Nabiz, and Boris Lohmann. Automatic adaptive sampling in parametric model order reduction by matrix interpolation. In *2017 IEEE International Conference on Advanced Intelligent Mechatronics (AIM)*, pages 472–477, 2017.

[70] Péter Baranyi and Yeung Yam. Tp model transformation based observer designto 2-d aeroelastic system. *Acta Polytechnica Hungarica*, 2004.

[71] András Molnár. Surveying archaeological sites and architectural monuments with aerial drone photos. *Acta Polytechnica Hungarica*, 2019.

[72] Bisera Andrić Gušavac, Milan Martić, Milena Popović, and Gordana Savić. Agricultural route efficiencies, based on data envelopment analysis (dea). *Acta Polytechnica Hungarica*, 2023.

[73] Ashraf Mahmud Rayed, Balasubramanian Esakki, Arunkumar Ponnambalam, Sajal Chandra Banik, and Karim Aly. Optimization of uav structure and evaluation of vibrational and fatigue characteristics through simulation studies. *Int. J. Simul. Multidisci. Des. Optim.*, 12:17, 2021.

[74] Tamás Réti and Károly Böröczky. Topological characterization of cellular structures. *Acta Polytechnica Hungarica*, 2004.

[75] Alan V. Oppenheim, Alan S. Willsky, and S. Hamid Nawab. *Signals & systems (2nd ed.)*. Prentice-Hall, Inc., USA, 1996.

[76] M.D. Plummer and L. Lovász. *Matching Theory*. North-Holland Mathematics Studies. Elsevier Science, 1986.

[77] Heiko Panzer, Jörg Hubele, Rudy Eid, and Boris Lohmann. Generating a parametric finite element model of a 3d cantilever timoshenko beam using matlab. Technical reports on automatic control, vol. trac-4,, Institute of Automatic Control, Technische Universität München, 2009.

[78] Maria Cruz Varona and Boris Lohmann. Model reduction of linear time-varying systems with applications for moving loads. *CoRR*, abs/1607.02846, 2016.

[79] Nguyen Thanh Son. A real time procedure for affinely dependent parametric model order reduction using interpolation on grassmann manifolds. *International Journal for Numerical Methods in Engineering*, 93(8):818–833, 2013.

[80] M. Geuss, D. Butnaru, B. Peherstorfer, H. J. Bungartz, and B. Lohmann. Parametric model order reduction by sparse-grid-based interpolation on matrix manifolds for multidimensional parameter spaces. In *2014 European Control Conference (ECC)*, pages 2727–2732, June 2014.

[81] George E. Forsythe, Michael A. Malcolm, and Cleve B. Moler. *Computer Methods for Mathematical Computations*. Prentice Hall Professional Technical Reference, 1977.

[82] Richard P. Brent. *Algorithms for Minimization without Derivatives*. Prentice-Hall, Englewood Cliffs, N.J., 1973.

[83] H. Panzer. *Model Order Reduction by Krylov Subspace Methods with Global Error Bounds and Automatic Choice of Parameters*. Verlag Dr. Hut, 2014.

[84] Abhineet Gupta, Claudia P. Moreno, Harald Pfifer, Brian Taylor, and Gary J. Balas. Updating a finite element based structural model of a small flexible aircraft. In *AIAA Modeling and Simulation Technologies Conference*, 01 2015.

[85] Alphose Zingoni. *Vibration Analysis and Structural Dynamics for Civil Engineers: Essentials and Group-Theoretic Formulations*. CRC Press, London, 2018.

[86] Norman Richard Draper and Harry Smith. *Applied regression analysis*. A Wiley-Interscience publication. Wiley, New York, NY [u.a.], 3. ed. edition, 1998.

[87] Charlie C. L. Wang and Gershon Elber. Multi-dimensional dynamic programming in ruled surface fitting. *Computer-Aided Design*, 51:39–49, 2014.

[88] J. N. Reddy. *Introduction to the Finite Element Method*. McGraw-Hill Education, New York, 4th edition edition, 2019.

[89] Igor A. Karnovsky and Olga I. Lebed. *Formulas for Structural Dynamics: Tables, Graphs and Solutions*. McGraw-Hill Education, New York, 1st edition edition, 2001.

[90] Jong-Shyong Wu. *Transfer Matrix Methods for Discrete and Continuous Systems*, chapter 4, pages 245–353. John Wiley & Sons, Ltd, 2015.

[91] Sondipon Adhikari. Rates of change of eigenvalues and eigenvectors in damped dynamic system. *AIAA Journal*, 37(11):1452–1458, 1999.

[92] Roger A. Horn and Charles R. Johnson. *Matrix Analysis*. Cambridge University Press, Cambridge; New York, 2nd edition, 2013.

[93] Kemin Zhou, John C. Doyle, and Keith Glover. *Robust and optimal control*. Prentice-Hall, Inc., USA, 1996.

[94] G. Regula, I. Gozse, and A. Soumelidis. Position estimation using novel calibrated indoor positioning system. In *Instrumentation and Measurement Technology Conference (I2MTC), 2012 IEEE International*, pages 1142–1147, May 2012.

[95] G. Regula, I. Gozse, and A. Soumelidis. 3d position and attitude estimation using novel marker detection method. In *Control Automation (MED), 2012 20th Mediterranean Conference on*, pages 1025–1030, July 2012.

[96] J.P. Dakin and R.G.W. Brown. *Handbook of Optoelectronics (Two-Volume Set)*. Handbook of Optoelectronics. Taylor & Francis, 2010.

List of Symbols and Abbreviations

$\mathbb{D}$	Unit disk on complex plane $\mathbb{D} := \{z \in \mathbb{C} : \lvert z\rvert < 1\}$
$d_h(\cdot,\cdot)$	Hyperbolic distance on Poincaré disk
$d_{hp}(\cdot,\cdot)$	Pseudo-hyperbolic distance on Poincaré disk
$\lvert.\rvert$	Absolute value
$\bar{\cdot}$	Bar means complex conjugate
$\lVert\cdot\rVert$	Norm
$\lVert\cdot\rVert_2$	Euclidean norm
$\lVert\cdot\rVert_\infty$	H-infinity norm
$H(z)$	Discrete time transfer function
$\hat{H}(z)$	Interpolated discrete time transfer function
$P(s)$	Continuous time transfer function
G	Symbol of a LTI system
$\hat{G}$	Symbol of an interpolated LTI system
$\delta_\nu(\cdot,\cdot)$	nu-gap metric

List of Figures

Acknowledgments

I would like to express my deepest gratitude to all those who supported and guided me throughout my PhD journey.

First and foremost, I am sincerely grateful to my former supervisor, Alexandros Soumelidis, at SZTAKI. His kindness, availability, and expertise shaped my early research path, and his guidance during the initial phase of my doctoral work provided a strong foundation for this dissertation.

I am deeply thankful to Tamás Péni, whose support extended far beyond technical advice. His help in developing my writing and his encouragement to explore a new subtopic played a crucial role in the evolution of my research. I also wish to thank Tamás Luspay for his steady support and helpful insights, and Zoltán Szabó, who was always willing to discuss mathematical questions and whose open-door attitude helped me resolve many mathematical issues.

After a long interruption in my doctoral work, I continued my PhD at Óbuda University, where I was fortunate to be guided by my new supervisor, Róbert Szabolcsi. His inspiration, unwavering support, and genuine selflessness were instrumental in helping me regain momentum and ultimately complete this dissertation. I am truly indebted to him for motivating me to finish this long journey.

Finally, I would like to express my heartfelt gratitude to my wife, Mónika, whose love, patience, and unwavering belief in me carried me through the most challenging periods of this work. Her support has been a constant source of strength, and this achievement is as much hers as it is mine.

To all of you, thank you for your dedication, patience, and belief in my work. This thesis would not have been possible without your contributions.